

Copyright

by

Valerie Ann Andres

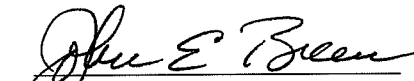
1995


---

**VERIFICATION OF FORCE DISTRIBUTION IN AN INNOVATIVE BRIDGE PIER**

APPROVED BY

SUPERVISING COMMITTEE:

  
\_\_\_\_\_  
John E. Breen

  
\_\_\_\_\_  
Michael E. Kreger

*to my parents, whose endless encouragement and support mean the world to me*

---

**VERIFICATION OF FORCE DISTRIBUTION IN AN INNOVATIVE BRIDGE PIER**

by

Valerie Ann Andres

Thesis

Presented to the Faculty of the Graduate School

of The University of Texas at Austin

in Partial Fulfillment

of the Requirements

for the Degree of

Master of Science in Engineering

The University of Texas at Austin

---

December 1995

## ACKNOWLEDGMENTS

This thesis was written with the encouragement and support of many people who are dear to me. Although this is the last page that I am writing, it is by far the most important to me and the hardest to write. I want to thank all of the people who have been a part of my life during this time, because I know I have not been the easiest person to deal with over the last 6 months.

I want to thank Dr. John Breen for his invaluable advising on this project. Just when I thought everything was gone awry, he provided a great deal of insight and encouragement to pull (or push) me along. Dr. Michael Kreger helped when I needed it the most - last minute reading time. I also want to thank Rodney Davis and Bryan Wood. Their help and patience in the field was priceless. Wade Bonzon provided a special enthusiasm for the project which kept me going when I wanted to quit.

I want to thank all of the staff at Ferguson Lab who made my life easier by cooperating with my “on-going student” status. Jenkins and Laurie Golding dealt patiently with my registration woes. Dr. Burns went out of his way to make certain I was accommodated during my last months at the lab. Sharon Cunningham was a life-saver when it came to putting my thesis together. Cindy McCright nourished me during my “homeless” days with her wide assortment of candies. All of the technicians were willing to help and didn’t laugh at my ignorance concerning the lab equipment.

I specifically want to thank the many friends who gave me words of support and made me laugh when I needed to laugh most. My roommate Sarah Billington was always just a phone call away no matter what part of Texas she was in, harassing the public. “Whispering” Jeff Schmitz was game for silly antics at any time of the day or night, and was always ready with words of encouragement like “up all night!”. Ron Peron literally saved my life by making sure that I had not a need in the world that wasn’t fulfilled, and that I ate dinner every night. Late nights at the computer lab were made less lonely by the constant computer room fixture - David Gwie. Willy Ramirez put in countless hours on a finite element model of the pier, which is not presented in this thesis. Lastly, I want to thank Sarah and Ron for their unselfish donation of countless hours to help me finish this thesis. If it weren’t for them I think I would have collapsed, never to finish my thesis.

## **ABSTRACT**

### **VERIFICATION OF FORCE DISTRIBUTION IN AN INNOVATIVE BRIDGE PIER**

by

Valerie Ann Andres, M.S.E.

The University of Texas at Austin

SUPERVISORS: John E. Breen and Michael E. Kreger

Construction of the US 183 Elevated highway in Austin provided a unique opportunity to investigate the behavior of innovative cast in situ reinforced concrete piers used to support the mainlanes of the precast segmental reinforced concrete superstructure. The study of the force distribution through the US 183 Elevated mainlane bridge piers was performed in order to further evaluate the use of strut-and-tie modeling (STM) for reinforced concrete design and to familiarize designers with the concept of STM and its possible uses. In order to investigate the behavior of a US 183 mainlane pier, one of these piers was instrumented during construction. The purpose of the instrumentation was to measure the flow of forces through the pier due to the superstructure dead load so that these forces could be compared to the forces predicted by a strut-and-tie model of the pier.

In summary, the field instrumentation of a US 183 Elevated mainlane bridge pier successfully provided researchers with valuable information regarding the distribution of forces in the pier. Information regarding temperature effects in the pier can be used to further study the behavior of similar structures. The measurements made prior to and during construction of the superstructure furnished researchers with the information needed to evaluate the use of strut-and-tie modeling for reinforced concrete design. The comparison of strut-and-tie models based on measured and predicted forces indicated the ability of strut-and-tie modeling to allow a designer to trace the flow of forces through a structure.

## TABLE OF CONTENTS

<b>List of Tables</b> .....	x
<b>List of Figures</b> .....	xi
<b>1 Introduction</b> .....	1
1.1 Introduction .....	1
1.2 US 183 Project Description .....	1
1.3 US 183 Mainlane Pier Description .....	1
1.4 Problem Statement and Objectives .....	3
1.5 Scope of Work .....	6
<b>2 Background</b> .....	7
2.1 Introduction .....	7
2.2 Previous Bridge Pier Studies .....	8
2.3 Strut-and-Tie Modeling .....	9
2.3.1 General .....	9
2.3.2 History .....	9
2.3.3 Assumptions .....	12
2.3.4 Development of a Strut-and-Tie Model .....	12
2.3.4.1 B-regions and D-regions .....	12
2.3.4.2 Layout of Struts and Ties .....	13
2.3.5 Struts .....	14
2.3.6 Ties .....	16
2.3.7 Nodes .....	16
2.3.8 Summary of Design Procedure .....	17
2.3.9 Benefits of Strut-and-Tie Modeling .....	17
2.3.10 Limitations of Research .....	19
<b>3 Pier Instrumentation</b> .....	20
3.1 Introduction .....	20
3.1.1 Instrumentation Systems .....	20
3.1.2 Instrumented Pier .....	20
3.2 Steel Strains - Strain Gages .....	21
3.2.1 Background .....	21
3.2.2 Application .....	21
3.2.3 Layout .....	22
3.3 Concrete Strains - Concrete Strain Devices .....	22
3.3.1 Background .....	22
3.3.2 Description and Application .....	22
3.3.3 Layout .....	26
3.3.4 Device Selection Procedure .....	26
3.3.4.1 Test Set-Up .....	27
3.3.4.2 Testing Procedure .....	29
3.3.4.3 Results .....	30
3.4 Concrete Strains - Demec Extensometer .....	35
3.4.1 Background .....	35
3.4.2 Description and Application .....	36

3.4.3	Layout.....	36
3.5	Temperature Gradient - Thermocouples.....	39
3.5.1	Background.....	39
3.5.2	Application.....	40
3.5.3	Layout.....	40
3.6	Deformation of the “Y” - Linear Potentiometers and Thermocouples.....	40
3.7	Data Acquisition System.....	43
<b>4</b>	<b>US 183 Construction and Data Collection.....</b>	<b>44</b>
4.1	Introduction.....	44
4.2	Pier Construction.....	44
4.3	Superstructure Erection.....	44
4.4	Data Collection.....	44
<b>5</b>	<b>Data Presentation.....</b>	<b>51</b>
5.1	Introduction.....	51
5.2	Background - Thermal Strains.....	51
5.2.1	Thermal Strains - Basic Principles.....	51
5.2.2	Thermal Restraint and Thermal Stresses.....	52
5.2.3	Thermal Stresses in Pier due to Temperature Gradient in Concrete.....	52
5.2.3	Thermal Stresses in Pier due to Temperature Gradient in Pipes.....	54
5.3	Measurements - Prior to Superstructure Erection.....	55
5.3.1	Temperature Measurements.....	55
5.3.2	Structural Steel Pipe Strains - Typical Sunny Day.....	64
5.3.3	Capital Strains - Typical Sunny Day.....	71
5.3.4	Shaft Strains - Typical Sunny Day.....	81
5.4	Measurements - During Superstructure Erection.....	86
5.4.1	Temperature Measurements.....	87
5.4.2	Structural Steel Pipe Strains.....	95
5.4.3	Capital Strains.....	96
5.4.4	Shaft Strains.....	106
<b>6</b>	<b>Superstructure Dead Load Data Analysis.....</b>	<b>113</b>
6.1	Introduction.....	113
6.2	Thermal Strains.....	113
6.2.1	Significance of Thermal Strains.....	113
6.2.2	Procedure for Extraction of Thermal Strains from Measured Strains.....	114
6.3	Superstructure Dead Load Strains in Pier.....	115
6.3.1	Pipe Strains.....	116
6.3.2	Capital Strains.....	116
6.3.3	Shaft Strains.....	119
6.4	Superstructure Dead Load Forces in Pier.....	121
6.4.1	Pipe Forces.....	121
6.4.2	Capital Forces.....	121
6.4.3	Shaft Forces.....	122
6.5	Strut-and Tie Model for US 183 Mainlane Pier.....	122
6.5.1	Strut-and-Tie Model Based on Measured Forces.....	124



6.5.1.1	Strut-and-Tie Model Based on Compressive Force Resultants in the Capital .....	124
6.5.1.2	Measured Force Distributions .....	125
6.5.2	Strut-and-Tie Model Based on an Elastic Frame Analysis .....	126
6.6	Comparison of Forces and Force Paths .....	127
<b>7</b>	<b>Conclusions, Recommendations &amp; Summary</b> .....	<b>130</b>
7.1	Introduction .....	130
7.2	Project Overview .....	130
7.3	Conclusions and Recommendations .....	131
7.3.1	Temperature Measurements .....	131
7.3.2	Superstructure Dead Load Measurements .....	132
7.3.3	Comparison of Measured Forces with Strut-and-Tie Models .....	133
7.4	Summary .....	134
	<b>Appendix</b> .....	<b>135</b>
	<b>References</b> .....	<b>151</b>
	<b>Vita</b> .....	<b>153</b>

## LIST OF TABLES

4.1	Data Collection Summary.....	45
5.1	Superstructure Erection Sequence Over Pier D6 .....	89
6.1	Comparison of Expected Gravity Strains and Measured Thermal Strains.....	114
6.2	Temperature Differential Locations Compared for Thermal Strain Extraction ...	115
6.3	Relative Temperatures for March 16 and March 30, 1995 .....	115
6.4	Superstructure Dead Load Strains Measured in Structural Steel Pipes: Thermal Strains Extracted .....	116
6.5	Average Superstructure Dead Load Strains Measured in the Capital: Thermal Strains Extracted .....	118
6.6	Average Measured Strains in Shaft due to Superstructure Dead Load: Thermal Strains Extracted .....	120
6.7	Forces Measured in Pipes due to Gravity Load.....	121
6.8	Compressive Forces Measured on One Branch of the Capital due to Superstructure Dead Load.....	122
6.9	Forces Measured in One Half of Shaft due to Superstructure Dead Load.....	122

## LIST OF FIGURES

1.1	Location Map .....	2
1.2	Photograph of US 183 Viaduct .....	3
1.3	US 183 Mainlane Pier: Elevation View .....	4
1.4	US 183 Mainlane Pier: Plan View .....	5
1.5	Structural Steel Pipe Assembly: Detail.....	5
2.1	US 183 Mainlane Pier .....	8
2.2	Typical Uses of Strut and Tie Models [4].....	11
2.3	St. Venant's Principle [3] .....	13
2.4	Strut Types [4] .....	14
2.5	Design Procedure for Structural Concrete [2].....	18
3.1	Strain Gage and Concrete Strain Device Layout: Elevation View.....	23
3.2	Strain Gage Locations: Pipe Assembly.....	24
3.3	Strain Gage and Concrete Strain Device Layout: Sections .....	25
3.4	Concrete Strain Device.....	25
3.5	Photograph of Concrete Strain Device .....	27
3.6	Concrete Strain Device Locations in Shaft.....	28
3.7	Concrete Strain Device Test Specimen .....	29
3.8	Comparison of Results; Specimen No. 1, Test 1.....	31
3.9	Comparison of Results; Specimen No. 2, Test 1.....	31
3.10	Comparison of Results; Specimen No. 3, Test 1.....	32
3.11	Comparison of Results; Specimen No. 1, Test 2.....	32
3.12	Comparison of Results; Specimen No. 2, Test 2.....	33
3.13	Comparison of Results; Specimen No. 3, Test 2.....	33
3.14	Side-by-Side Comparison for Test 1 .....	34
3.15	Side-by-Side Comparison for Test 2 .....	34
3.16	Demec Extensometer .....	35
3.17	Demec Point Installation .....	36
3.18	Demec Point Locations on Shaft.....	37
3.19	Demec Point Locations on Side of Shaft and Capital .....	38
3.20	Demec Point Locations on Inside Face of Capital .....	39
3.21	Thermocouple Locations .....	41
3.22	Set-up to Read Deformation in "Y" .....	42
4.1	Casting of Pier Column Concrete .....	46
4.2	Construction of Pier Capital .....	46
4.3	Typical Mainlane Pier .....	47
4.4	Pier Bracket.....	48
4.5	Partially Mounted Pier Bracket.....	48
4.6	Pier Bracket Supporting Truss.....	49
4.7	Construction Procedure for Typical Span Completion .....	49
4.8	Completed Span .....	50
5.1	Example Problem Examining Temperature Effects.....	53
5.2	Temperature Effects in Column.....	53
5.3	Temperatures Over a Typical Day .....	54
5.4	Temperature History.....	57
5.5	Ambient Temperatures for March 11, 1995 .....	57

5.6	Thermocouple Locations .....	58
5.7	Structural Steel Pipe Temperatures: Typical Sunny Day .....	58
5.8	Structural Steel Pipe Temperature Changes: Typical Sunny Day.....	59
5.9	Temperatures in Concrete “Shell”: Typical Sunny Day.....	59
5.10	Temperature in Concrete “Core”: Typical Sunny Day.....	60
5.11	Temperature Lag to Concrete “Core”: Typical Sunny Day.....	60
5.12	Ambient Temperatures During March 1, 1995 .....	62
5.13	Structural Steel Pipe Temperatures: Typical Cloudy Day .....	62
5.14	Structural Steel Pipe Temperature Changes: Typical Cloudy Day .....	63
5.15	Temperatures in Concrete “Shell”: Typical Cloudy Day.....	63
5.16	Temperature in Concrete “Core”: Typical Cloudy Day.....	64
5.17	Strain Gage Locations on Structural Steel Pipes .....	66
5.18	Strain Variations Along Structural Steel Pipe: Exterior Pipe.....	67
5.19	Strain Variations Along Structural Steel Pipe: Interior Pipe.....	68
5.20	Pipe Strain Change and Temperature Change.....	69
5.21	Pipe Strain Change and Temperature Change.....	69
5.22	Pipe Strain Change and Temperature Change.....	70
5.23	Pipe Strain Change and Temperature Change.....	70
5.24	Capital Instrument Locations.....	73
5.25	Strain Variation Instruments Located in Top Section of Capital - Typical Sunny Day .....	74
5.26	Strain Variation Instruments Located in Middle Section of Capital - Typical Sunny Day .....	75
5.27	Strain Variation Instruments Located in Bottom Section of Capital - Typical Sunny Day .....	76
5.28	Comparison of Temperature Change and Strain Variation for Instruments Located Near the Top of the Capital.....	77
5.29	Comparison of Temperature Change and Strain Variation for Instruments Located Near the Bottom of the Capital.....	77
5.30	Variation of Strain Vertically Along the “Y”: Concrete Core.....	78
5.31	Variation of Strain Vertically Along the “Y”: Concrete Core.....	78
5.32	Variation of Strain Vertically Along the “Y”: Concrete Shell .....	79
5.33	Variation of Strain Vertically Along the “Y”: Concrete Shell .....	79
5.34	Variation of Strain Vertically Along the “Y”: Concrete Shell .....	80
5.35	Variation of Strain Vertically Along the “Y”: Concrete Shell .....	80
5.36	Location of Instruments in Column .....	82
5.37	Strain Variation: Top of Column .....	83
5.38	Strain Variation: Middle of Column.....	83
5.39	Strain Variation: Bottom of Column.....	84
5.40	Comparison of Column Strain Variation and Surface Temperature Change: Concrete “Shell” .....	84
5.41	Comparison of Column Strain Variation and Surface Temperature Change: Core Concrete.....	85
5.42	Column Strains Near Surface: Typical.....	85
5.43	Column Strains in Core: Typical .....	86
5.44	Ambient Temperature Readings During Superstructure Erection (As Reported by the National Oceanic and Atmospheric Administration).....	90

5.45	Temperatures Measured on the Structural Steel Pipe During Construction.....	91
5.46	Concrete Temperatures Measured Near the Top of the Capital During Construction .....	92
5.47	Concrete Temperatures Measured Near the Bottom of the Capital During Construction .....	93
5.48	Concrete Temperatures Measured at the Base of the Capital During Construction .....	94
5.49	Strain Change Measured in the Interior Structural Steel Pipe During Construction .....	98
5.50	Strain Change Measured in the Exterior Structural Steel Pipe During Construction .....	99
5.51	Strain Change Measured near Top of Capital During Superstructure Erection.....	100
5.52	Strain Change Measured near Mid-Height of Capital During Superstructure Erection.....	101
5.53	Strain Change Measured near Bottom of Capital During Superstructure Erection.....	102
5.54	Comparison of Strain Change “Vertically” on Capital During Superstructure Erection: Core Near Inside Face of "Y" .....	103
5.55	Comparison of Strain Change “Vertically” on Capital During Superstructure Erection: Core Near Outside Face of "Y" .....	104
5.56	Comparison of Strain Change “Vertically” on Capital During Superstructure Erection: Shell Near Outside Face of "Y" .....	105
5.57	Strain Change Near Top of Shaft Measured During Superstructure Erection .....	108
5.58	Strain Change Near Mid-Height of Shaft Measured During Superstructure Erection.....	109
5.59	Comparison of Strain Change “Vertically” in Shaft During Construction of Superstructure.....	110
5.60	Comparison of Strain Changes at Varying Distances from the Transverse Centerline of the Pier During Superstructure Construction (C107, C108).....	111
5.61	Comparison of Strain Changes at Varying Distances from the Transverse Centerline of the Pier During Superstructure Construction (C105).....	112
6.1	Strain Locations on Structural Steel Pipe.....	117
6.2	Strains Measured in Capital due to Superstructure Dead Load: Thermal Strains Extracted .....	118
6.3	Strain Distribution Across Each Section of the Capital: Thermal Strains Extracted .....	119
6.4	Strains Measured in the Shaft due to Superstructure Dead Load: Thermal Strains Extracted .....	120
6.5	Basic Force Path in the US 183 Mainlane Piers .....	124
6.6	Calculation of the Orientation of the Compression Strut in the Capital Based on Measured Compressive Centroids.....	126
6.7	Comparison of Measured Forces and Strut-and-Tie Model Forces.....	129

# CHAPTER 1

## INTRODUCTION

### 1.1 Introduction

Construction of the US 183 Elevated highway in Austin provided a unique opportunity to investigate the behavior of a post-tensioned segmental box girder bridge with innovative strut-and-tie type pier substructures. The behavior of this elevated highway was monitored through extensive field instrumentation of portions of the superstructure and substructure. Funding for this project was provided by the Texas Department of Transportation in conjunction with the Federal Highway Administration.

Research presented in this thesis focuses on the behavior of the innovative cast in situ reinforced concrete piers used to support the mainlanes of the precast segmental reinforced concrete superstructure. Other reports from this project will focus on the superstructure and on precast segmental post-tensioned piers.

The purpose of this chapter is to present an overview of the US 183 Elevated Project, including a detailed description of the pier studied. The problem statement, objectives, and scope of work of the project are also included in this chapter.

### 1.2 US 183 Project Description

US 183 currently carries 6 lanes of traffic along the northern perimeter of Austin, as depicted in Figure 1.1. These lanes will serve as frontage roads for the elevated portion currently under construction. The US 183 Elevated Project consists of two phases as shown in the shaded areas in Figure 1.1. The main traffic lanes of this project consist of twin viaducts which are precast segmental box girders. One nearly completed viaduct is shown in Figure 1.2. The superstructure is supported by innovative and aesthetically pleasing reinforced concrete piers, which are the focus of this thesis.

### 1.3 US 183 Mainlane Pier Description

The piers for the mainlane portion of US 183 Elevated are attractive “Y-shaped” reinforced concrete piers with structural steel tension ties across the top of the “Y”, as



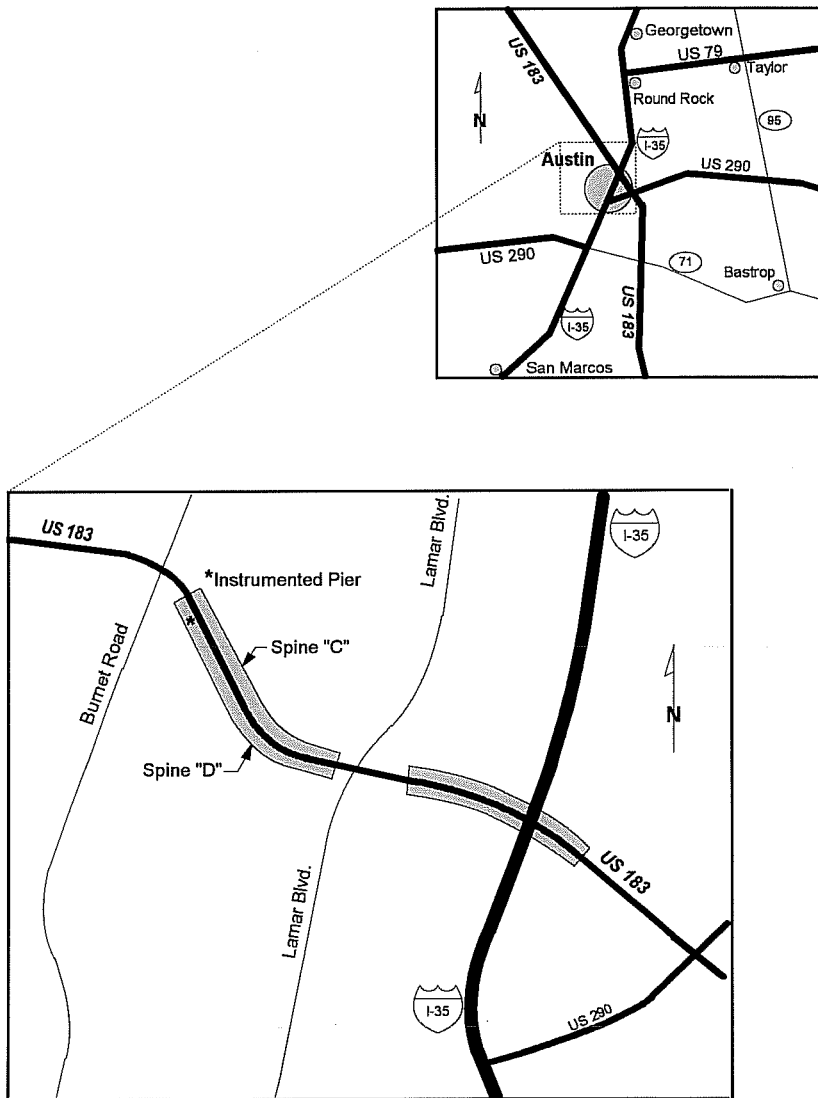


**Figure 1.1 - Location Map**





**Figure 1. 2 - Photograph of US 183 Viaduct**

shown in Figure 1.3 and in Figure 1.4. The shaft of the piers is of variable height, “H”. The capital has a constant height of 3200 mm (10’-6”). The structural steel pipes are AASHTO Extra Strong M270 steel and are 203 mm (8”) in diameter. The pipes are anchored in the concrete by steel plates at two locations as seen in Figure 1.5.

#### **1.4 Problem Statement and Objectives**

The US 183 mainlane piers were designed using strut-and-tie modeling (STM). This is a design method that is generally not taught in universities in the United States (USA) as a standard method for reinforced concrete design. However, interest in the use of STM in design is increasing in the USA. Since this type of modeling was only recently mentioned in USA codes, many engineers are unfamiliar with its possible uses and benefits. The research performed on the US 183 mainlane piers will be used to further evaluate the use of STM for reinforced concrete design and to familiarize designers with the concept of STM and its possible uses. Since STM is a plasticity based concept for ultimate limit state design, it has a limited capability to detect compatibility and constraint induced stresses. Therefore, the possibility of thermal induced deformations was investigated.

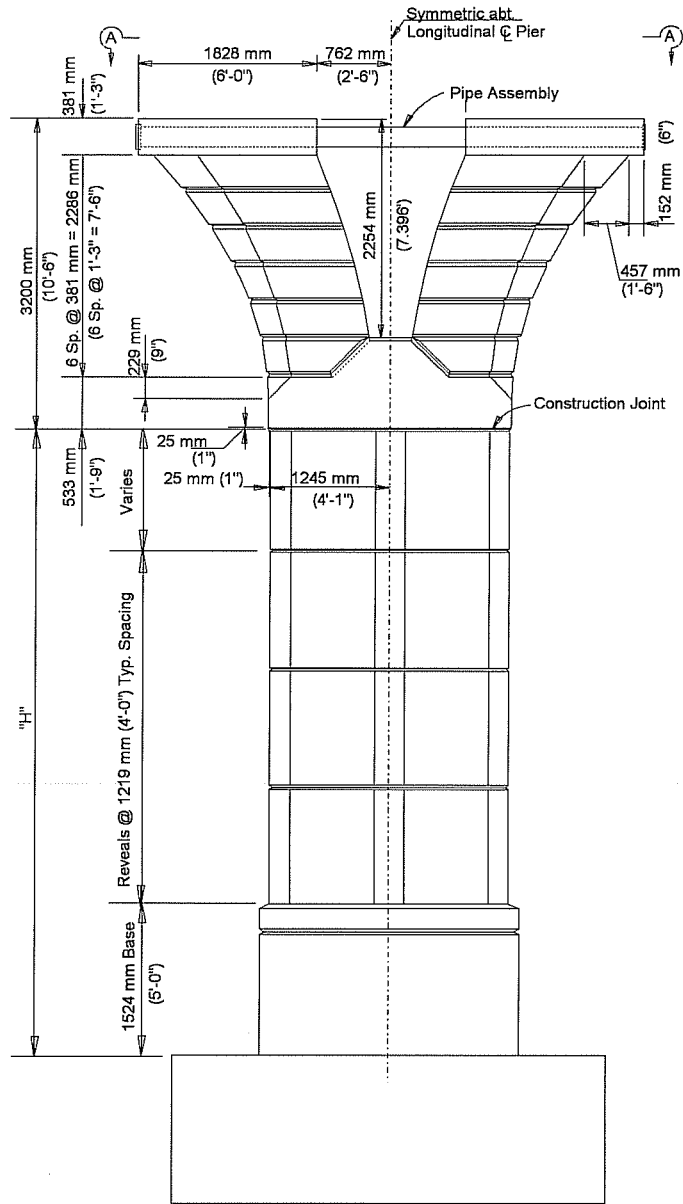


**Figure 1. 3 - US 183 Mainlane Pier: Elevation View**

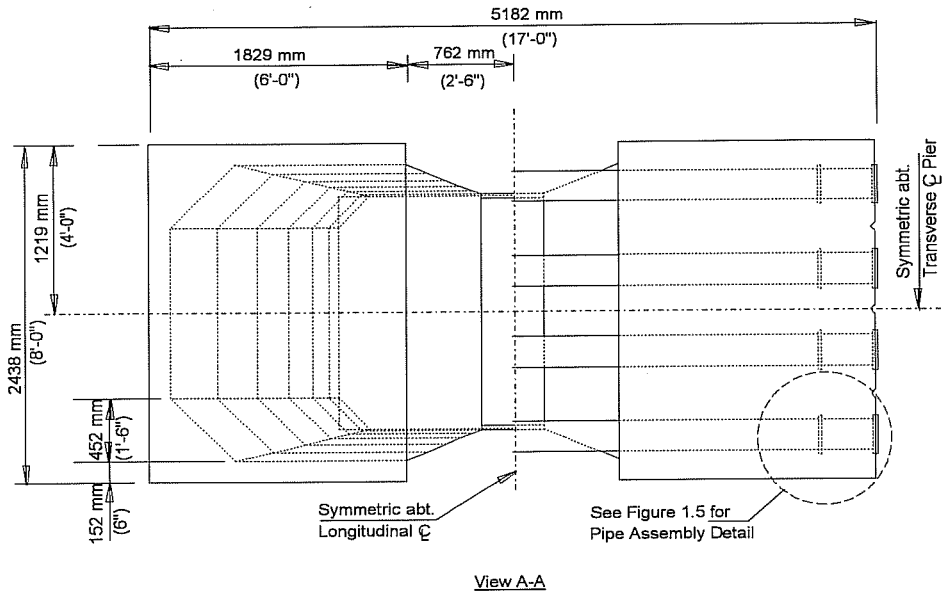


**Figure 1. 4 - US 183 Mainlane Pier: Plan View**

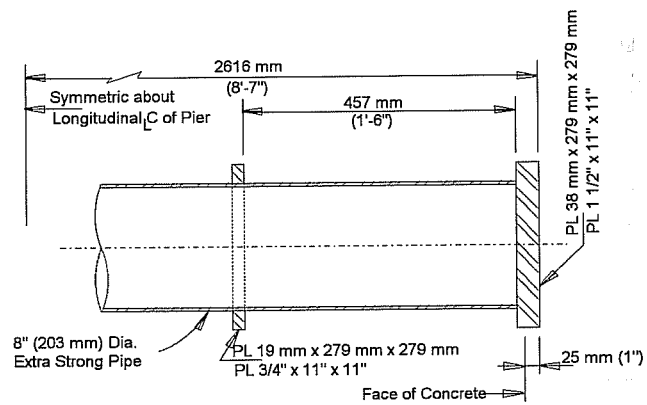


**Figure 1. 5 - Structural Steel Pipe Assembly: Detail**

The objectives of this project are as follows:

1. to instrument a US 183 mainlane pier in order to measure force distribution and thermal gradients through the pier;
2. to develop a strut-and-tie model of the pier in order to evaluate the use of STM for structural concrete design;
3. to compare measured force distributions with those predicted by strut-and-tie modeling; and
4. to make any indicated recommendations for additions or changes to bridge design and construction regulations.

### **1.5 Scope of Work**

The scope of work for this project included selection and extensive field instrumentation of a single mainlane pier. Construction and service load deformations were measured to determine force distribution throughout the pier. A detailed strut-and-tie model was used to compare analytical values with experimentally determined force distributions in order to further investigate the validity of STM for reinforced concrete design. Thermal gradients across the steel tension ties were monitored to identify additional forces induced in the pier due to this gradient.

## **CHAPTER 2**

### **BACKGROUND**

#### **2.1 Introduction**

The purpose of this chapter is to present background information. A literature review of previous bridge studies is discussed. The significance of the US 183 mainlane bridge pier study is presented. A description of strut-and-tie modeling and procedures for development of strut-and-tie models are presented.

#### **2.2 Previous Bridge Pier Studies**

Previous research pertaining to overall load distribution throughout all components of a bridge and general behavior of bridge piers is minimal. Most previous load distribution studies have focused exclusively on distribution among the various superstructure elements. The study of load transfer between girders and similar studies are examples of this trend.

Bridge pier design in most state departments of transportation has become highly standardized. Designs for piers that have worked in the past are often used, and many states minimize creativity in this area of bridge design as a means of minimizing cost. Piers are very conservatively designed, and minimum reinforcement ratios tend to govern. Due to these circumstances, structural problems with bridge piers do not often arise. Consequently, research in this area is lacking.

The US 183 mainlane bridge piers are not typical highway bridge piers. They are functional and are also innovative and aesthetically pleasing, as shown in Figure 2.1. As such, they provide an opportunity to investigate behavior of non-standard bridge substructures.

Through their form, these piers provide a visual representation of their structural behavior. Most observers will intuitively realize that as vertical load is placed on the bearings, the “Y” will tend to “spread apart”, placing the steel members across the “Y” into tension. Although this behavior is intuitive, detailing and dimensioning involved in the pier design may be quite difficult.

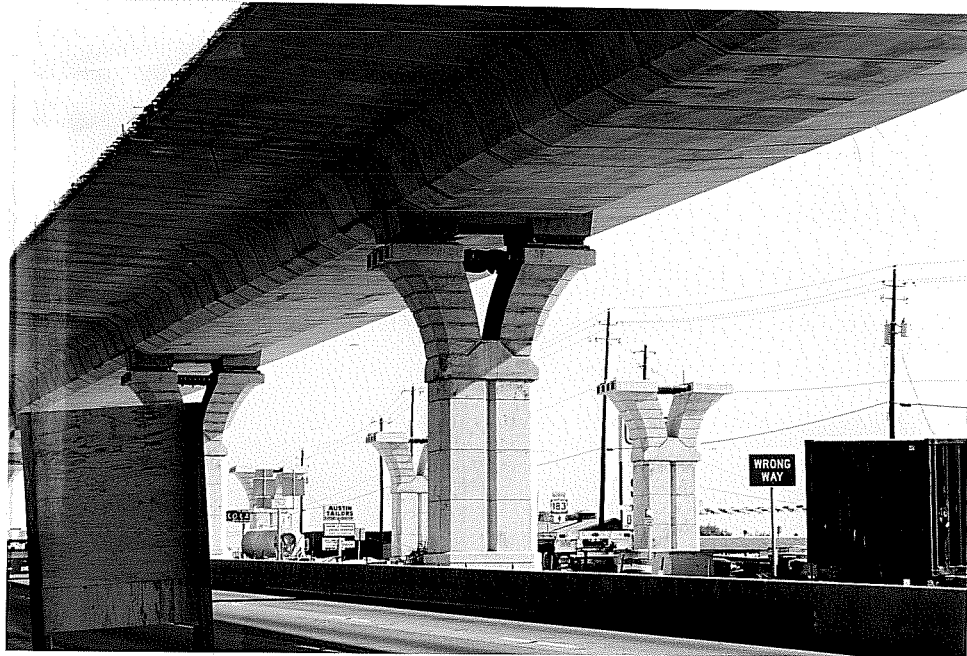


**Figure 2.1 - US 183 Mainlane Pier**

Structural failures have shown that detailing and dimensioning of structural concrete are of utmost importance to the integrity of a structure [1]. This is especially true in areas where geometric discontinuities and concentrated loads occur. However, no consistent method for detailing structural concrete is codified in the US. Most detailing recommendations included in codes do not provide a conceptual model to aid the engineer in visualizing behavior. In order to insure structural integrity, the engineer's focus must be redirected to the flow of forces and overall structural behavior. The introduction of rational, transparent models could greatly improve detailing [1].

Since the US 183 mainlane pier was accessible for instrumentation purposes during construction, researchers had the opportunity to measure deformations and deduce the flow of forces through the pier. Once obtained, these forces could be compared to forces predicted by a strut-and-tie model of the pier to evaluate the use of strut-and-tie modeling for design of structural concrete.

## 2.3 Strut-and-Tie Modeling

The US 183 mainlane pier was designed using strut-and-tie modeling. This is a design method that uses compression struts, tension ties, and interconnecting nodes to model the equilibrium state of a structure at ultimate load. Strut-and-tie modeling allows the designer to visualize the main structural action by tracing the flow of forces through a structure.

### 2.3.1 *General*

As previously stated, strut-and-tie modeling utilizes struts, ties, and nodes to idealize the flow of forces through a structure. Struts represent the flow of compressive forces through three dimensional (3-D) stress fields in the concrete. Ties represent the flow of tensile forces provided by reinforcement or concrete tensile strength. For practical design purposes, concrete tensile strength is neglected. Nodes link the strut and tie forces together, and must be in equilibrium.

Strut-and-tie modeling provides a rational framework for a detailing method that can be applied to a variety of structural components [2]. With strut-and-tie models, the stress distribution is idealized as a static force system. Forces in the struts and ties are calculated and then used to evaluate compressive stresses in the concrete and to proportion the reinforcement [3]. Although a full study of strut-and-tie modeling is beyond the scope of this research, the following discussion is provided as background information.

### 2.3.2 *History*

Strut-and-tie modeling can trace its origin to 1899 with William Ritter's introduction of the truss model for shear design of reinforced concrete beams and Morsch's introduction of the truss analogy for design of web reinforcement in 1902. Strut-and-tie modeling is a generalized application of the truss analogy. Marti and Mueller created strut-and-tie model's scientific basis for a rational application working with Thürliman at the Swiss Federal Institute of Technology, using the theory of plasticity [4]. Leonhardt had advanced the practical use of STM at the University of Stuttgart and in his consulting practice [5]. Schlaich further developed STM as a consistent method by which structural concrete can be designed. His landmark PCI Journal paper was the first major introduction

of STM into US literature [4]. A thorough history of strut-and-tie modeling can be found in Bergmeister [2].

Truss models for beams and STM for discontinuity regions are seen as attractive alternatives to empirical approaches for detailing structural concrete because of their transparency and adaptability to many design situations [2]. Strut-and-tie modeling is particularly useful for irregularly shaped zones and areas subject to high concentrated loads. Typical uses for strut-and-tie modeling include the design of corbels, deep beams, and walls with openings as shown in Figure 2.2. Strut-and-tie modeling is also frequently used in segmental bridge design in anchorage zones and deviator blocks.

Although strut-and-tie modeling is used in the situations listed above, it is by no means a widely used design method in the US. This may be attributed to the background of most US engineers. Section analysis is emphasized in US universities, and engineers therefore become comfortable and familiar with this type of analysis. While section analysis is very useful in many situations, it is not sufficient for detailing structural concrete in unusual circumstances where stress concentrations occur. Section analysis does not force an engineer to focus on the overall behavior of a structure. When unique conditions occur, lack of a consistent design method for all portions of a structure may cause problems.

US codes, other than the 1989 AASHTO Design Specification for Design and Construction of Segmental Concrete Bridges [6] and the 1994 AASHTO LRFD Bridge Design Specifications [7] do not currently contain a consistent design method for detailing and dimensioning structural concrete in areas of geometric discontinuity or areas where strain distribution becomes disturbed. This forces the designer to rely on empirical procedures, rules of thumb, and guess-work when dealing with these situations.

The ACI 318-89 Building Code Requirements [8] contains no information on strut-and-tie modeling. The AASHTO Specifications previously mentioned contain information concerning where the use of strut-and-tie modeling may be appropriate. These codes also contain some design examples. However, no consistent guidelines exist through which a designer can learn and apply strut-and-tie modeling.



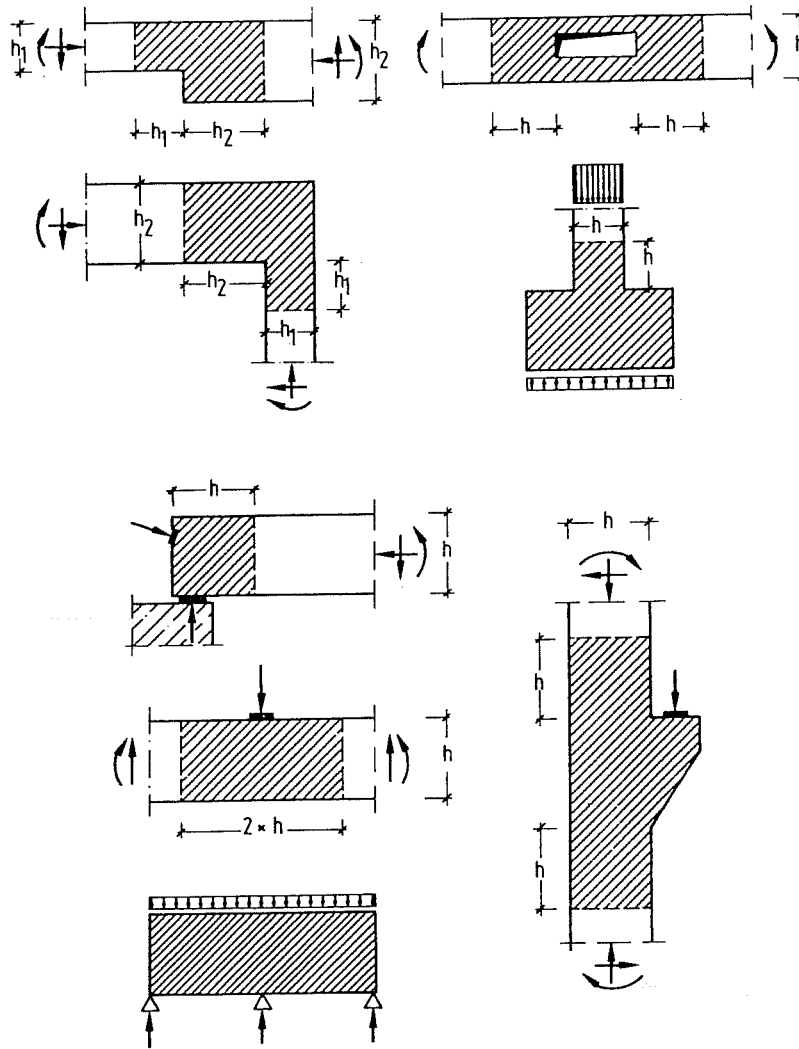


Figure 2.2 - Typical Uses of Strut-and-Tie Models [4]

### 2.3.3 Assumptions

The most important assumptions of which a designer should be aware when using strut-and-tie models are the following [2]:

1. Failure coincides with the formation of a mechanism caused by yielding of one or more of the ties.
2. Crushing of the concrete struts should not occur prior to yielding of the ties. Crushing is prevented by limiting the stress levels in the concrete.
3. All forces in the struts and ties are assumed as uniaxial.
4. All external loads are applied at the nodes of the strut-and-tie model. The model must be adequately formulated to realistically represent the load distribution when distributed loads are present.
5. Reinforcement must be detailed properly in order to prevent local bond or anchorage failure.

Also important is the adherence of strut-and-tie modeling to the lower bound theorem of the theory of plasticity. The lower bound theorem states that a load system which does not violate the yield condition and is based on a statically allowable stress field is a lower bound of the ultimate load. Equilibrium equations and statical boundary conditions must be satisfied by the statically allowable stress distribution. The lower bound theorem will be conservative in all cases [2].

### 2.3.4 Development of a Strut-and-Tie Model

#### 2.3.4.1 B-regions and D-regions

In order to apply the strut-and-tie modeling procedure to a structure, Schlaich [4] suggests dividing the structure into B-regions and D-regions. B-regions are those areas of a structure in which the Bernoulli hypothesis of plane strain distribution is assumed valid. D-regions are areas of a structure where strain distribution becomes *d*isturbed; near concentrated loads, corners, and openings [4].

The size of D-regions can be estimated by using the principle of St. Venant. Stress distribution varies from nominal in regions of stress concentrations. St. Venant's principle states these localized effects disappear at some distance from the point of application of the load [9]. This distance is shown as "h" in Figure 2.3. As depicted by Figure 2.3, a load on

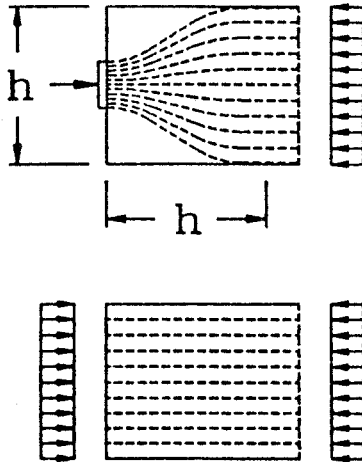


**Figure 2.3 - St. Venant's Principle [3]**

a structure can be replaced by a set of statically equivalent loads without changing the state of stress in the structure beyond the distance in which localized effects disappear. This distance is approximately equal to the distance between the statically equivalent applied loads [3].

#### 2.3.4.2 Layout of Struts and Ties

Two recommended methods exist for determining the orientation of struts and ties [4]. These are the load path method and the elasticity analysis method. The load path method can be easily used for structures in which the flow of forces is intuitive or known from previous experience. The elasticity analysis method is normally used in structures with very unusual configurations, where the flow of forces is not intuitive.

In the load path method, the outer equilibrium of the D-regions are determined. Once a structure has been divided into B- and D-regions, the forces in the B-regions can be found from flexural theory. The outer forces acting on a D-region are then the externally applied loads as well as these newly determined internal forces at the boundary between the

B- and D-regions. Strut-and-tie models can be developed to determine the load paths in the D-region. A detailed approach for the load path method can be found in Bergmeister [2].

With the elasticity analysis method, the strut-and-tie model is based on the principal stress pattern as determined from an elastic analysis. An elastic finite element program may be used for unusual cases. The struts and ties are then located at the center of gravity of the corresponding stress fields [2].

There is no unique solution for a given structural problem. While developing and subsequently evaluating a strut-and-tie model, a designer should be aware that loads will tend to use the path of least resistance, or the path with the least forces and deformations. Therefore, the model with the least and shortest ties is the best since the steel ties are much more deformable than the concrete struts [4].

### 2.3.5 Struts

Compression forces are transferred from node to node through struts. Three basic strut types are suggested for use by Schlaich [4]. These are the “prism”, the “fan”, and the “bottle” struts as shown in Figure 2.4.

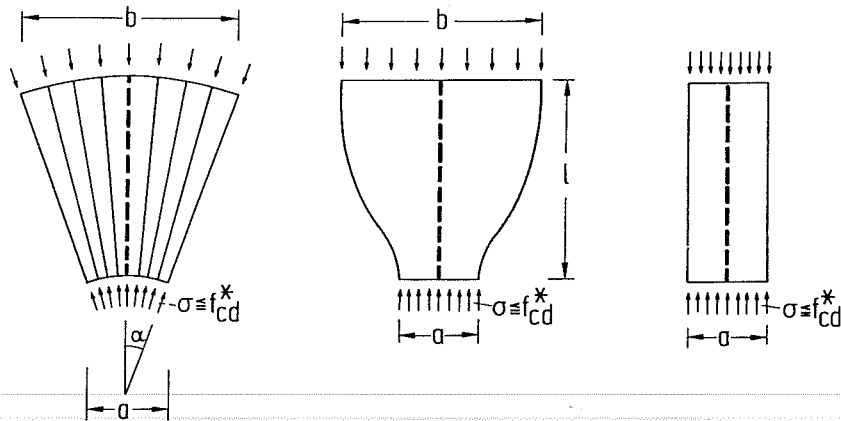


Figure 2.4 - Strut Types [4]

### 2.3.6 Ties

The ties of a strut-and-tie model are tension carrying members provided by reinforcing steel or concrete tensile strength. Reliance on concrete tensile strength for ties should be approached with caution since previous loading conditions, such as shrinkage or thermal loads, may reduce the tension carrying capacity of the concrete. For most practical cases, concrete tensile strength is ignored.

Once the orientation of the ties is determined and forces in the ties are calculated from equilibrium analysis, reinforcing steel can be proportioned. The following relationship is used for this purpose:

$$T_n = A_s f_y$$

where

$A_s$  = the area of steel reinforcement

$f_y$  = the yield stress of the steel

Tie forces are usually resisted by placing the reinforcement symmetrically along the entire length of the tie and about the line of action of the force. Proper anchorage for the reinforcement at the nodes should be provided. Reinforcement should be provided such that the bars will just reach yield at ultimate load. Yielding of the reinforcing bars must occur prior to the crushing of the concrete.

In addition to proportioning reinforcement to resist the tie force, special attention should be given to assuring that brittle failures, such as stability failures, are precluded. To ensure satisfactory performance at service load levels, crack control reinforcement should supplement that required by strut-and-tie modeling. This additional reinforcement is not critical in terms of ultimate capacity as long as adequate reinforcement is provided for the primary load path [3].

### 2.3.7 Nodes

Nodes are defined as the intersection points of three or more straight struts or ties [4]. They are points where forces change direction. The strut and tie forces that meet at a node must be balanced in equilibrium at the node. If the deviation of forces at a node is locally concentrated and the node is small, the node is referred to as a “singular node”.

Where stress fields joined by the node are large, the node is referred to as a “smeared node”. Nodes are further classified depending on the type of elements they connect. The classifications are [2]:

CCC: Compression-Compression-Compression

CCT: Compression-Compression-Tension

CTT: Compression-Tension-Tension

TTT: Tension-Tension-Tension

Node dimensioning is limited by two constraints [2]:

1. The lines of action of struts, ties, and external loads must coincide.
2. The relative angles and widths of struts and ties restrict the geometry of the nodes.

The forces of a node balance each other in compression in most cases. An idealized tension tie, represented as a tie anchor, transfers load from “behind” the node. Detailed information on checking strength for various node types can be found in Schlaich [4] and Bergmeister [2].

### ***2.3.8 Summary of Design Procedure***

Bergmeister [2] presents a generalized design procedure for structural concrete based on the utilization of strut-and-tie models. This procedure is shown in Figure 2.5.

### ***2.3.9 Benefits of Strut-and-Tie Modeling***

Strut-and-tie modeling redirects the designer’s focus to overall structural behavior. The method is rational and transparent. It allows the engineer to visualize the flow of forces through a structure. It provides a consistent design approach for an entire structure and is adaptable to many situations. Proportioning of reinforcing steel is simple with the use of strut-and-tie modeling.

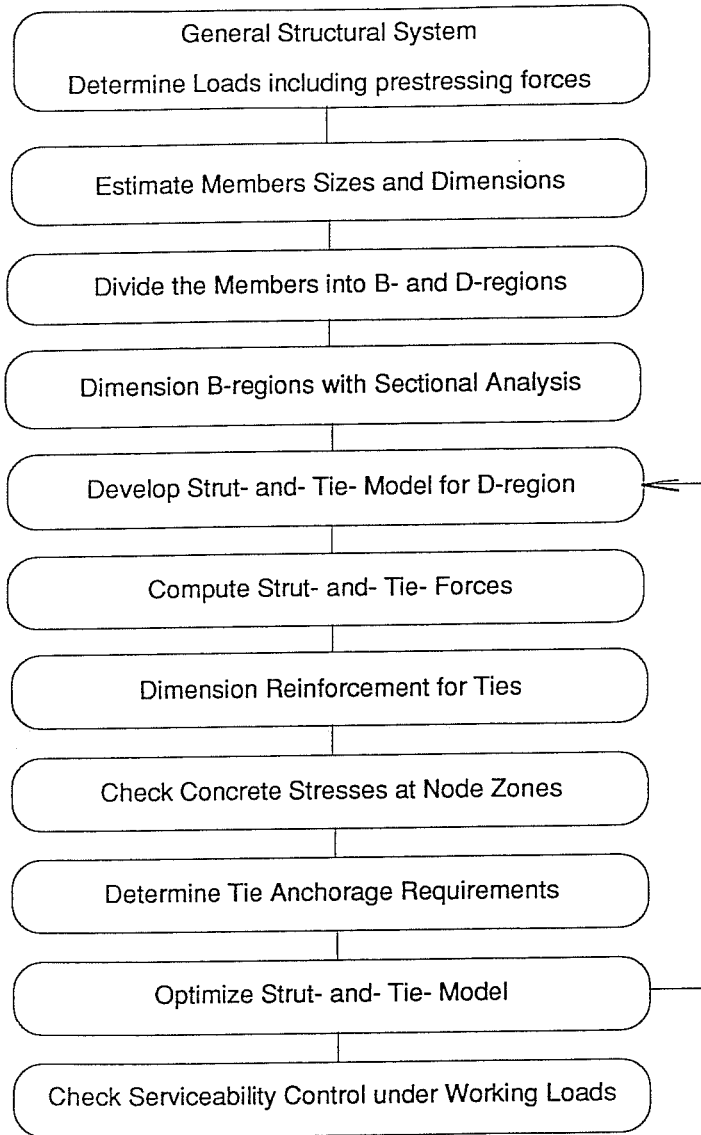


**Figure 2.5 - Design Procedure for Structural Concrete [2]**

Since STM is a lower bound plasticity model, it is conservative for design. STM is appropriate for design of structural concrete in areas where discontinuities occur because the behavior of the region in question is simplified into discrete load carrying members [4]. In summary, strut-and-tie modeling can lead to a better understanding of structural behavior. By providing a consistent method for detailing and dimensioning, STM can improve the integrity of concrete structures.

#### ***2.3.10 Limitations of Research***

The ultimate load of the US 183 mainlane pier could not be investigated in this study. The strut-and-tie model developed for research purposes is not the one used for pier design, which considered dead load, live loads, and wind loads. Since this study was limited to dead load conditions, a different STM was developed using dead loads only. The purpose of this STM was only to trace the flow of dead load forces through the pier in order to compare the model forces with forces deduced from field measurements.



## CHAPTER 3

### PIER INSTRUMENTATION

#### 3.1 Introduction

This chapter describes the instrumentation of the US 183 mainlane bridge pier. Instrumentation systems are discussed in detail. A description of the pier selection process is also discussed.

##### 3.1.1 Instrumentation Systems

In order to measure the transfer of forces through the pier and to investigate the effects of thermal gradient in the pier, the following measurements were determined to be of importance:

- steel strains
- concrete strains
- temperature gradient
- deformation of the “Y”

Systems were chosen based on previous studies performed by Arréllaga [10] and from previous experiences of Roberts [11] on the instrumentation of the San Antonio “Y” segmental box girders.

##### 3.1.2 Instrumented Pier

The selection of the instrumented pier was based on several criteria; (1) the contractor’s schedule, (2) the research schedule, and (3) the height of the pier. In order to avoid compromising the research schedule, a pier was chosen which was located at the beginning of the first construction phase of the project. The pier was also chosen such that its location coincided with the instrumentation of a portion of the superstructure. The height of the pier was kept to a minimum in order to provide an accessible and safe working environment.

Pier D6, which supports superstructure spans 5 and 6, was chosen for instrumentation. This pier is located as shown in Figure 1.1. The dimension “H”, as shown in Figure 1.3, for pier D6 is 4572 mm (15'-0”). Only one quadrant of the pier was instrumented since the final loading is symmetrical.

Background, application, and layout for all instrumentation systems are discussed in the following sections. Strain gage and concrete strain device locations are shown in Figure 3.1 - Figure 3.3 and in Figure 3.6. Demec point locations are shown in Figure 3.19 - Figure 3.21. Thermocouple locations are shown in Figure 3.4, Figure 3.21, and Figure 3.22.

### **3.2 Steel Strains - Strain Gages**

Electrical resistance strain gages were used to measure steel strains. These gages work based on a direct relationship between the change in length of the wire embedded in the gage and the change in electrical resistance of the wire as its length is changed due to stress. A complete description of the method of operation of electrical resistance strain gages may be found in Arréllaga [10].

#### ***3.2.1 Background***

A 350 ohm strain gage, as opposed to a standard 120 ohm strain gage, was chosen for measuring the reinforcing steel strain. The gage resistance was chosen so that the small strain variations expected could be read with accuracy. The signal to noise ratio is reduced with the use of a larger resistance strain gage [11]. The size of the gage was chosen so that the gage could be easily placed on small areas such as the rods used for the concrete strain devices discussed in Section 3.3.

#### ***3.2.2 Application***

Strain gages were bonded directly to the steel reinforcing cage of the pier and to the structural steel pipes at the construction site. Acrylic, rubber, and epoxy were layered on the gages in order to protect them from exposure to water and from damage due to vibration of the concrete.

### **3.2.3 Layout**

Strain gages were located on reinforcement in areas where tension was expected and on the structural steel pipes. The layout of strain gages is shown in Figure 3.1 - Figure 3.3. Strain gages are labeled with the designation "S".

## **3.3 Concrete Strains - Concrete Strain Devices**

A concrete strain device was manufactured in the laboratory in order to measure the strain in the concrete. The concrete strain device was selected to minimize the time required to place instruments in the field. Prefabrication of the devices in a controlled environment allowed for greater certainty that the strain gage would be protected against infiltration by water and against various construction procedures that are detrimental to the gages.

### **3.3.1 Background**

A detailed study of concrete strain measuring devices can be found in Arréllaga [10]. A concrete strain measuring device was developed for this instrumentation project based on the modified Mustran Cell [10] and on research performed by Stone [12]. This device basically consists of an electrical resistance strain gage mounted on a steel rod. The device is firmly anchored in the concrete by nuts and washers placed at each end of the steel rod.

### **3.3.2 Description and Application**

The concrete strain measuring device developed is shown in Figure 3.4. It consists of a 4.76 mm (3/16") diameter steel rod approximately 235 mm (9 1/4") long with an effective gage length of 203 mm (8"). A strain gage, as described in Section 3.2, was bonded to the rod in the center of the effective gage length. Acrylic was placed on the gage to protect it from moisture. Heat shrink tubing was then placed over the length of the rod.

A washer and two nuts were placed at each end of the rod to insure strain compatibility and to minimize the inclusion effect. A series of tests were performed. The shortest gage length producing acceptable strain measurements was selected.

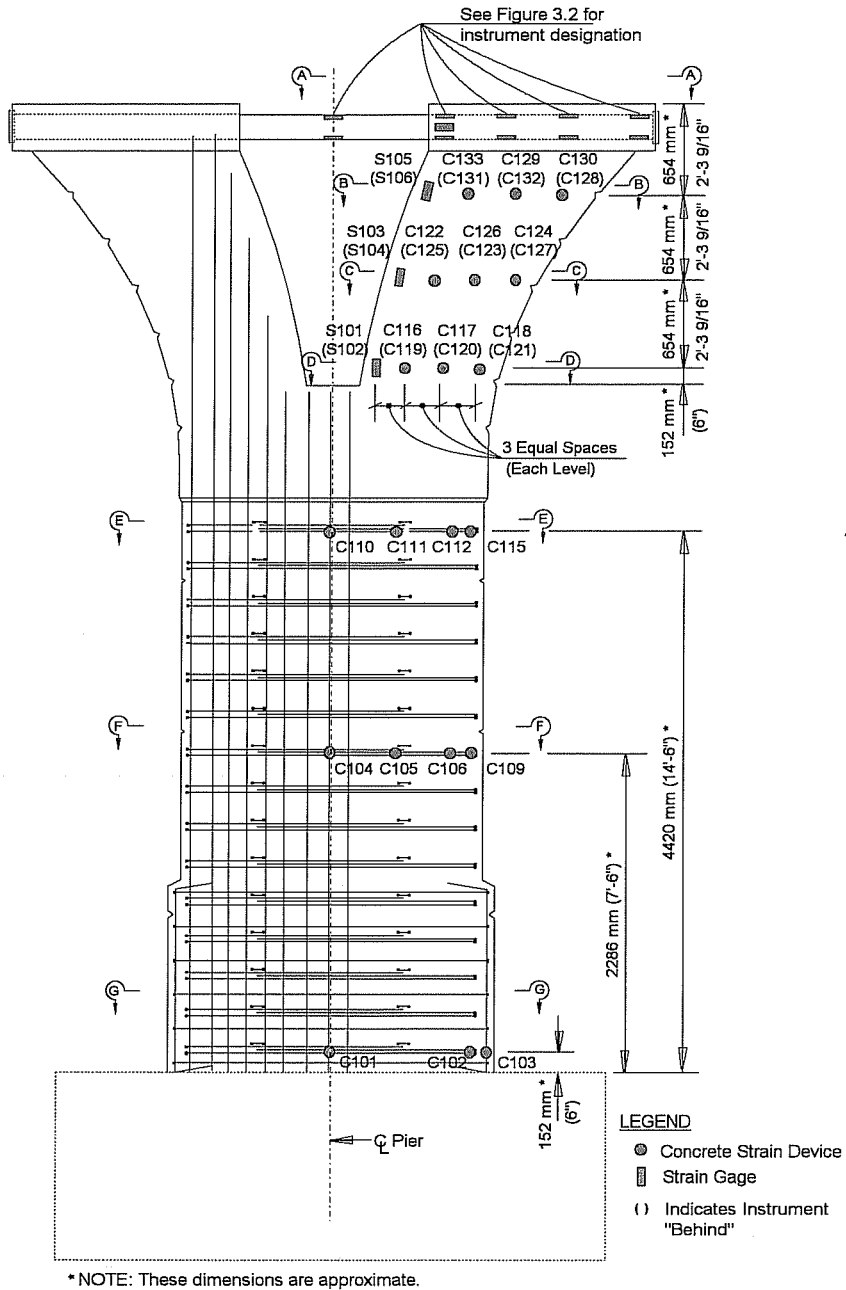
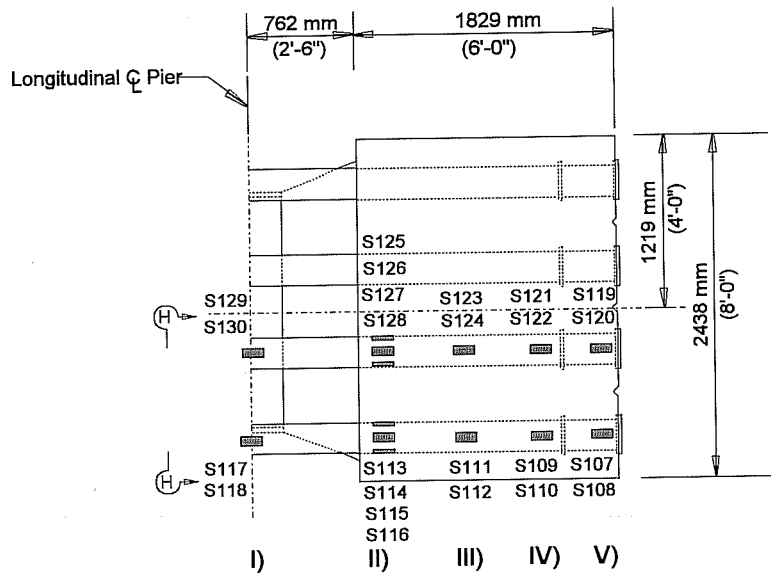
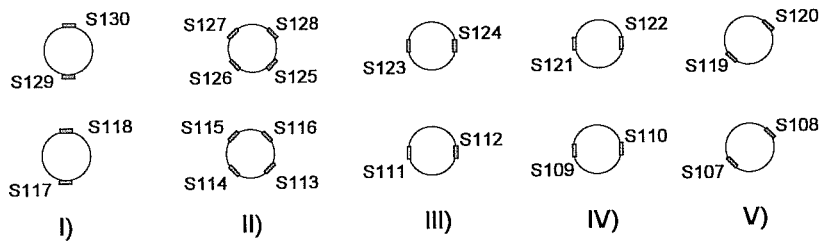


**Figure 3.1- Strain Gage and Concrete Strain Device Layout: Elevation View**



Plan View of Capital



Section H-H

**Figure 3.2 - Strain Gage Locations: Pipe Assembly**

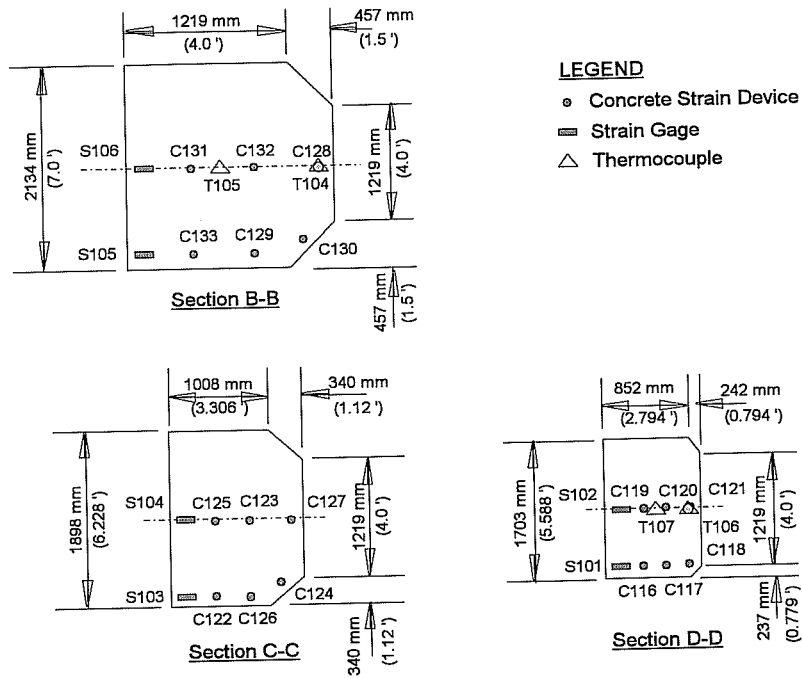


Figure 3.3 - Strain Gage and Concrete Strain Device Layout: Sections

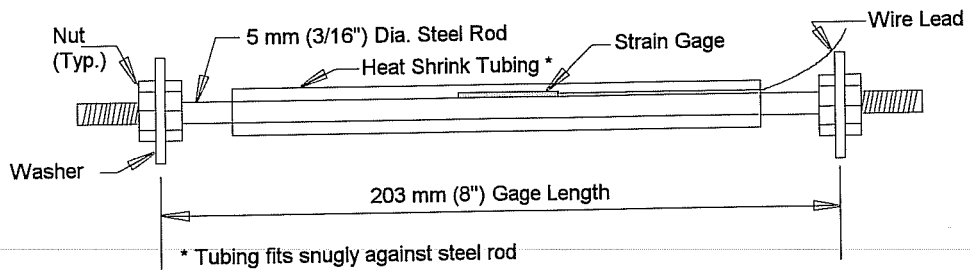


Figure 3.4 - Concrete Strain Device

For placement in the field, the devices were secured between two pieces of welded wire fabric for placement in the reinforcing cage, as shown in Figure 3.5. The wire cage allowed for ease of placement and greater options for placement. It also served to protect the instrument from the vibrator during casting and from adjustments to the reinforcing cage prior to concrete placement. Electrical wires were routed up reinforcing steel to the top of the pier.

### ***3.3.3 Layout***

The locations for concrete strain devices are shown in Figure 3.1, Figure 3.3, and Figure 3.6. Concrete strain devices are labeled with the designation “C”.

### ***3.3.4 Device Selection Procedure***

Strain compatibility was provided by careful selection of the material for the shaft of the device. Both the coefficient of thermal expansion and Young’s Modulus of the shaft material were considered. Steel was selected as the optimum material. The thermal coefficients of expansion of steel and concrete are similar. Strain compatibility is maintained if the device is firmly anchored in the concrete at each end of the gage.

Minimizing inclusion effects was an important consideration when developing the concrete strain measuring device. An inclusion effect is a disturbance of the strain field in a material due to the presence of an object of differing material, such as a strain measuring device. This effect is related directly to the relative stiffness of the materials being considered and to the geometry of the inclusion. The magnitude of error in the output of the strain measuring device is dependent on the length to width ratio of the device [10]. The axial stiffness of the device was optimized to minimize inclusion effects. The smallest diameter rod on which a strain gage could be easily placed was chosen.

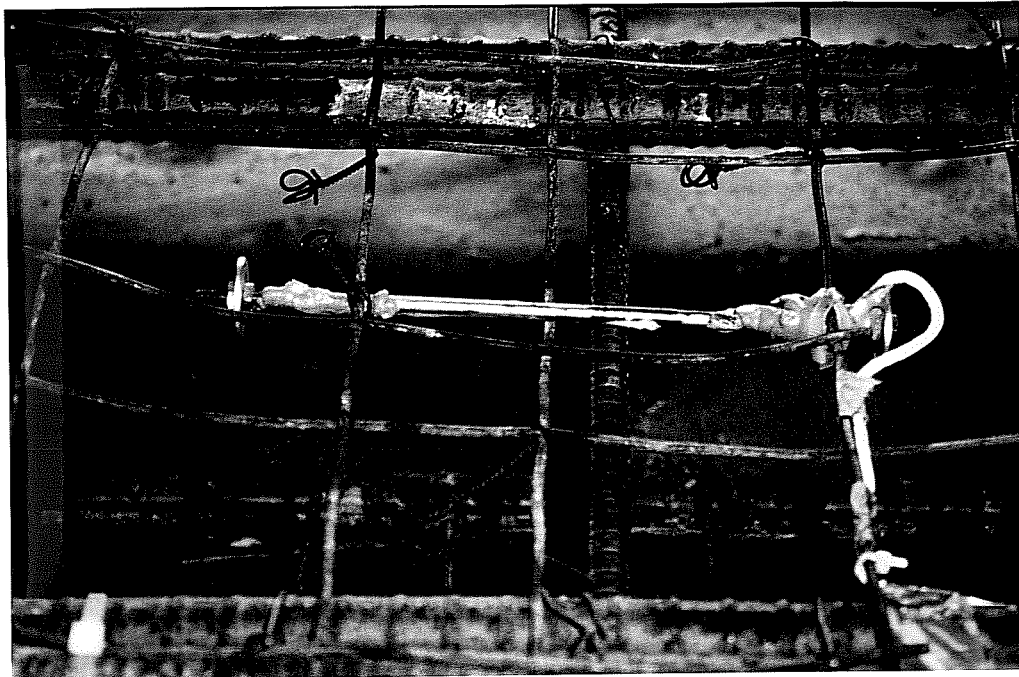


**Figure 3.5 - Photograph of Concrete Strain Device**

A testing procedure was performed in order to develop the concrete strain measuring device. The goals of these tests were to develop an instrument that would provide easy installation, minimize inclusion effects, and give accurate and consistent results. Preliminary tests were performed on 102 mm (4"), 152 mm (6"), and 203 mm (8") devices. Based on handling ease, the 102 mm (4") and 152 mm (6") devices were eliminated as options. Final tests were performed on the 203 mm (8") device.

#### 3.3.4.1 Test Set-Up

Three identical concrete specimens were prepared for testing the 203 mm (8") device. A typical test specimen is shown in Figure 3.7. A 203 mm (8") device was placed in the center of each of the concrete specimens with the lead-wire exiting the concrete at the top of the specimen. These wires were connected to a Campbell 21X Datalogger [13] for electronic monitoring. One set of Demec extensometer points was placed on each face of the specimen using the modified installation method as depicted in Figure 3.17.



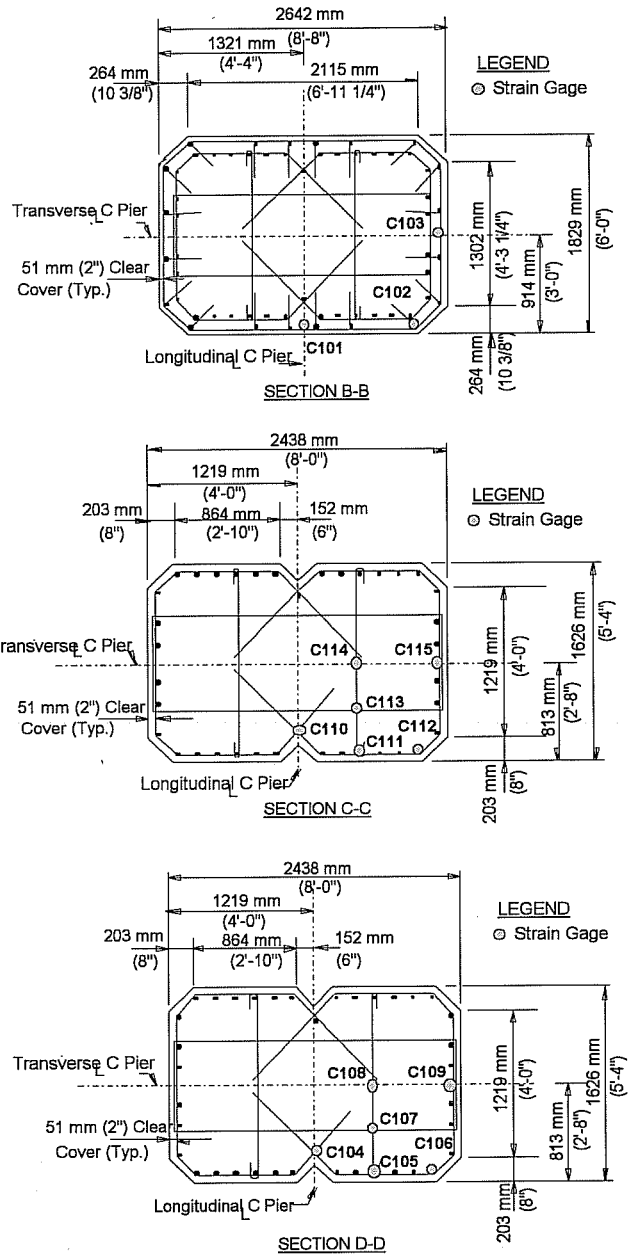


**Figure 3.6 - Concrete Strain Device Locations in Shaft**

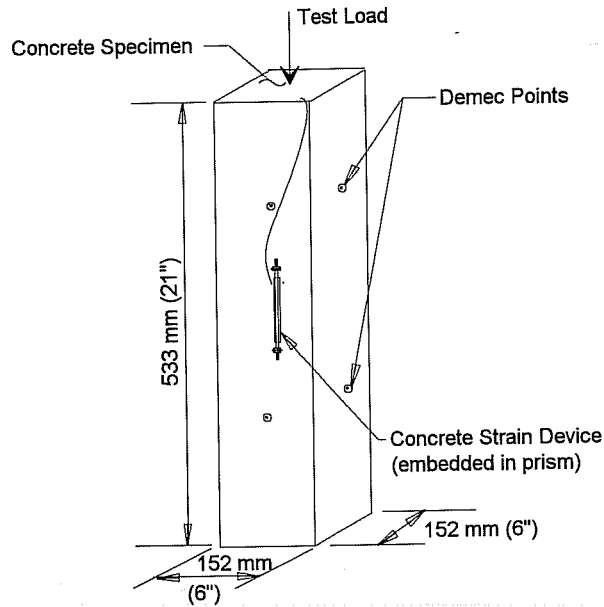


**Figure 3.7 - Concrete Strain Device Test Specimen**

#### 3.3.4.2 Testing Procedure

A test consisted of axially loading the specimen in a hydraulic testing machine. The specimen was loaded in 44.48 kN (10 kip) increments to a maximum load of 222.4 kN (50 kips). While the specimen was loaded, concrete strain device readings were taken electronically with the data acquisition system. External concrete strains were measured using the Demec extensometer on all four faces of the specimen at each 44.48 kN (10 kip) load increment. Two tests were performed on each specimen.

### 3.3.4.3 Results

The readings obtained from the concrete strain device correlated well with the Demec readings as shown in Figure 3.8 - Figure 3.13.

#### Test 1

Figure 3.8 through Figure 3.10 represent the first tests performed on the specimens. The results from the Demec extensometer for Specimen Nos. 1 and 2 do not align well with the Campbell datalogger readings from the concrete strain devices. The linear stress-strain behavior provided by the electronic readings indicate more credible behavior. The erratic behavior of the Demec readings in this first test may be due to crushing of the concrete around the outermost edges of the specimen as load was applied. Results from Specimen No. 3 show no indication of this behavior and the readings correlate well with a 1.3 % difference. The maximum difference occurs in Specimen No. 2 and is 6.7 %.

#### Test 2

Figure 3.11 - Figure 3.13 represent the second tests performed on the specimens. Results for Specimen No. 1 indicate a maximum difference of 12 %. A maximum strain of approximately 0.000315 mm/mm (0.000315 in/in) was maintained throughout Tests 1 and 2 for all specimens. However, the maximum strain given by the Demec readings for Specimen No. 1, Test 2, is much greater than 0.000315 mm/mm (0.000315 in/in).

The Demec output for this specimen was again not linear. Performance of the Demec points in Specimen No. 1 is questionable. Specimen Nos. 2 and 3 give close results between the two measurement systems, with a maximum difference of 5 %.

A side-by-side comparison of all devices from each test is shown in Figure 3.14 and Figure 3.15. These results indicate that the 203 mm (8") concrete strain devices give consistent results and acceptable strain measurement error.

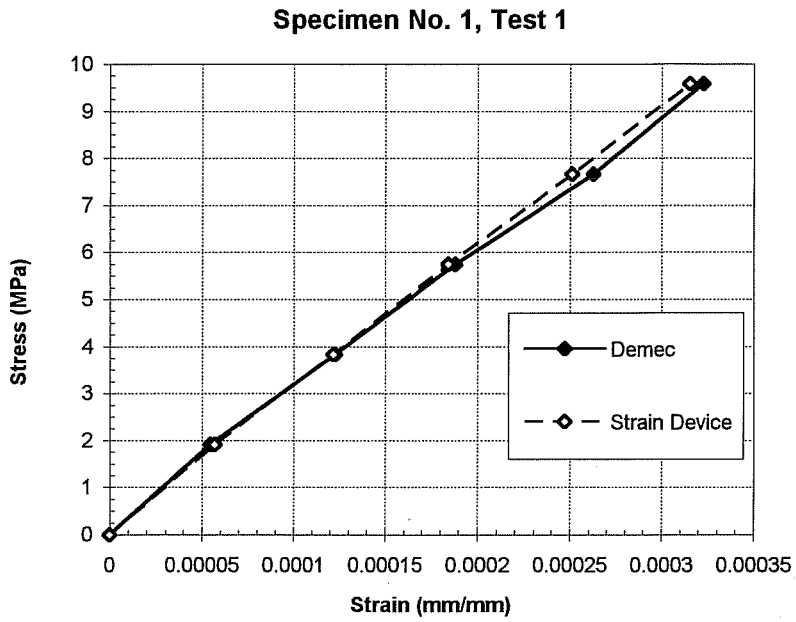


**Figure 3.8 - Comparison of Results; Specimen No. 1, Test 1**

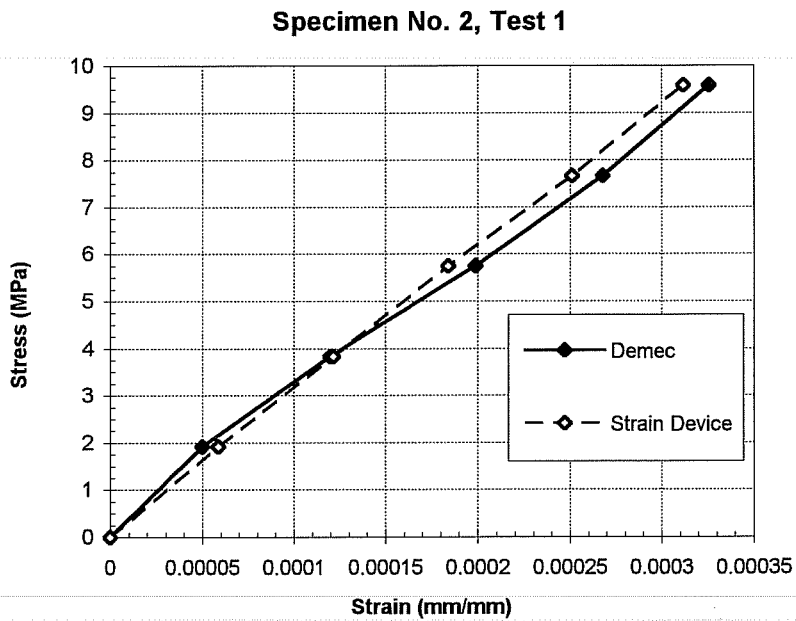


**Figure 3.9 - Comparison of Results; Specimen No. 2 Test 1**

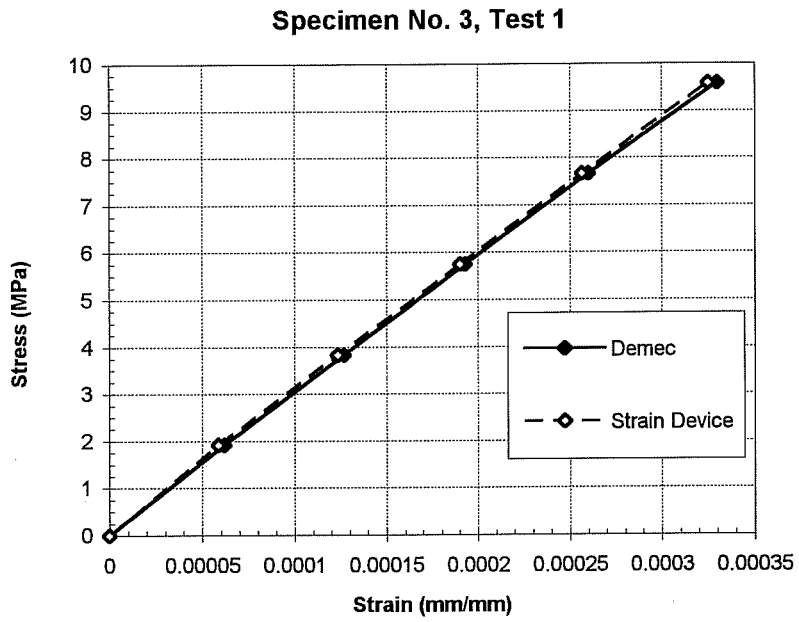


Figure 3.10 - Comparison of Results; Specimen No. 3, Test 1

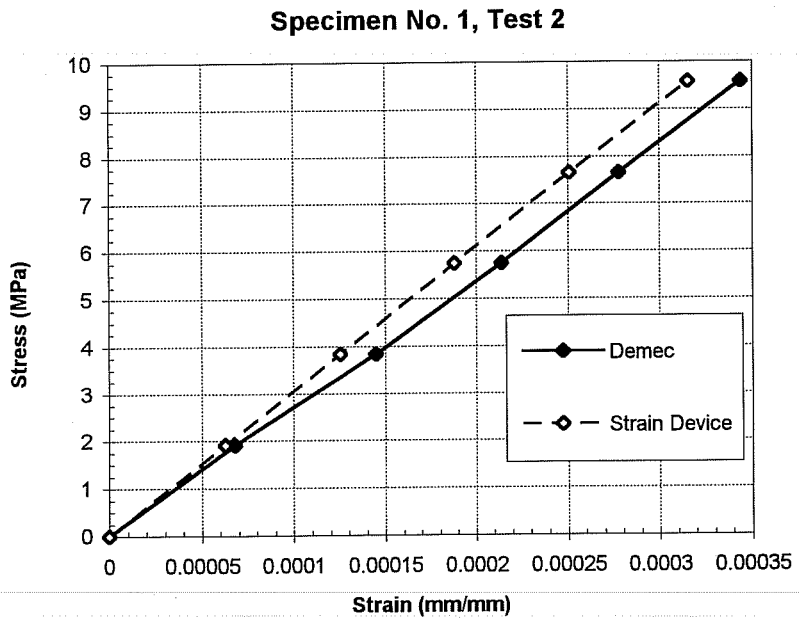
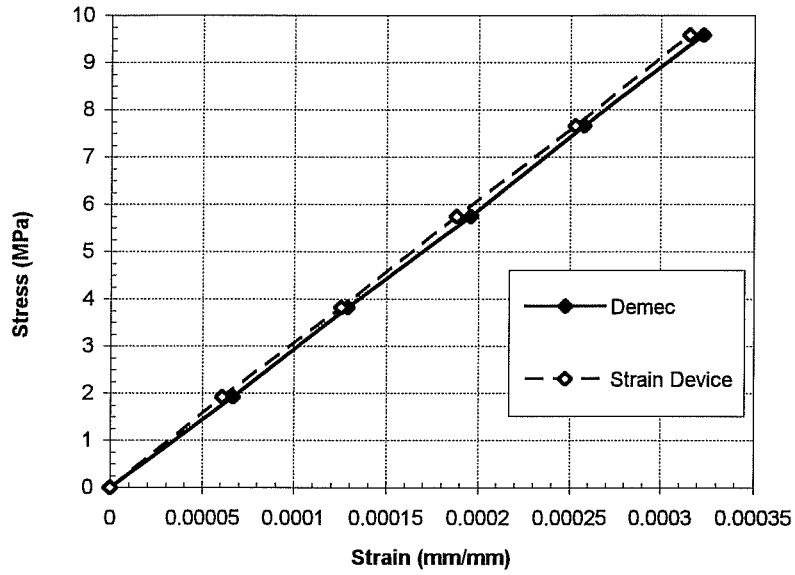


Figure 3.11 - Comparison of Results; Specimen No. 1, Test 2

**Specimen No. 2, Test 2**



**Figure 3.12 - Comparison of Results; Specimen No. 2, Test 2**

**Specimen No. 3, Test 2**

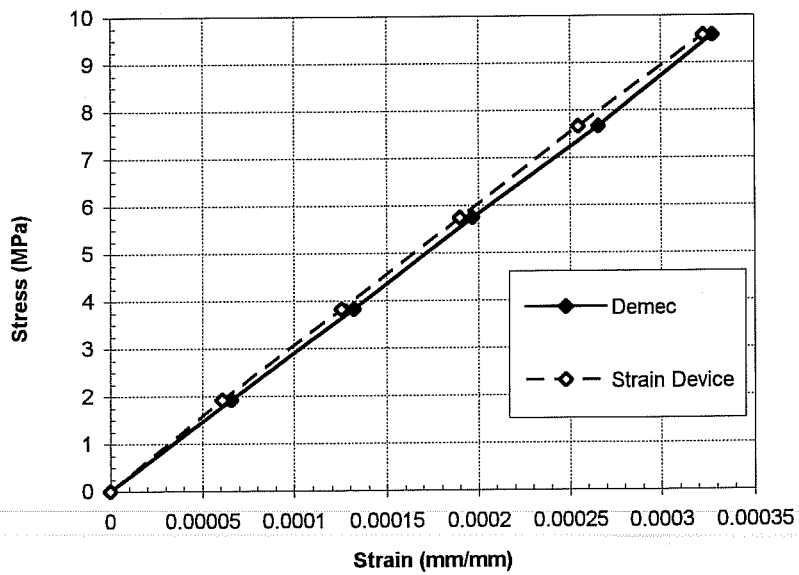


**Figure 3.13 - Comparison of Results; Specimen No. 3, Test 2**

**8" Strain Devices - Test 1  
Side-by-Side Comparison**

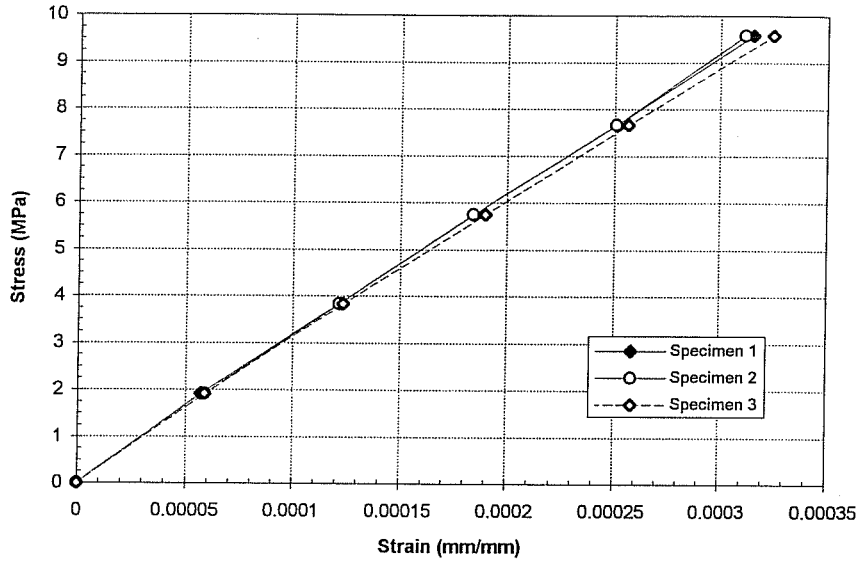


**Figure 3.14 - Side-by-Side Comparison for Test 1**

**8" Strain Devices - Test 2  
Side-by-Side Comparison**

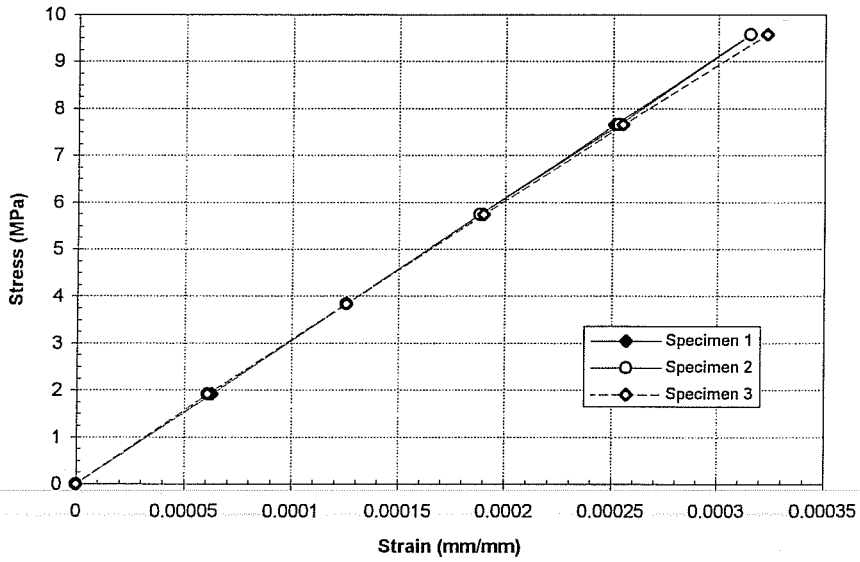


**Figure 3.15 - Side-by-Side Comparison for Test 2**

### 3.4 Concrete Strains - Demec Extensometer

A mechanical device known as a Demec extensometer was used to verify strain readings obtained from the electronic devices in the experiments reported in Section 3.3 and in field applications where instantaneous loads were applied to the structure. The Demec extensometer, as depicted in Figure 3.16, is a mechanical device which consists of an invar bar with conical locating discs at each end. One of these points is fixed, and the other pivots. Metal discs with holes drilled in them the size of the pivot points are mounted on the surface of the material being measured. An in-depth description of this measuring system can be found in Arréllaga [10].

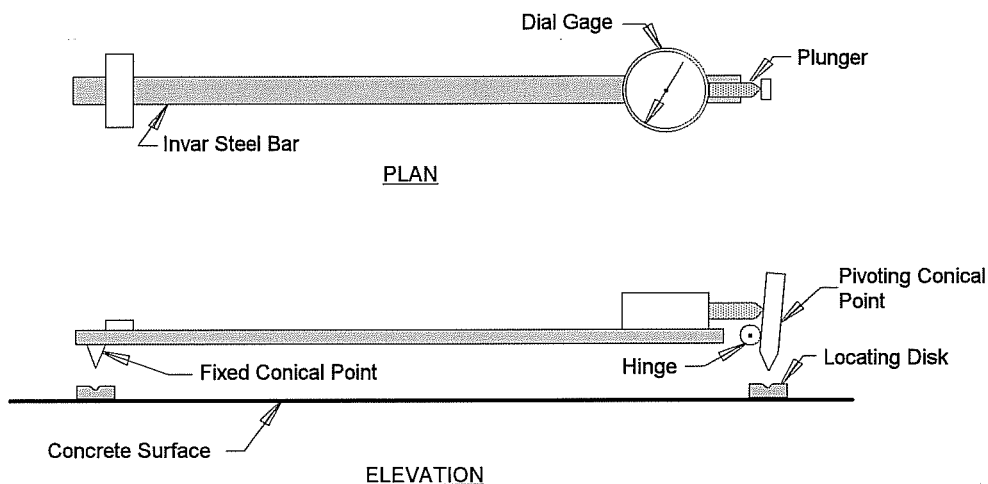


Figure 3.16 - Demec Extensometer

#### 3.4.1 Background

The Demec system was studied by Arréllaga [10] and utilized by Roberts [11] for the San Antonio “Y” instrumentation project. Based on the success of the system used by Roberts, the Demec system was chosen for backup use in current field studies.

The Demec extensometer is best used to measure strains due to instantaneous load. This is due to the fact that temperature effects cannot be accounted for through use of this



device. The Demec system was intended for use during a live load test for the instrumented pier.

### 3.4.2 Description and Application

The Demec system consists of a mechanical device called a Demec extensometer and two metal locating discs called Demec points. The Demec points are mounted on the surface of the test specimen. The modified installation method recommended by Arrélega [10] was used as shown in Figure 3.17. An aluminum template was manufactured to insure proper spacing of the drilled holes for placement in the field.

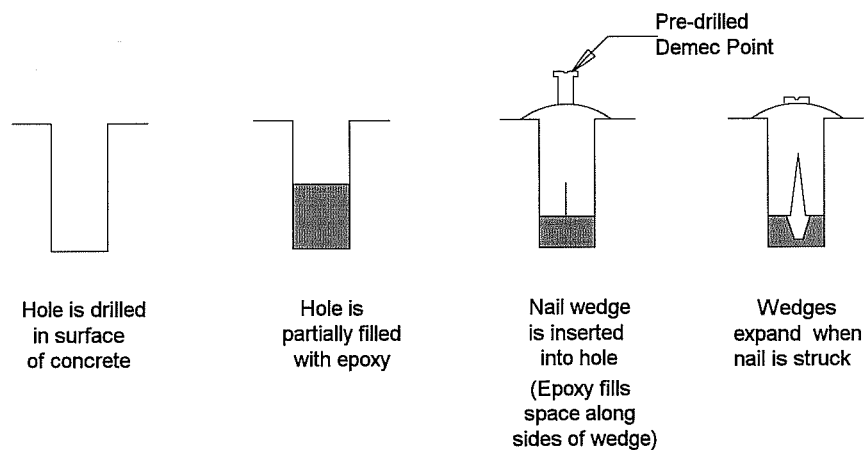


**Figure 3.17 - Demec Point Installation**

### 3.4.3 Layout

The layout of the Demec points used on the studied pier is shown in Figure 3.18, Figure 3.19, and Figure 3.20. The points were placed at locations that corresponded to the elevations of the electronic strain measuring devices. The original Demec points placed at the lowest elevation on the pier had to be relocated to a higher elevation due to the grade at the base of the pier. Demec points are labeled with the designation "D".

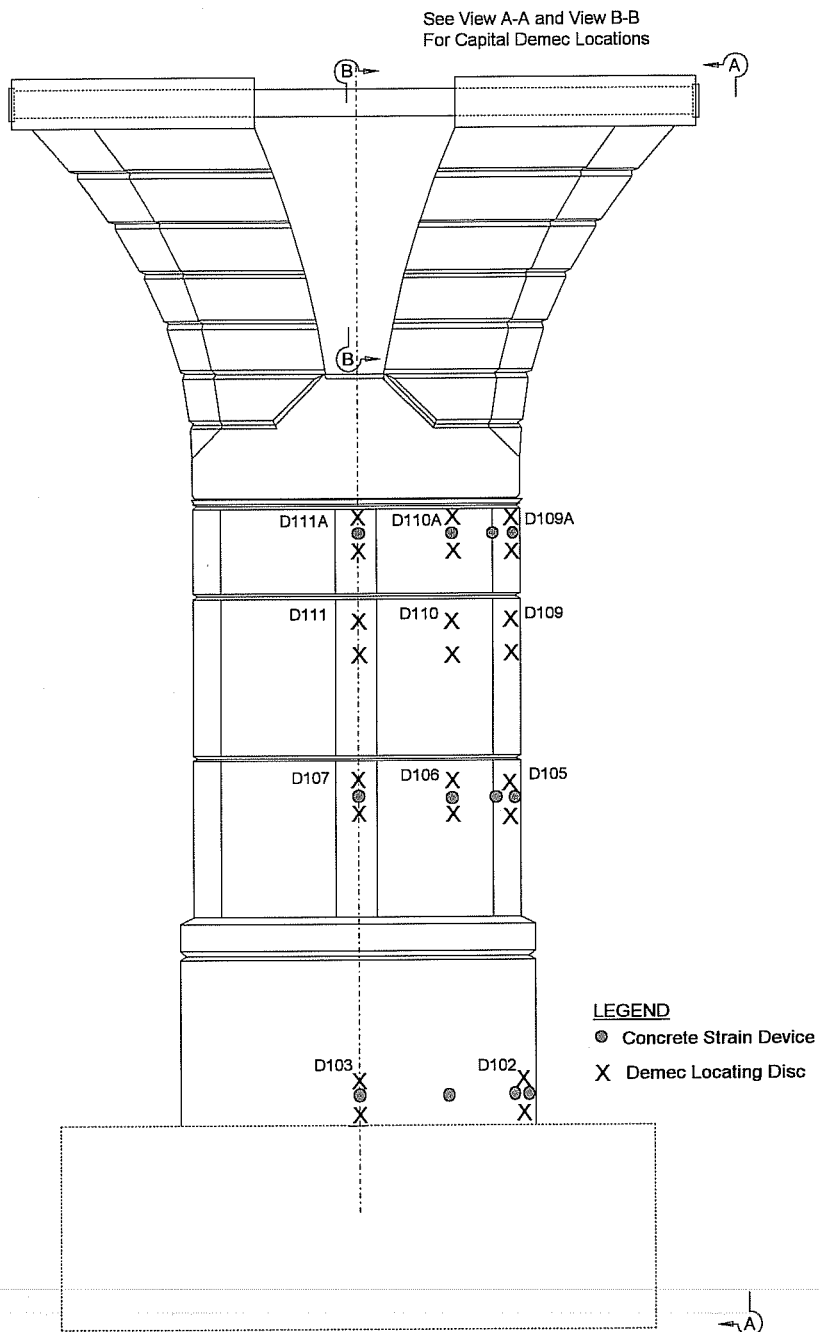


**Figure 3.18 - Demec Point Locations on Shaft**

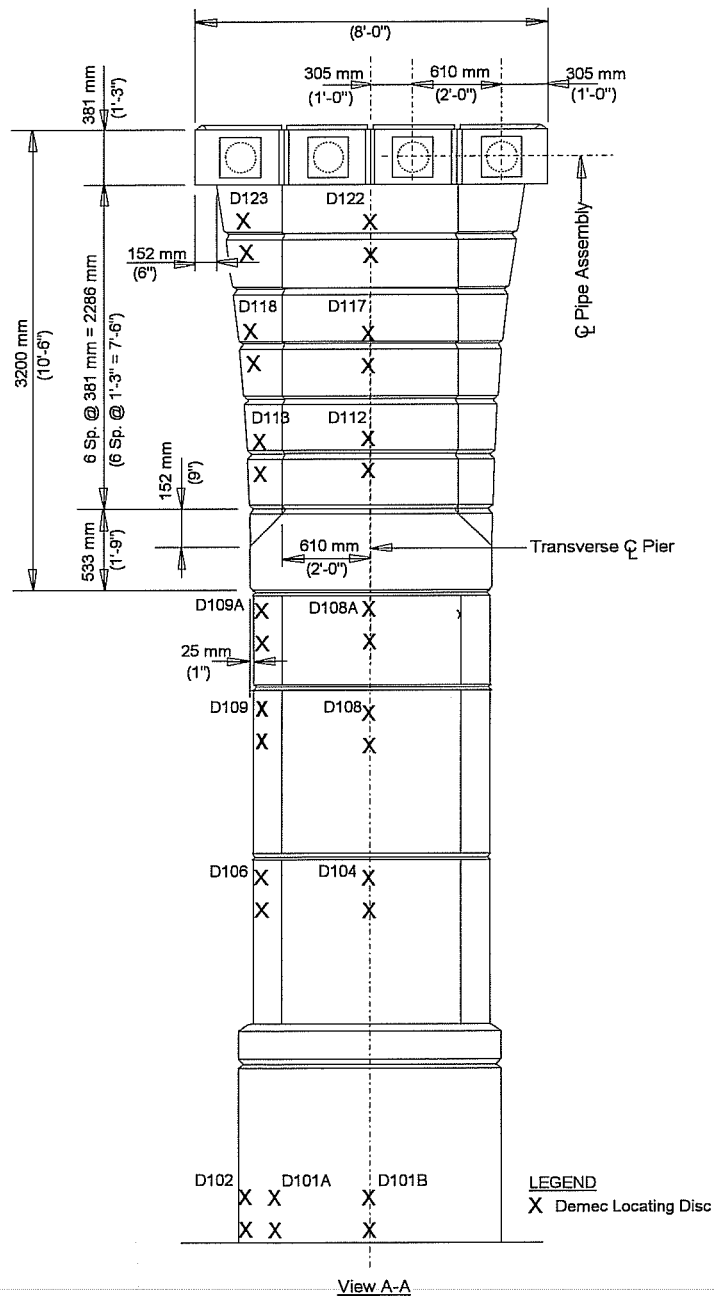
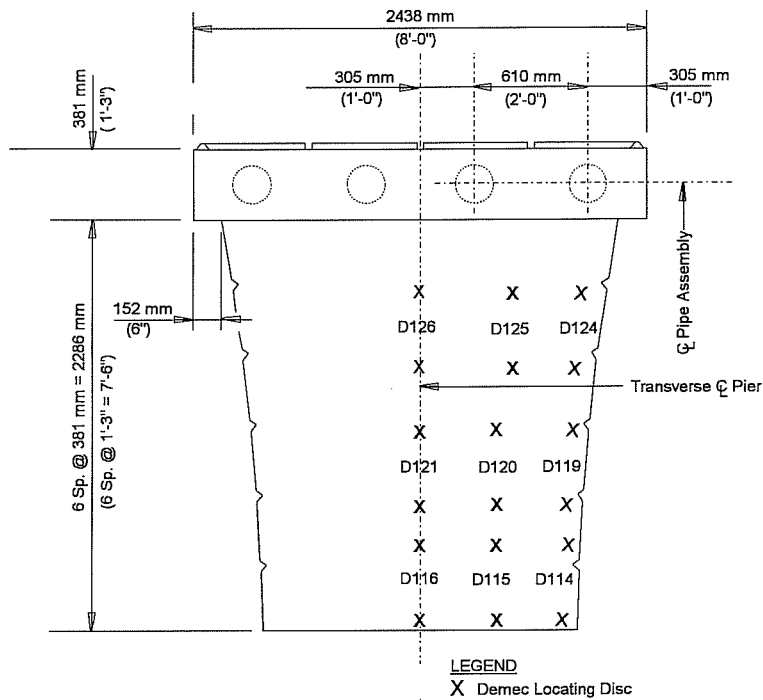


Figure 3.19 - Demec Point Locations on Side of Shaft and Capital



View B-B

**Figure 3.20 - Demec Point Locations on Inside Face of Capital**

### 3.5 Temperature Gradient - Thermocouples

The thermal characteristics of the pier are of particular concern in this study. The effects of thermal gradients across the structural steel tension ties and in the concrete were investigated.

#### 3.5.1 Background

A thermocouple consists of two wires of dissimilar metals. These wires are connected at each end. When one of the ends is heated, a continuous current flows through

the circuit. The temperature at the connected ends can then be read. Thermocouples were used to measure temperatures on the steel pipes and in the concrete of the pier.

Type T thermocouple wires were used. Type T thermocouples are made of copper and constantan and are the most common type used for embedment in concrete [10] due to the fact that both of these materials only mildly oxidize in concrete.

### ***3.5.2 Application***

The thermocouples were placed on the steel pipe as well as inside the concrete. Thermocouples placed on the steel pipe (T102 and T103) were mounted on the surface of the pipe. Thermocouples were placed inside the concrete (T101, T104-T109) by tying the thermocouple lead wire to reinforcing bars at the location where temperature readings were desired.

### ***3.5.3 Layout***

In order to investigate the magnitude of the effect of thermal gradients in the pier, thermocouples were placed as shown in Figure 3.21. Thermocouples were labeled with the designation "T".

## **3.6 Deformation of the "Y" - Linear Potentiometers and Thermocouples**

Measurement of the deformation of the "Y" under loading was done using linear potentiometers mounted on steel angles placed in the inner portion of the "Y". The set-up for these measurements is shown in Figure 3.22. Deformation was measured at the face of each side of the pier. Thermocouples were used to measure the temperature gradient along the steel angles so that any temperature effects could be taken into account. Three thermocouples were placed on each angle as shown in Figure 3.22. The thermocouples were labeled T110-T112 on one angle and T113-T115 on the other.

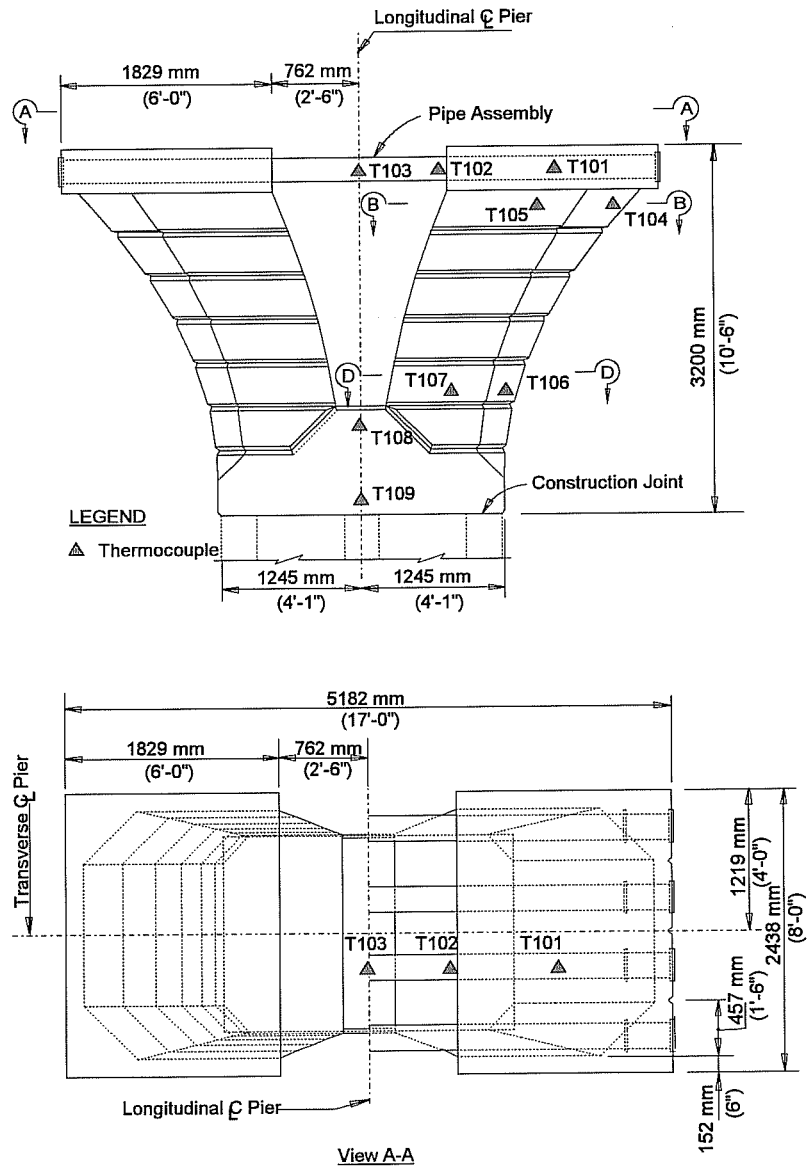


Figure 3.21 - Thermocouple Locations

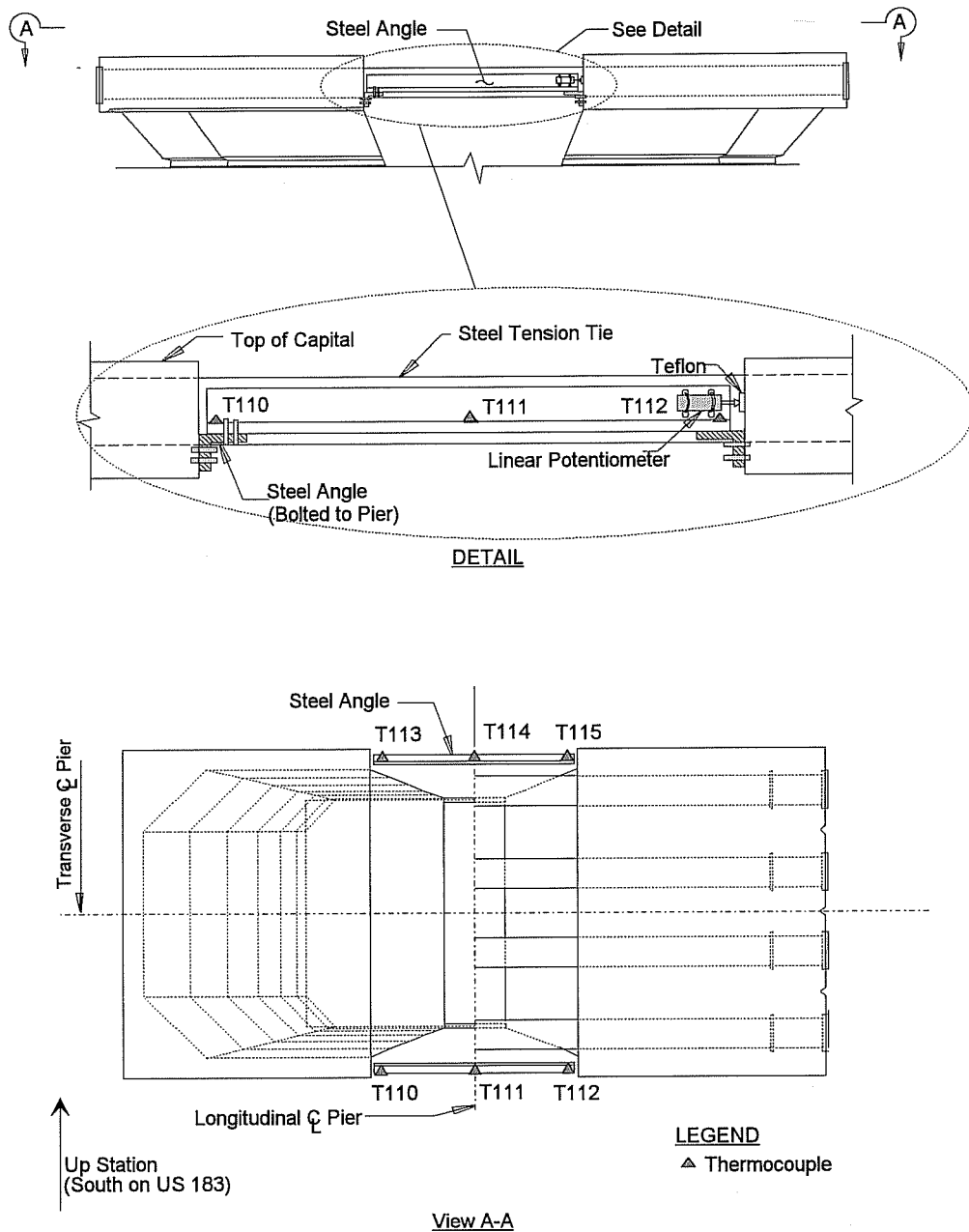


Figure 3.22 - Set-up to Read Deformation in the "Y"

### **3.7 Data Acquisition System**

A data acquisition system was used to record measurements from the electronic instruments. The selection of this acquisition system was made based on studies by Arrélega [10]. The Campbell Scientific 21X Datalogger was used in conjunction with the Campbell Scientific AM416 Multiplexers to temporarily store data. Roberts [11] reported good performance of this system for the San Antonio “Y” project.

The wires from the electronic instruments were routed adjacent to a centrally located reinforcing bar and out the top of the pier. All measurements taken prior to the superstructure erection were taken using a temporary data acquisition system located at the bottom of the “Y”.

Once span D5 was erected, the wires were routed into the superstructure at the adjacent live end of the span and connected to a permanent acquisition unit which was mounted on the interior face of the box girder web.



## **CHAPTER 4**

### **US 183 CONSTRUCTION AND DATA COLLECTION**

#### **4.1 Introduction**

The purpose of this chapter is to describe the pier construction and superstructure erection. Collection of data throughout these procedures is also discussed.

#### **4.2 Pier Construction**

The US 183 Mainlane piers were constructed in two concrete lifts. The first lift consisted of the column portion of the pier, "H" (see Figure 1.3), and is shown in Figure 4.1. Subsequent to the hardening of the column concrete, the capital reinforcing steel was tied, the structural steel tension ties placed, and the concrete cast for the capital. Figure 4.2 shows the capital during construction. A completed typical mainlane pier is shown in Figure 4.3.

#### **4.3 Superstructure Erection**

The superstructure consists of a simple span precast concrete segmental box girder system erected by the span-by-span method. Since the US 183 Elevated project is flanked on either side by the existing US 183 frontage roads, the use of falsework to temporarily support the superstructure while under construction was not feasible. The US 183 mainlane piers were designed with this constraint in mind.

The piers were used to support a truss system which in turn supported the superstructure while under construction. In order for the piers to support the steel truss system, a steel "pier bracket" was mounted in the "Y" of the pier. Figure 4.4 shows the pier bracket. A partially mounted pier bracket can be seen in Figure 4.5. The truss system was supported on the bracket as shown in Figure 4.6. A completed span can be seen in Figure 4.7. The basic construction procedure is shown schematically in Figure 4.8.

#### **4.4 Data Collection**

All instruments were monitored weekly after installation until approximately one month prior to construction of the superstructure. At this time, a temporary data acquisition

system was assembled and placed in a ventilated water-resistant box. This system was placed in the “Y” of the pier. Prior to pier bracket placement, this box was moved to the top of the capital and left in place until the segments of span 5 were epoxied and temporarily tensioned together.

The acquisition system was then disconnected for approximately three days while the instrumentation of span 5 was performed. During those three days, all construction activity was stopped. Pier instrument wires were re-routed into the box girder and connected to a permanent acquisition system mounted to the wall of the box girder.

During construction of span 5, all instruments were monitored more frequently during the stressing procedure. The instruments were observed frequently until span 5 was placed on the bearings of pier D6. Subsequent to span 5 placement on pier D6, regular hourly readings were resumed. A data collection summary can be found in Table 4.1.

**Table 4.1 - Data Collection Summary**

<b>EVENT</b>	<b>DATE</b>	<b>READINGS</b>
<b>Pier Finished</b>	8/23/94	<i>Each Week</i>
<b>Prior to Span 5 Erection</b>	12/1/94 - 4/19/95	<i>Each Hour</i>
<b>Instrumentation of Span 5</b>	4/19/95 - 4/21/95	<i>None</i>
<b>Stressing of Span 5</b>	4/22/95	<i>Each Minute</i>
<b>After Stressing</b>	4/22/95	<i>Each Half Hour</i>
<b>After Placement on Bearings</b>	4/22/95 - Present	<i>Each Hour</i>



**Figure 4.1 - Casting of Pier Column Concrete**



**Figure 4.2 - Construction of Pier Capital**



**Figure 4.3 - Typical Mainlane Pier**



**Figure 4.4 - Pier Bracket**

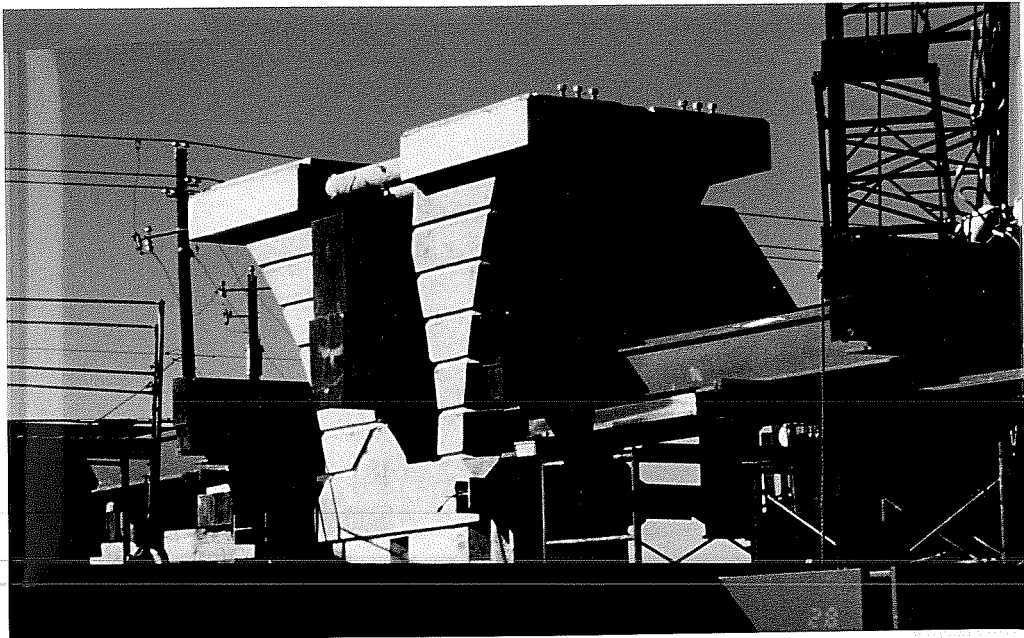


**Figure 4.5 - Partially Mounted Pier Bracket**



**Figure 4.6 - Pier Bracket Supporting Truss**



**Figure 4.7 - Completed Span**

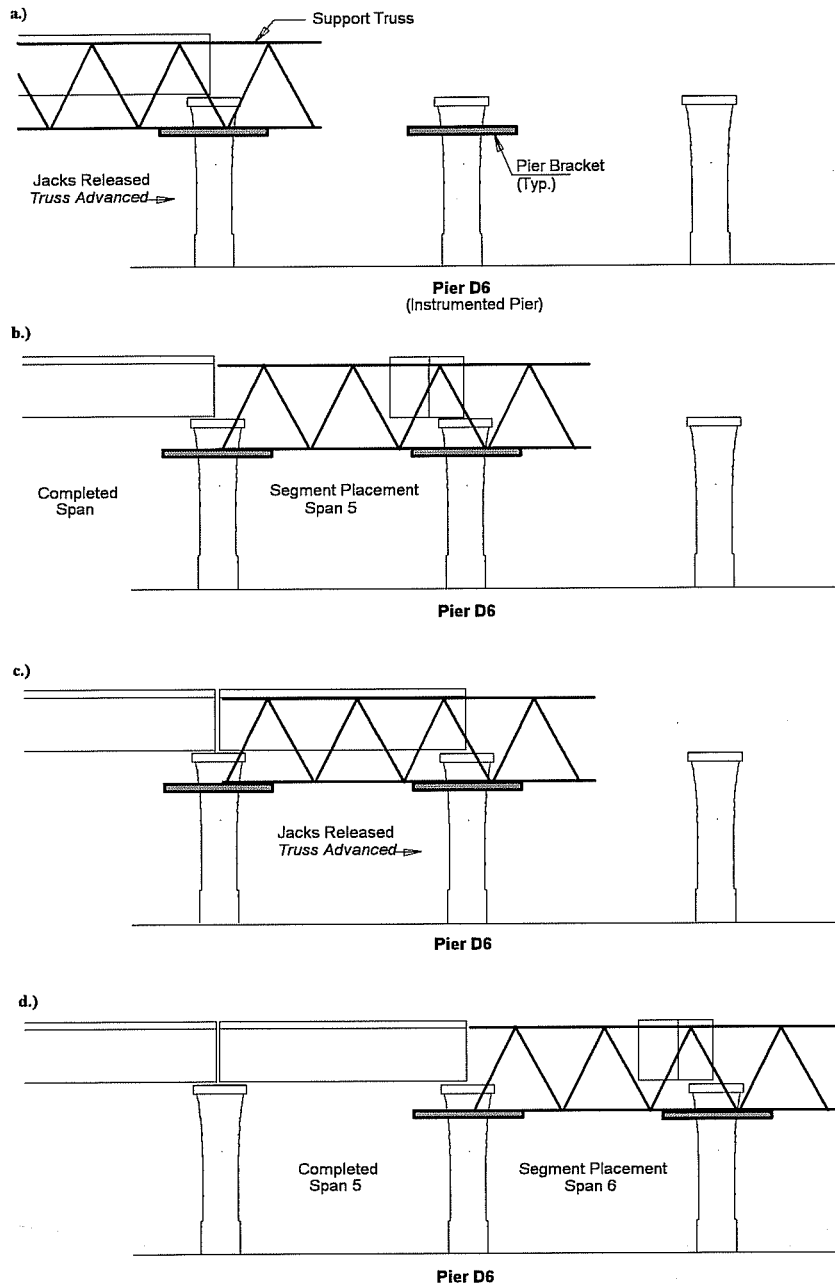


**Figure 4.8 - Construction Procedure for Typical Span Completion**

## CHAPTER 5

### DATA PRESENTATION

#### 5.1 Introduction

The purpose of this chapter is to present background information and data in order to describe the behavior of pier D6 under temperature and gravity loads.

#### 5.2 Background - Thermal Strains

As mentioned in Chapter 1, the limited capability of the equilibrium based STM to predict compatibility and constraint-induced stresses requires that strains induced due to thermal loading be investigated and separated from those due to gravity loading. The approach for separating thermal strains from gravity strains for each load case is discussed in detail in Chapter 6.

##### 5.2.1 Thermal Strains - Basic Principles

Heating causes most unrestrained engineering materials to expand. Similarly, cooling causes contraction. The ratio of this expansion or contraction to the original length is known as thermal strain. The strain induced in a material due to a one degree temperature change is called the coefficient of thermal expansion of the material, or  $\alpha$ . The following formula is used to calculate  $\epsilon_T$ , the strain due to temperature change [9]:

$$\epsilon_T = \alpha(\Delta T)$$

where

$\alpha$  = coefficient of thermal expansion

$\Delta T$  = change in temperature



### ***5.2.2 Thermal Restraint and Thermal Stresses***

Thermal stresses are induced by thermal strains if the material is restrained while temperature change takes place. Provided behavior remains elastic, thermal stresses can be calculated as follows [9]:

1. Assume the member is permitted to move freely
2. Apply the forces that cause the member to assume the configuration that the restraint would cause.

The principle of superposition may be used to add thermally induced stresses to other stresses existing prior to the temperature change. Material properties can be changed due to temperature induced strain. However, most engineering materials undergo very small material property changes for a temperature change of a few hundred degrees near room temperature [9].

### ***5.2.3 Thermal Stresses in Pier due to Temperature Gradient in Concrete***

The following example will provide a basis for the description of a typical US 183 mainlane pier. Den Hartog [14] provides the problem shown in Figure 5.1 as an example of temperature effects.

Consider the bolt shown in Figure 5.1. The bronze is shrunk on so that no slippage occurs. A uniform increase in temperature is applied to the brass encased bolt. Since  $\alpha_b$  is greater than  $\alpha_s$ , the bronze will want to expand to a greater length than the steel. Since the two materials are connected such that no slippage occurs, the bronze will not be able to expand to its desired length and will therefore be placed in compression. The steel will be pulled along by the bronze and will be placed in tension as a result [14].

The shaft or “column” portion of the US 183 mainlane pier closely resembles the bolt example given above. Rather than consisting of two materials of differing  $\alpha$  and a uniform  $\Delta T$ , the column consists of a core and a shell of the same material but with a differing  $\Delta T$ . This concept is shown in Figure 5.2. Since the concrete is so massive, it does not heat and cool uniformly with ambient temperature change. An outer “shell” of concrete

tends to heat and cool more rapidly than the inner core, which stays more constant in temperature. Evidence of this behavior over a typical day can be seen in Figure 5.3.

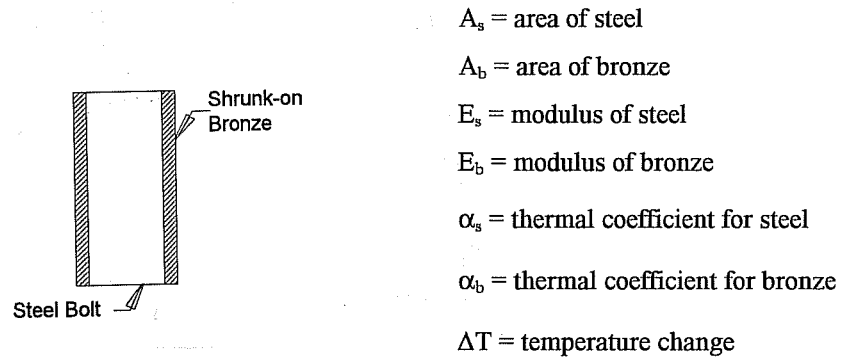


**Figure 5.1 - Example Problem Examining Temperature Effects**

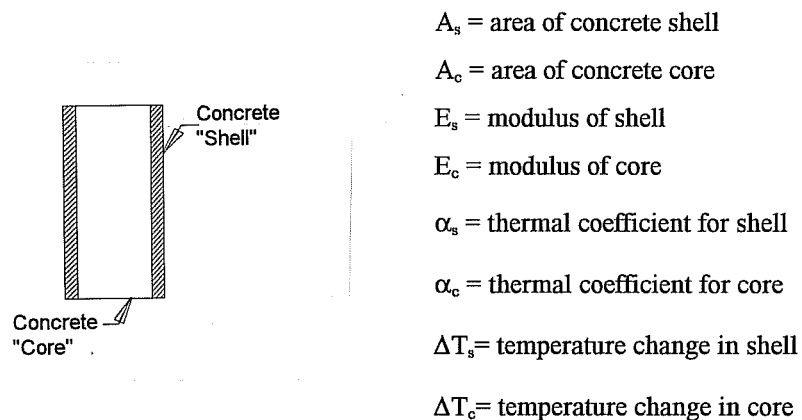


**Figure 5.2 - Temperature Effects in Column**

If the concrete shell undergoes a greater  $\Delta T$  than the core, then the shell will want to expand more than the core. Assuming no pre-existing stresses exist on the member, the shell will then be placed in compression due to restraint from the core. Like the brass

encased steel bolt in the previous example problem, the core will be in tension for this case. If stress is present prior to the temperature change, then the shell will undergo a compressive strain change. However, the final state of stress may not necessarily be compression. Each branch of the “Y” portion of the capital would be expected to behave in a similar fashion, perhaps with a smaller effect since the concrete is less massive in this area.

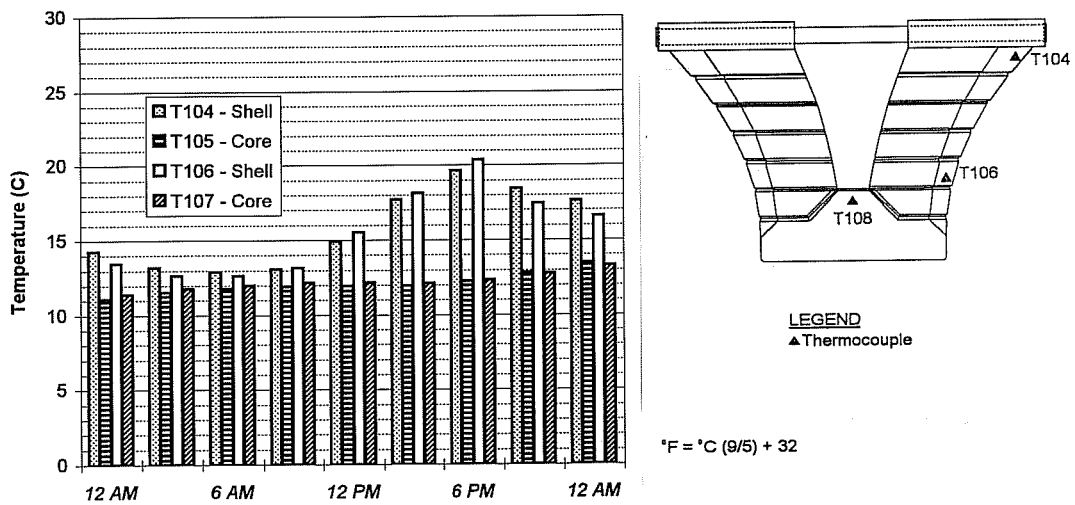


Figure 5.3 - Temperatures Over a Typical Day

#### 5.2.4 Thermal Stresses in Pier due to Temperature Gradient in Pipes

Thermal stresses in both the structural steel pipes and the concrete of the pier may also be induced due to temperature change along the structural steel pipes. If the temperature of the pipes increase, the steel will want to expand. If the steel expansion is restrained by the concrete at the pipe ends, the full desired expansion will not be reached, and a thermal stress will be set up in the structural steel pipes.

The concrete will also be affected by this pipe expansion. As noted, the concrete is trying to resist the expansion of the steel. This action causes the concrete to accumulate bending stresses due to the temperature changes in the pipes.

### 5.3 Measurements - Prior to Superstructure Erection

This section presents field measurements made prior to the erection of the superstructure. The purpose of investigating behavior before gravity loading is to consider the effects of thermal gradients across the concrete and across the structural steel pipes.

The measurements presented in this section have not been adjusted for temperature effects. As indicated in Table 4.1, continuous hourly measurements were taken for pier D6 beginning in December of 1994. In order to observe behavior prior to the superstructure erection, March 11, 1995, was chosen as a typical sunny day.

Temperature trends from day to day become consistent beginning around this date. Also, several days during which no precipitation occurred preceded March 11. As seen in Figure 5.4, temperature patterns prior to this time were not consistent from day to day due to weather fluctuations. As such, March 11 provides information for a typical sunny day during the time frame prior to any superstructure load. Figure 5.5 shows ambient temperatures as reported by the National Oceanic and Atmospheric Administration [15] for March 11, 1995. Climatological data can be found in the Appendix. Also shown in Figures 5.5 are the pipe temperatures at the center of the pipe. The temperatures show excellent correlation with the ambient temperatures. Therefore, thermocouple T103 can be used as a "local thermometer" at the project site.

#### 5.3.1 Temperature Measurements

Thermocouples were placed in the concrete "Y" portion of the pier and on the structural steel pipes as shown in Figure 5.6. Temperature variation along the structural steel pipes can be seen in Figure 5.7. As the day progresses, the pipe undergoes a cooling trend in the morning followed by a heating trend in the afternoon. In the evening, the pipes begin to cool. The greatest difference between the temperature on the fully exposed portion of the pipe and the fully embedded pipe occurs at 3:00 P.M. and is approximately 8 °C (11.5 °F).

Temperature changes along the pipe during March 11 are depicted in Figure 5.8. Although the entire length of the pipe shows similar trends, thermocouple T103 (located at

the center of the pipe) undergoes a more drastic temperature change than thermocouple T102 (located at the concrete/steel interface). This trend indicates that the concrete is absorbing heat from the pipe. Thermocouple T102 undergoes a greater temperature change than T101, which is located in the concrete. At the latter location, the pipe is insulated from the sun's radiation by the concrete.

The thermocouples located near the surface of the concrete are T104, T106, and T108. Temperatures for these devices during March 11 are shown in Figure 5.9. Similar to thermocouples T101, T102, and T103, a morning cooling trend, afternoon heating trend and evening cooling trend can be observed. These thermocouples exhibit very similar temperatures and temperature changes throughout the day.

Thermocouple T108 begins a cooling trend earlier in the evening than T104 and T106. Thermocouples T104 and T106 are located on the southwest corner of pier D6. As such, they are directly exposed to the setting sun. Thermocouple T108 is shaded by the "Y" during this time, allowing it to begin cooling earlier in the day.

Thermocouples located in the core of the concrete are T105, T107, and T109. Temperatures for these devices during March 11 are shown in Figure 5.10. These thermocouples do not exhibit heating and cooling trends similar to the rest of the thermocouples. They are not exposed directly to the environment at any time and are not as immediately affected by ambient temperature changes as other thermocouples due to the massiveness and low conductivity of the concrete. These core thermocouples exhibit only a slight heating trend over the course of a typical day.

Assuming thermocouple T103 represents the ambient temperature, certain observations can be made about the temperature 'lag' in the concrete "core" based on Figure 5.11. In early morning, as the ambient temperature is cooling, the core instruments still exhibit an increase in temperature. As the ambient temperature rises during mid-day, the core instruments show almost no change in temperature. During the latter part of the day, as ambient temperature is decreasing, the core is again heating.

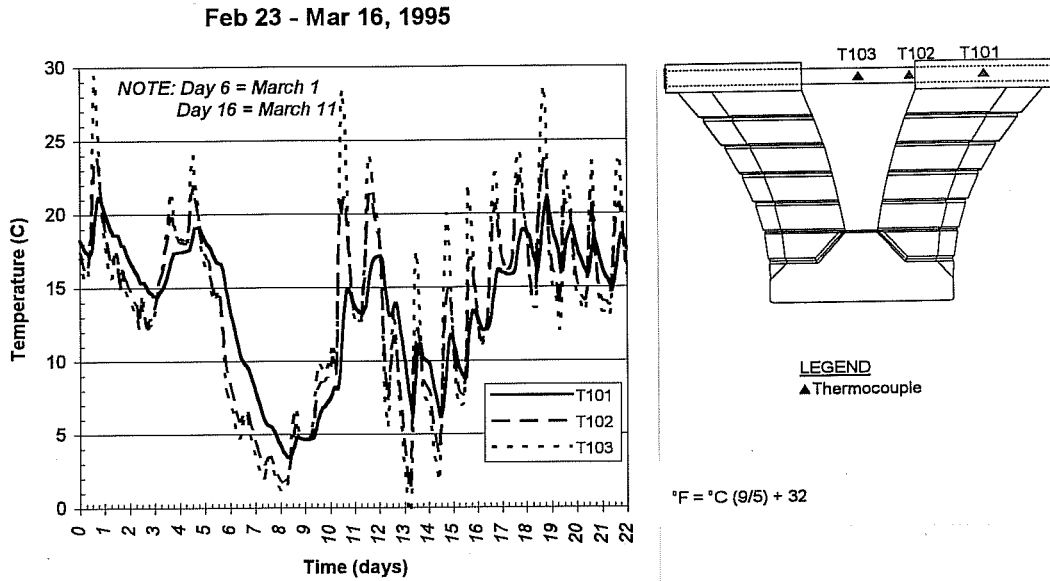


**Figure 5.4 - Temperature History**

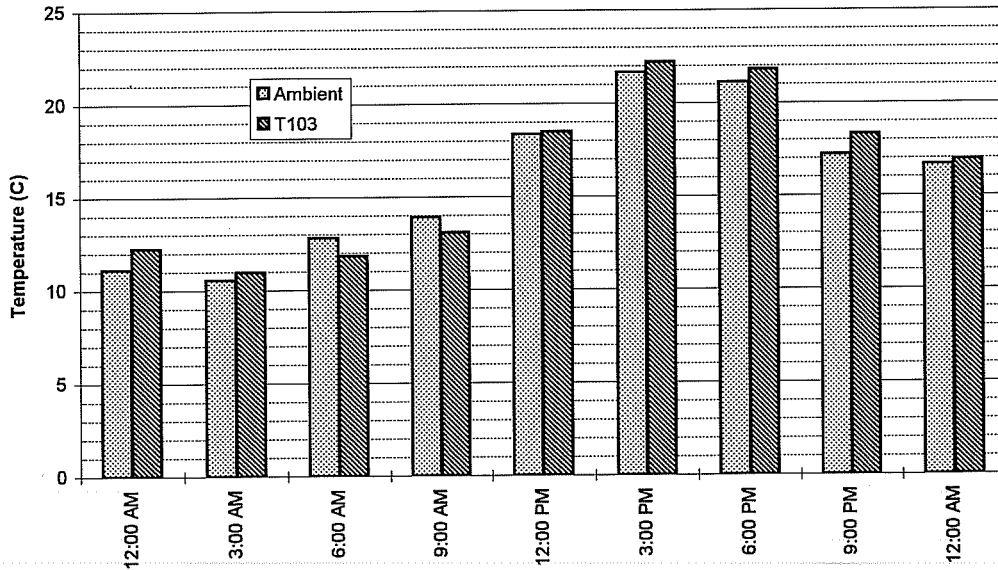


**Figure 5.5 - Ambient Temperatures for March 11, 1995**

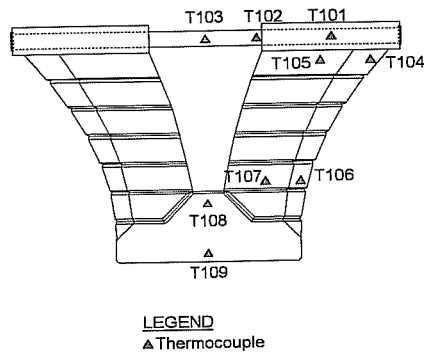


**Figure 5.6 - Thermocouple Locations**

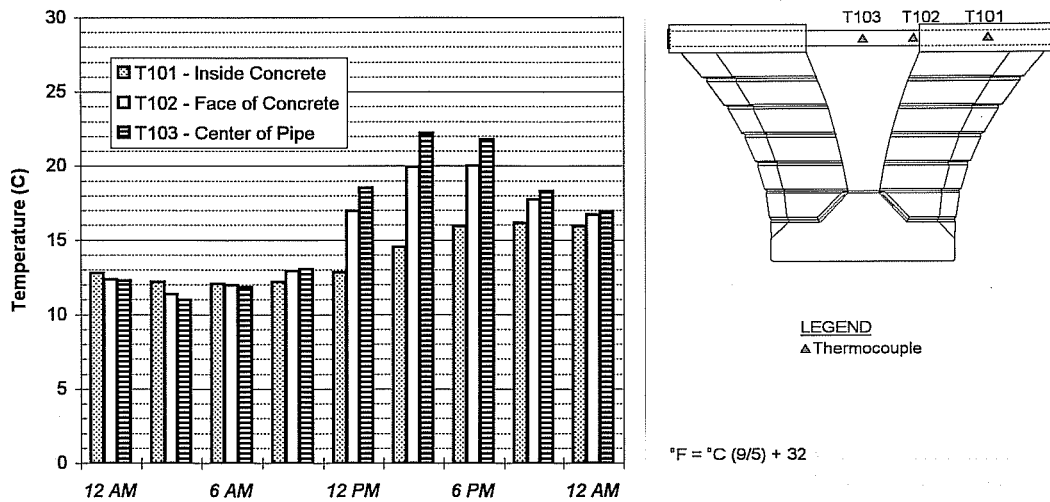


**Figure 5.7 - Structural Steel Pipe Temperatures: Typical Sunny Day**

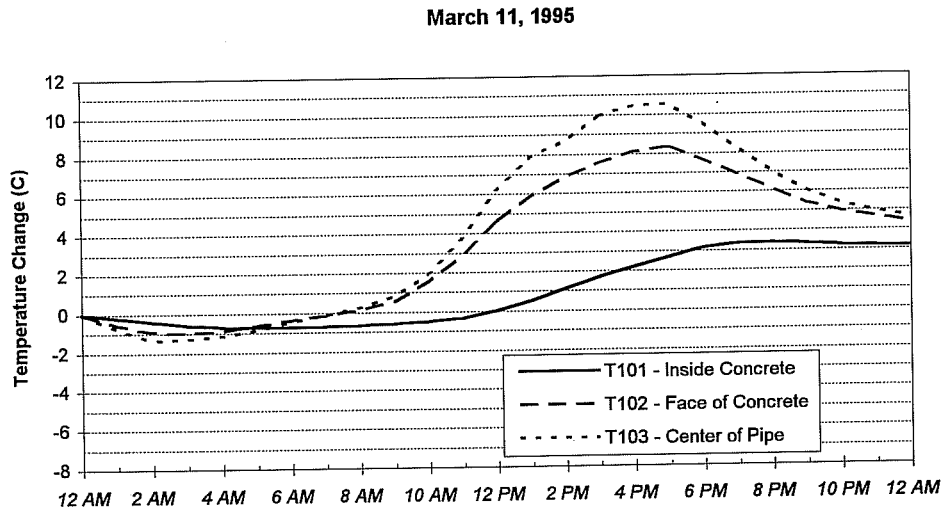


Figure 5.8 - Structural Steel Pipe Temperature Changes: Typical Sunny Day

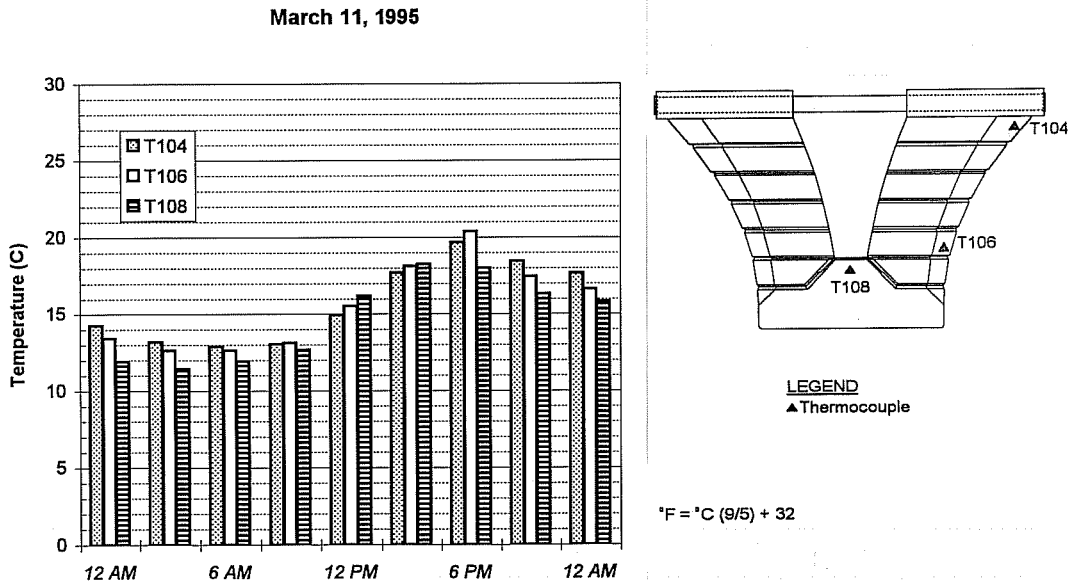
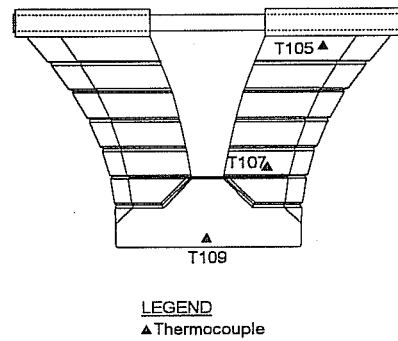
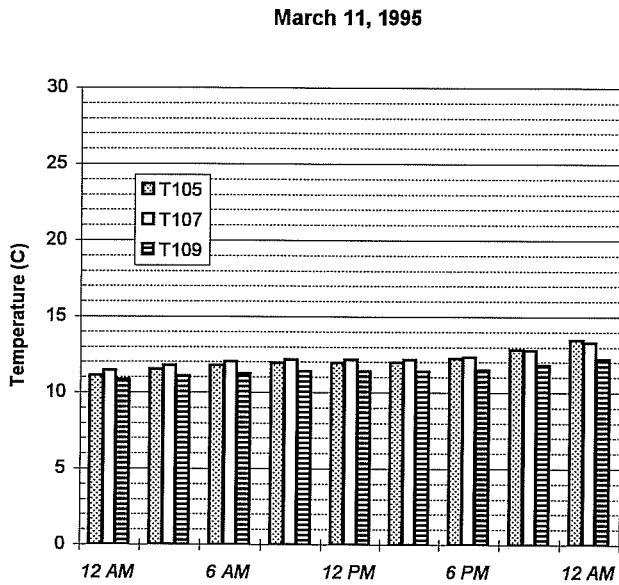


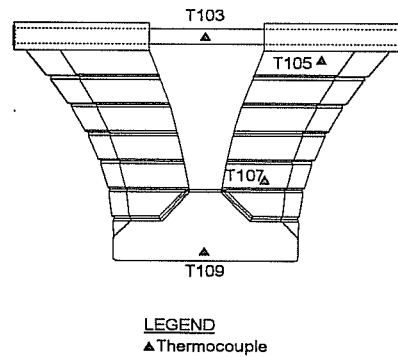
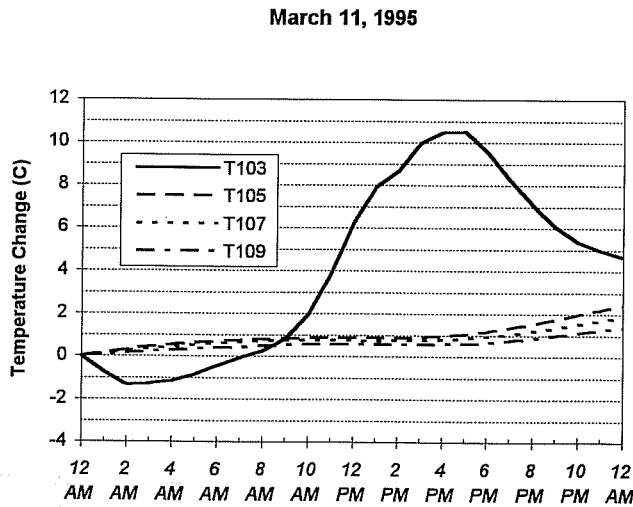
Figure 5.9 - Temperatures in Concrete "Shell": Typical Sunny Day





$^{\circ}\text{F} = ^{\circ}\text{C} (9/5) + 32$

**Figure 5.10 - Temperature in Concrete “Core”: Typical Sunny Day**



$^{\circ}\text{F} = ^{\circ}\text{C} (9/5) + 32$

**Figure 5.11 - Temperature Lag to Concrete “Core”: Typical Sunny Day**

In order to provide contrast to a typical sunny day, a cloudy day was chosen for presentation. Figure 5.4 indicates that a general cooling trend occurred during the days surrounding March 1, 1995. As reported by the National Oceanic and Atmospheric Administration, ambient temperatures for this day are shown in Figure 5.12. Again, the temperatures measured by T103 at the center of the pipe are in excellent agreement with the ambient temperatures. Climatological data indicate that the four days prior to March 1 were cloudy and rainy. A large temperature drop occurred on March 1 as well.

Temperature variation along the structural steel pipes can be seen in Figure 5.13. As the day progresses, T102 and T103 show an overall cooling trend with a slight warming in the afternoon. Thermocouple T103 is consistently cooler than T102, indicating that heat stored in the concrete from previous warmer days is being transferred to the pipe. Thermocouple T101, which is embedded in the concrete, shows only cooling during the day but is consistently warmer than T102 and T103. As shown in Figure 5.14, there is heat transfer from the concrete to the pipes.

Temperatures from “shell” thermocouples T104, T106, and T108 are shown in Figure 5.15. Each of these thermocouples shows an overall cooling for the day with a slight warming in mid-afternoon. Thermocouple T108 follows the same evening cooling trends as T104 and T106 since the cloudiness of March 1 protects all of the thermocouples from the late afternoon sun.

Thermocouples embedded in the concrete “core” were also affected by the cool and cloudy weather of March 1, as shown in Figure 5.16. Thermocouples T105, T107, and T109 exhibit decreasing temperatures as the day progresses. Also, the temperature of the concrete core is higher than the concrete shell.

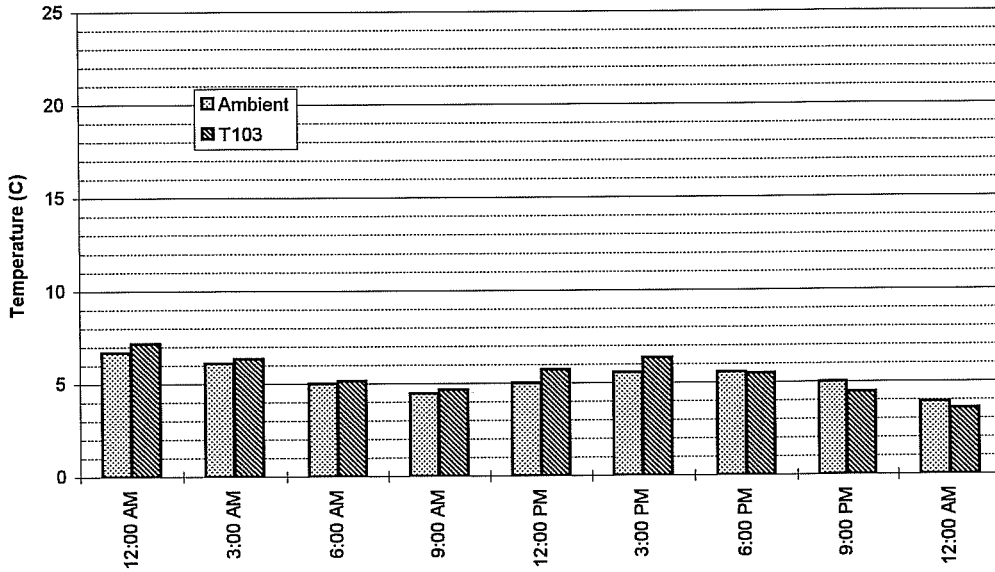
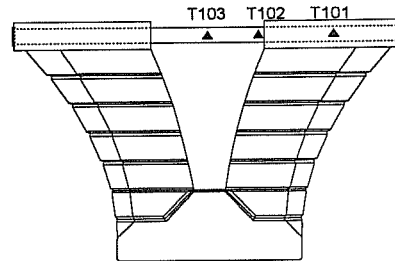
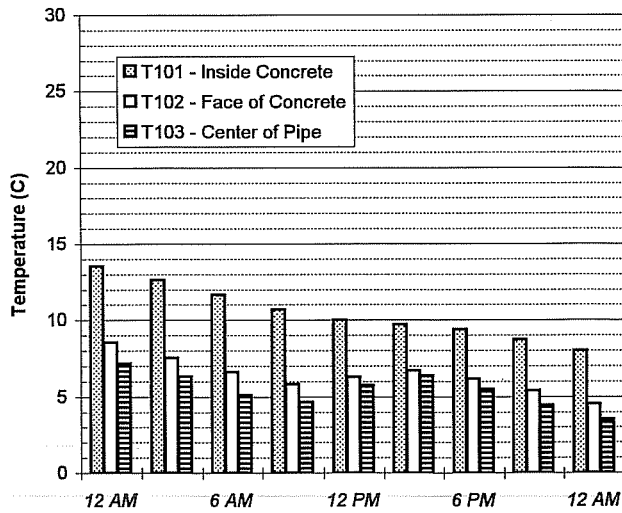


Figure 5.12 - Ambient Temperatures During March 1, 1995

March 1, 1995



LEGEND  
▲ Thermocouple

$^{\circ}\text{F} = ^{\circ}\text{C} (9/5) + 32$

Figure 5.13 - Structural Steel Pipe Temperatures: Typical Cloudy Day

March 1, 1995

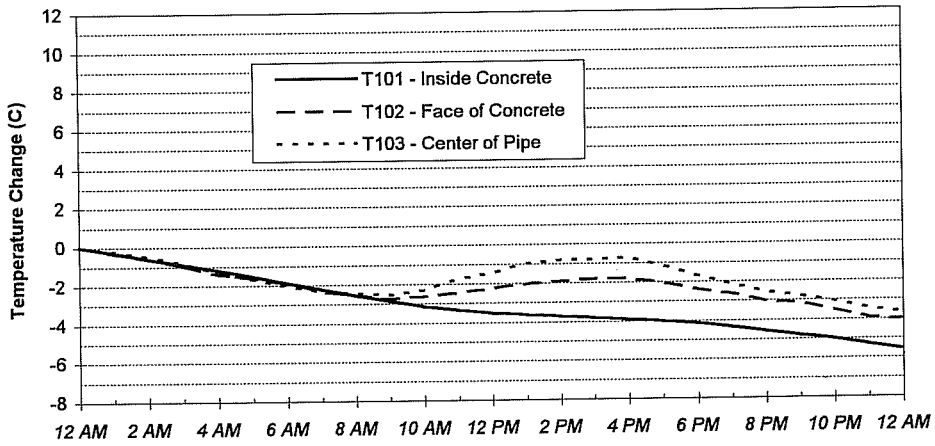


Figure 5.14 - Structural Steel Pipe Temperature Changes: Typical Cloudy Day

March 1, 1995

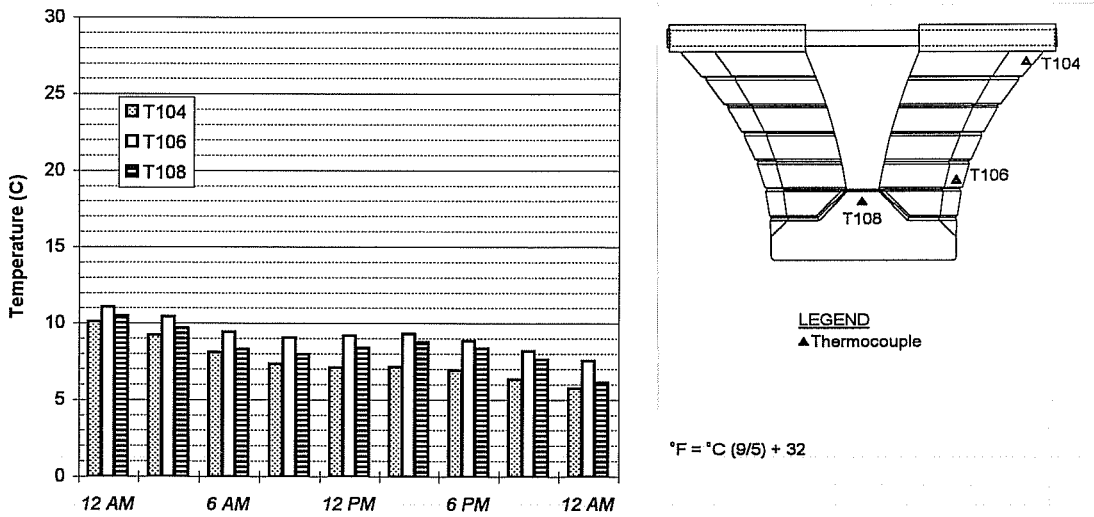
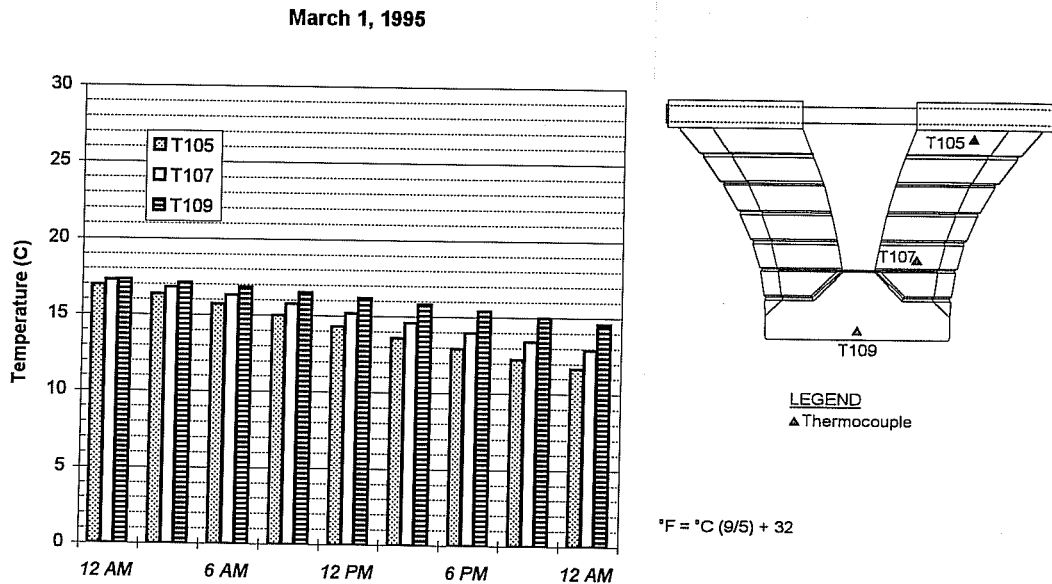


Figure 5.15 - Temperatures in Concrete "Shell": Typical Cloudy Day



**Figure 5.16 - Temperatures in Concrete “Core”: Typical Cloudy Day**

### 5.3.2 Structural Steel Pipe Strains - Typical Sunny Day

Strain gages were mounted along the length of two of the structural steel pipes as shown in Figure 5.17. Strain variations measured on March 11, 1995, along the pipes can be seen in Figure 5.18 and Figure 5.19. These plots indicate that although the gravity load on the pier is unchanged during this time period, pipe strains are changing throughout the day. These changes can only be induced due to temperature effects. The maximum changes would correspond to pipe strain changes of  $\pm 2.8$  MPa ( $\pm 400$  psi), which are relatively unimportant when compared to the pipe allowable stress.

Both pipes show similarities in behavior along their lengths. In general, as the temperature increases over a day, tensile strain changes occur. As the temperature decreases, compressive strain changes occur. These tensile and compressive strain changes occur at different times over the course of the day.

Figure 5.20 shows strain changes and temperature changes for transducers located near the middle of the enclosed portion of the pipes. T101 is located approximately between strain gages S121, S122 and S123, S124. As temperature decreases, tensile change in strain occurs. As temperature increases, compressive strain changes occur.

Strain gages S109, S110 and S111, S112 show a trend similar to strain gages S121, S122 and S123, S124. The strain changes associated with this exterior pipe are larger than those of the interior, especially during the second half of the day. These larger strain changes may be due to the fact that the exterior pipe is provided less insulation by the concrete since the cover is less on the exterior side face of the concrete. Also, the exterior pipe is directly exposed to the setting sun. This may cause the significantly larger strain change during the latter part of the day.

Figure 5.21 shows strain changes and temperature changes for strain gages and thermocouples located near the concrete/steel pipe interface. The interior and exterior pipes exhibit differing behavior. This may again be due the difference in concrete cover and location of the pipe relative to the position of the sun.

Strain gages S126-S128 exhibit behavior indicating that the concrete portion of the capital is not restraining expansion and contraction of the steel at this location. As temperatures decrease, compressive strain changes occur. As temperatures increase, tensile strain changes occur.

Strain gages S113-S116 indicate a tensile strain change as temperatures increase in the early morning. As the temperature increase continues into early afternoon, the strain change for S113-S116 becomes compressive until the temperature starts to decrease at approximately 5 P.M. At this time, strain change becomes tensile.

Figure 5.22 shows temperature change and strain change for the thermocouples and strain gages located in the center of the pipe. Strain gages S117, S118 exhibit behavior similar to S126-S128. Strain gages S129, S130 exhibit behavior similar to S113-S116.

Strain gages S119, S120 and S107, S108 are located near the ends of the pipes. There is no thermocouple in this location. The strain changes are compared to thermocouple T101 in Figure 5.23. As temperature decreases, the strain change for strain gages S107, S108 is tensile. As temperature increases, the strain change is compressive. Gages S119,

S120 showed similar behavior. However, S119, S120 exhibited larger strain change as the daytime heating occurred.

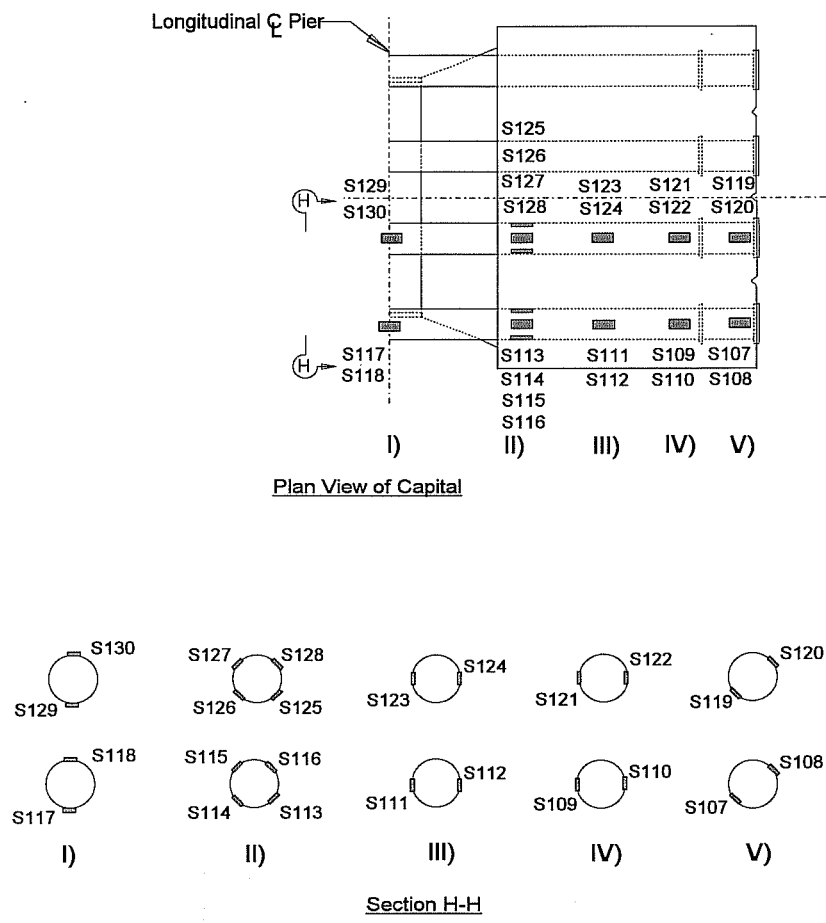


Figure 5.17 - Strain Gage Locations on Structural Steel Pipes

March 11, 1995

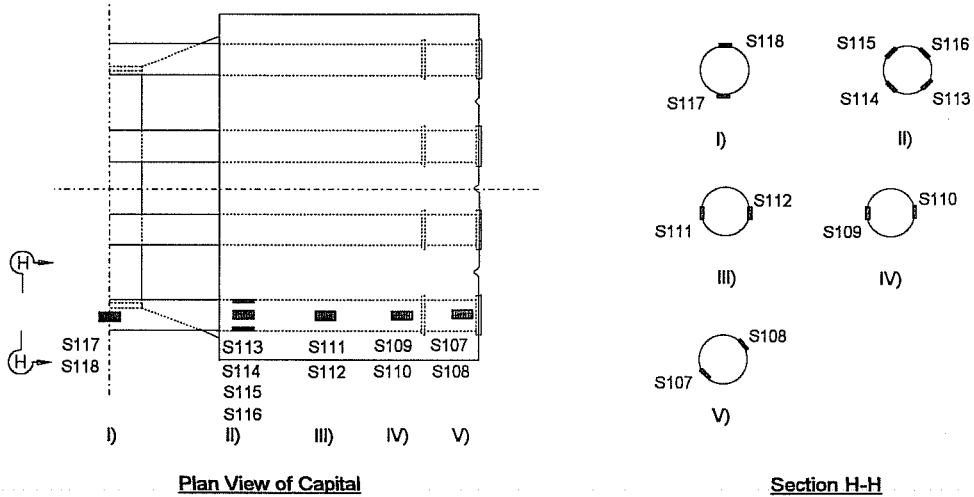
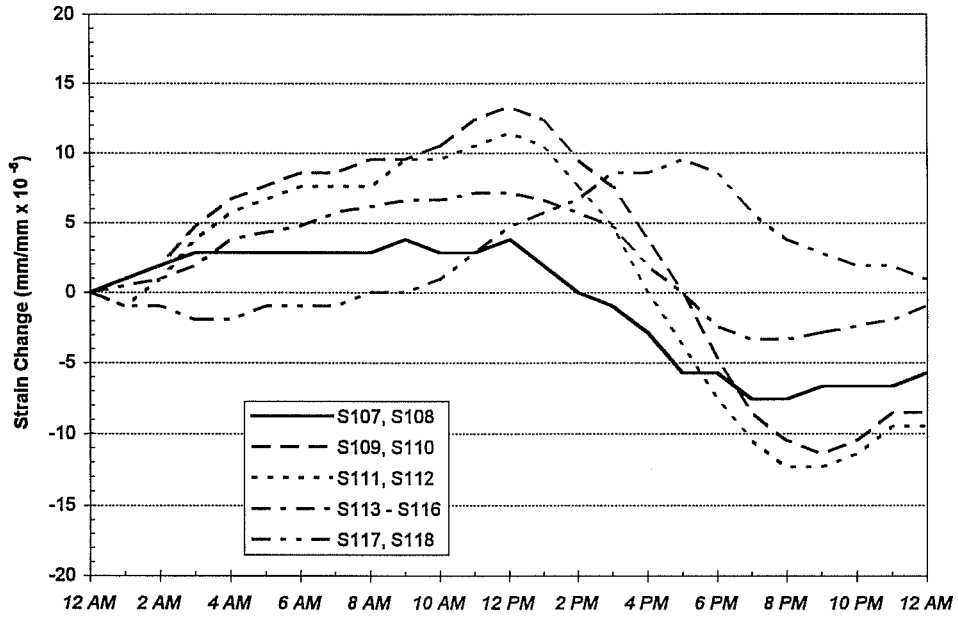


Figure 5.18 - Strain Variations Along Structural Steel Pipe: Exterior Pipe



March 11, 1995

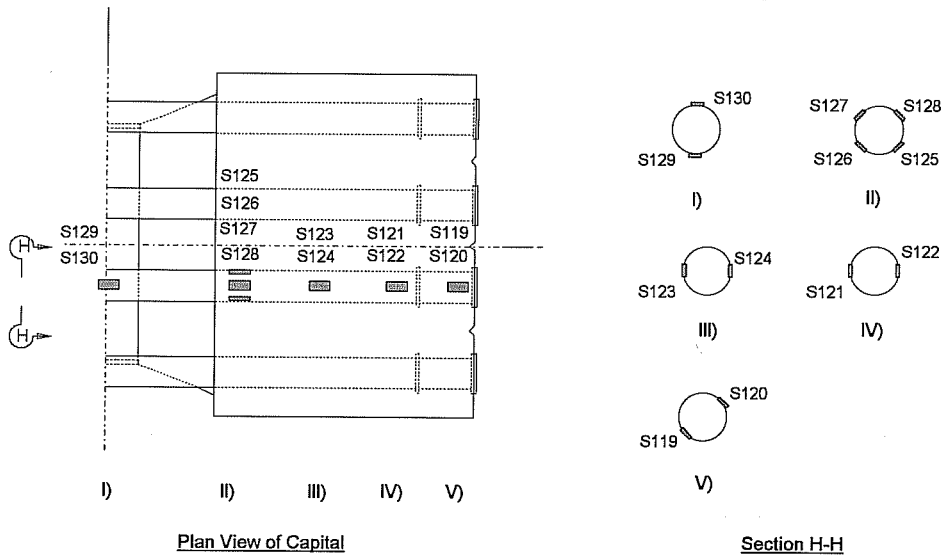
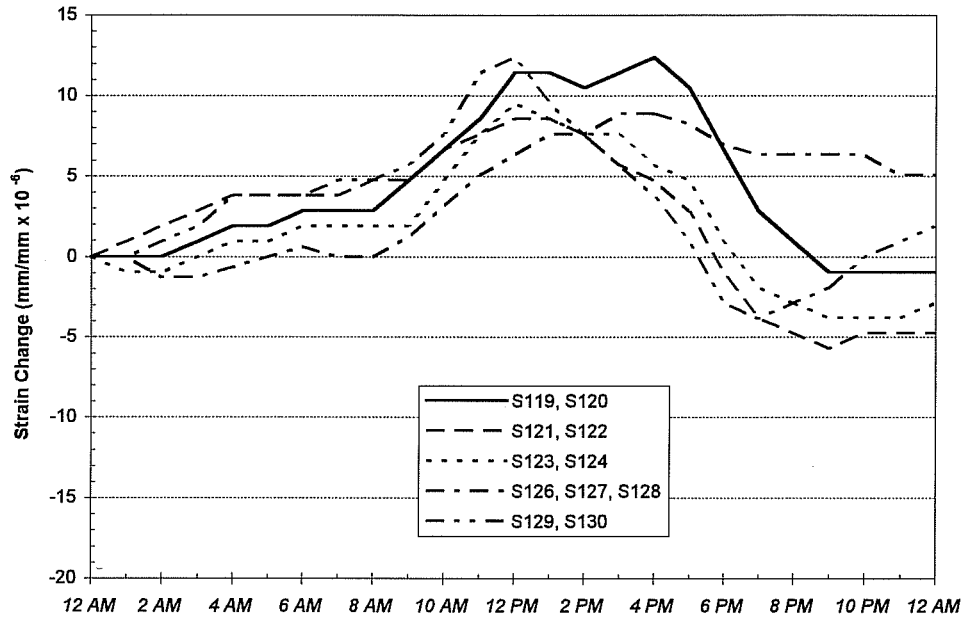
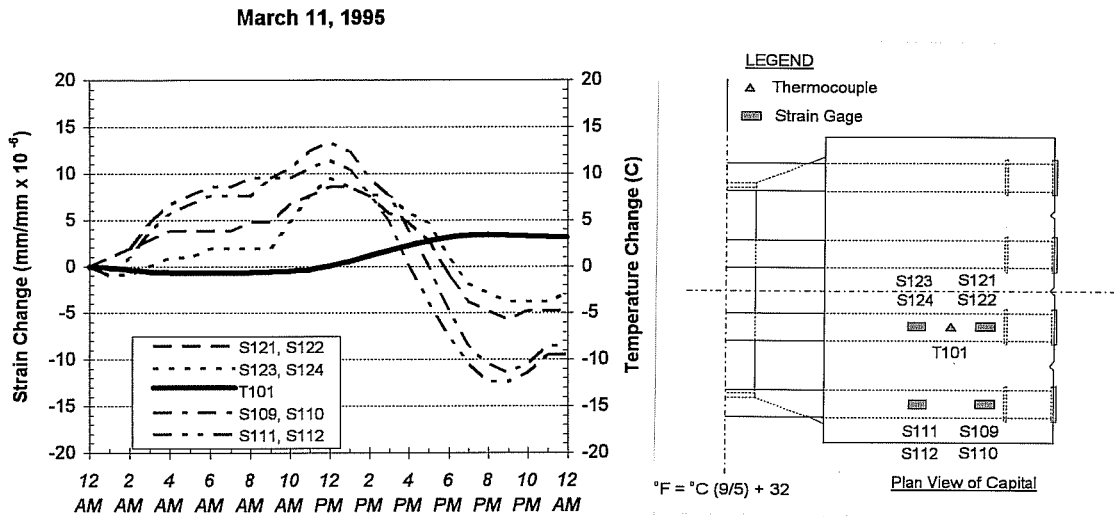
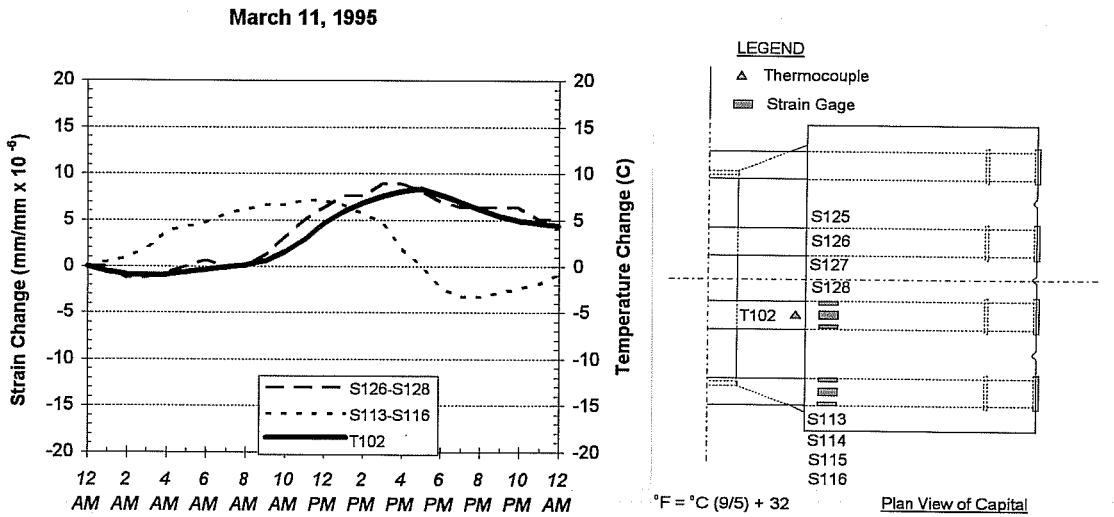


Figure 5.19 - Strain Variations Along Structural Steel Pipe: Interior Pipe



**Figure 5.20 - Pipe Strain Change and Temperature Change**



**Figure 5.21 - Pipe Strain Change and Temperature Change**

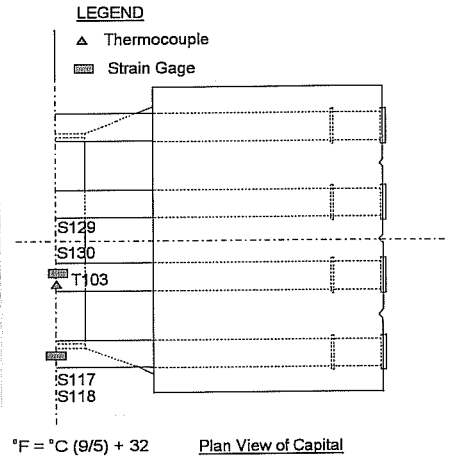
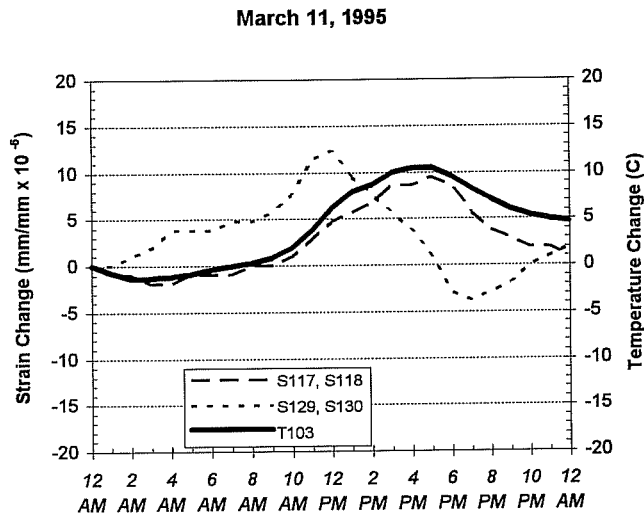


**Figure 5.22 - Pipe Strain Change and Temperature Change**

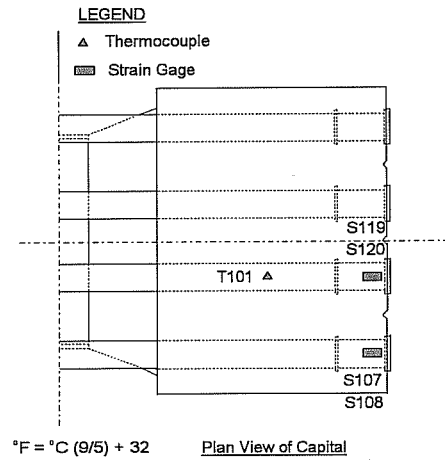
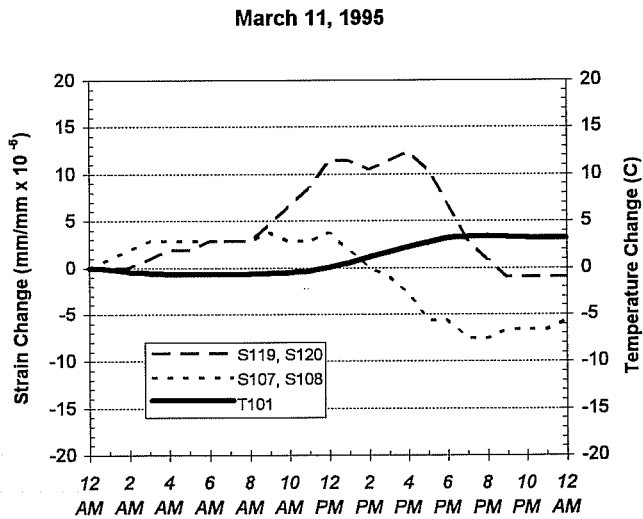


**Figure 5.23 - Pipe Strain Change and Temperature Change**

### 5.3.3 *Capital Strains - Typical Sunny Day*

Concrete strain device, strain gage, and thermocouple locations for the concrete portion of the capital are shown in Figure 5.24. Concrete strain device variations over the course of March 11, 1995, are shown in Figure 5.25 - Figure 5.27.

Figure 5.25 shows strain change for concrete strain devices located near the top of the capital. Interesting to notice is the fact that devices located near the surface on the outside face of the "Y" exhibit much larger strain changes throughout the day than do the devices located on the shell near the side face of the "Y" and in the core of the capital.

This supports the idea discussed in Section 5.2.4 concerning the effect of the expansion and contraction of the structural steel pipes due to temperature changes. In the morning, the temperature of the pipe is cooling. The pipes contract as they cool, pulling the "Y" together. Flexural tensile strains may be caused on the outside face of the "Y" due to this pulling. As the day progresses and pipe temperatures increase, the outside face of the "Y" experiences compressive strain changes due to the expansion of the "Y".

Figure 5.26 shows the strain changes over the course of a typical day for the concrete strain devices located in the middle section of the capital. Again, as with the devices located in the top of the capital, the strain changes associated with the outside face of the "Y" are larger than any other strain changes across the middle section.

The strain changes for concrete strain devices near the surface are less than those for strain devices located near the top of the capital. The devices located near the top of the capital are more affected by the expansion and contraction of the structural steel pipes over the course of the day.

Figure 5.27 shows strain changes over the course of the day for concrete strain devices located near the bottom of the capital. The strain changes across this section follow the same trends as for the sections located at the top and middle of the "Y".

For each of the sections shown in Figure 5.25 - Figure 5.27, the concrete strain devices located in the core of the "Y" exhibit compressive strain changes during temperature decreases and tensile strain changes during temperature increases. With the exception of strain device C122, the devices located in the shell exhibit behavior opposing the core

devices. Decreases in temperature cause tensile strain changes, and increases in temperature cause compressive strain changes.

This is consistent with the concept discussed in Section 5.2.3 which states that an ambient temperature increase causes the concrete located in the shell to undergo compressive strain changes and the concrete in the core to undergo tensile strain changes. Again, this is caused by the temperature lag existing across a given concrete section due to the massiveness and poor insulating properties of the concrete.

Figure 5.28 and Figure 5.29 compare strain variation over March 11 with temperature change. In each case, the temperatures depicted are measurements from thermocouples located very close to the strain devices from which strain variation was measured. In the case of strain devices located in the core, an average value of strain for two devices located on either side of the thermocouple was used.

Temperature trends are indicated by plots of thermocouples T104 - T107 as seen in Figure 5.28 and Figure 5.29. As the surface concrete is cooling during the early morning, the core concrete is heating up. This indicates a lag of heat transfer across the cross section of the pier due to the low conductivity of concrete. The surface concrete undergoes a large temperature increase in the afternoon. During this time, the core concrete is maintaining a fairly steady temperature. By the evening, the surface concrete is beginning to cool down. The core concrete is heating up in the evening; the afternoon heating trend of the surface is reaching the core at this time. As the core heats slightly in the early morning, compressive strains occur. As the shell concrete undergoes substantial temperature increase during the afternoon, the core is "pulled" along and tensile strains are induced in the core.

Depending on the time of day, the surface and core concrete are restraining each other from undergoing the desired expansion or contraction. This effect is indicated by the strain variation observed for each location. Strain gages located near the surface of the concrete exhibit compressive strain changes during heating of the concrete surface and tensile strain changes during cooling of the concrete surface. If the expansion or contraction of the concrete due to temperature changes were free, heating would cause tensile strain changes and cooling would cause compressive strain changes.

Figure 5.30 through Figure 5.35 show the variation of strain vertically along the capital. Figure 5.30 and Figure 5.31 show the variation of strain along the core of the

concrete. Each strain gage shows trends similar to those discussed above. Figure 5.32 and Figure 5.33 show variation of strain along gages located near the surface of the concrete on the side face of the “Y”. Figure 5.34 and Figure 5.35 show variation of strain along gages located near the surface of the concrete on the outside face of the “Y”. Important to notice is the much larger strain change exhibited by the gages located on the outside face of the “Y”.

Vertical strain variations appear to be consistent along each “vertical” line down the capital. This indicates that temperature effects are fairly consistent at each cross section where instrumentation was placed.

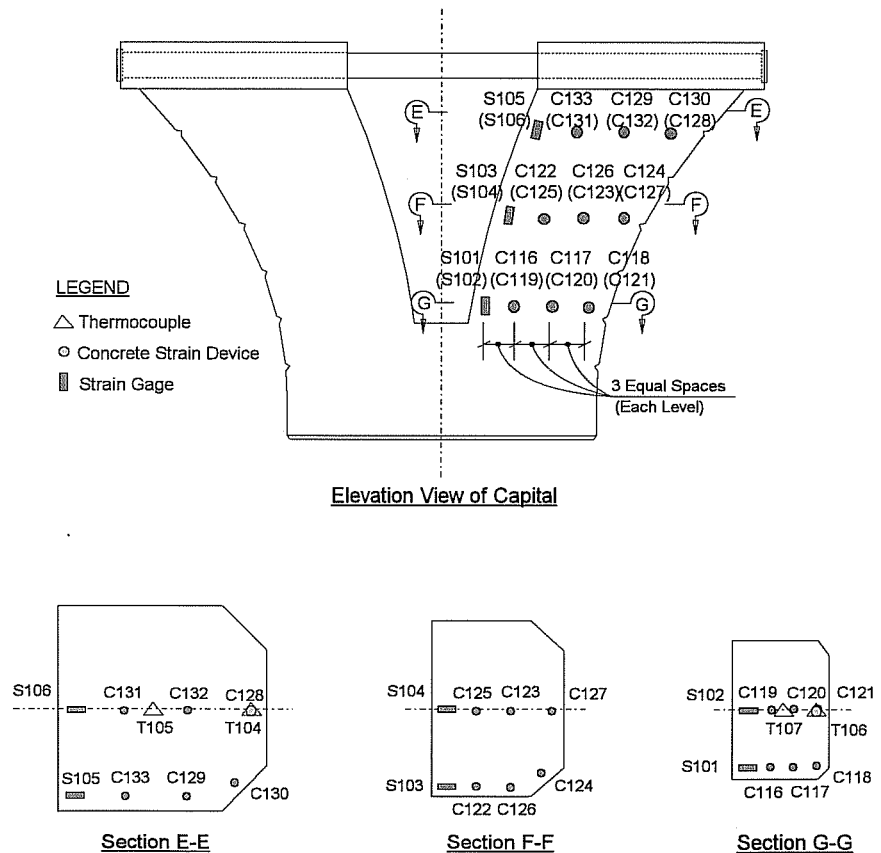
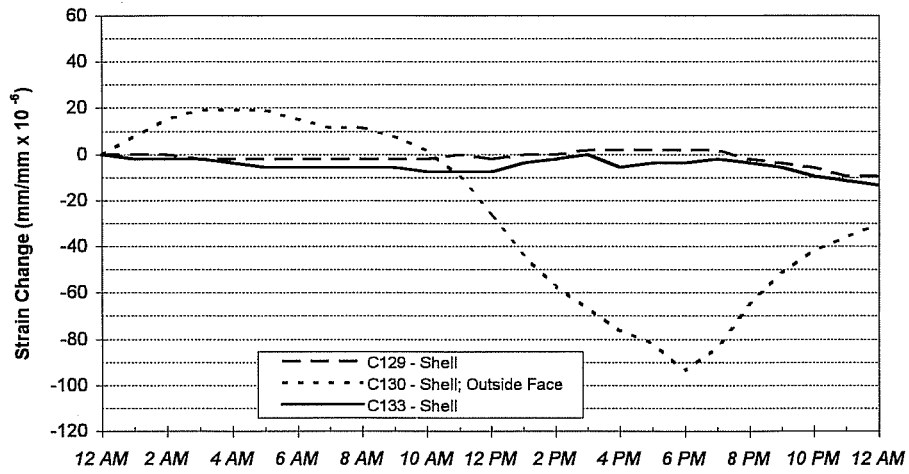


**Figure 5.24 - Capital Instrument Locations**

March 11, 1995



March 11, 1995

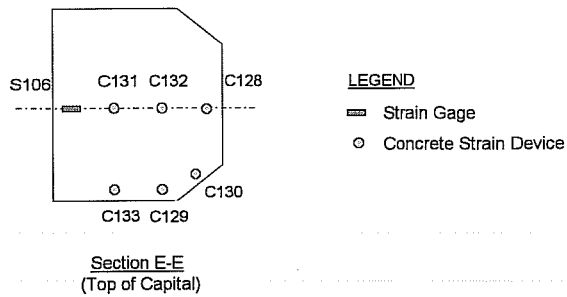
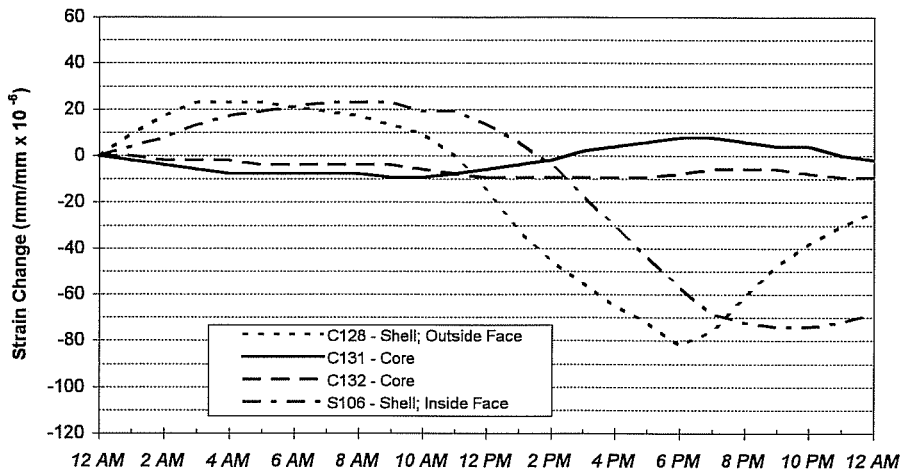
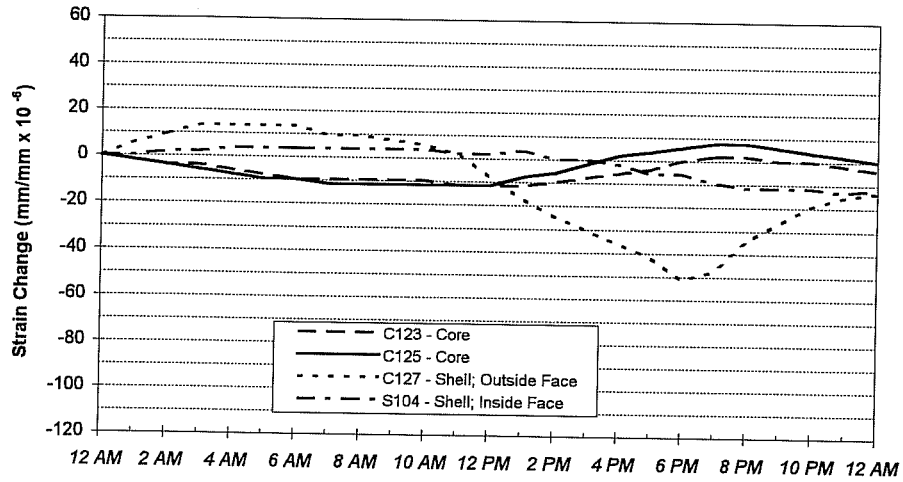


Figure 5.25 - Strain Variation Instruments Located in Top Section of Capital - Typical Sunny Day

March 11, 1995



March 11, 1995

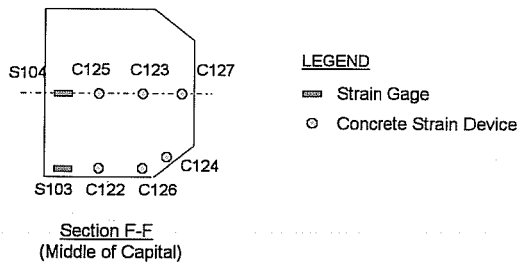
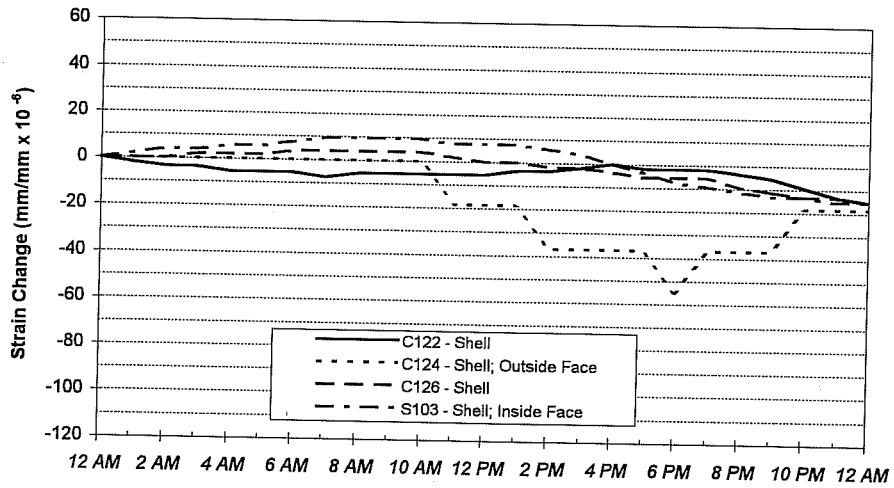
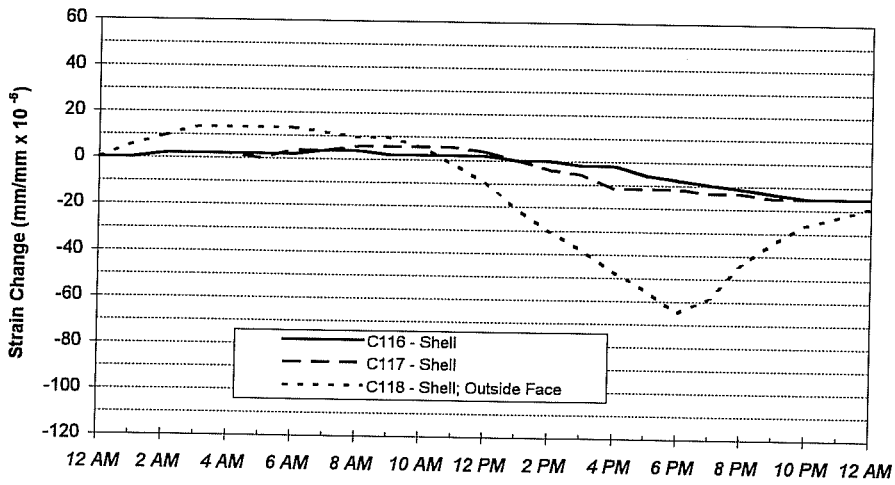


Figure 5.26 - Strain Variation Instruments Located in Middle Section of Capital - Typical Sunny Day



March 11, 1995



March 11, 1995

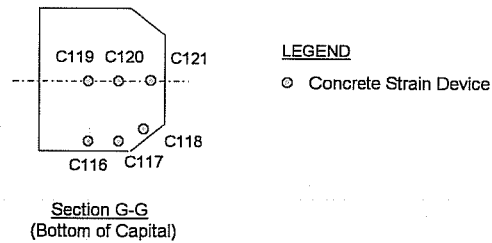
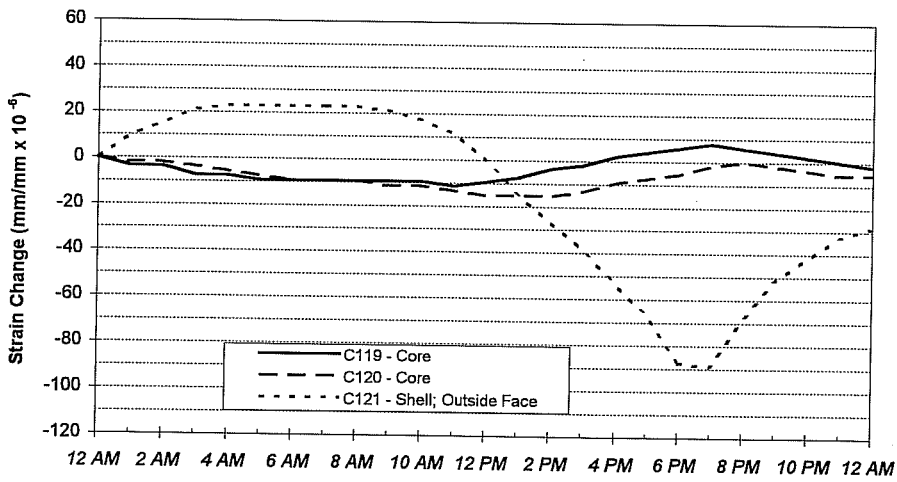


Figure 5.27 - Strain Variation Instruments Located in Bottom Section of Capital - Typical Sunny Day

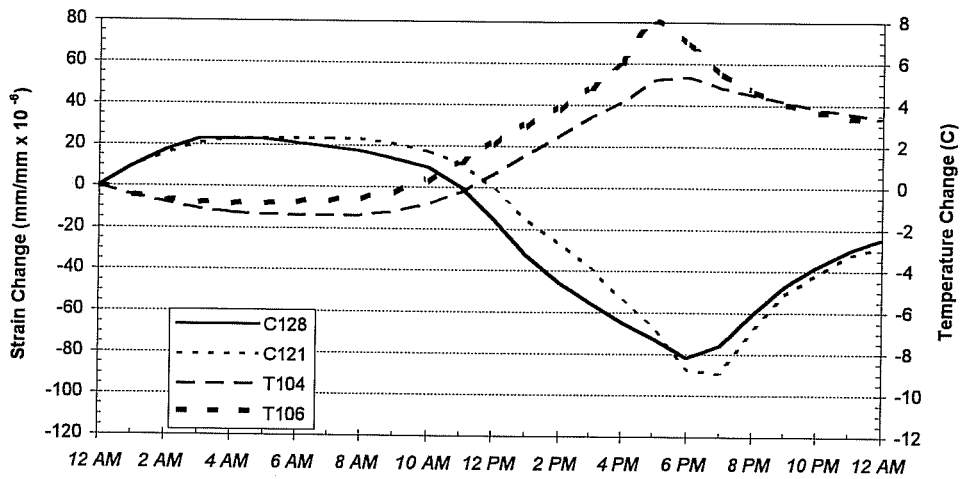


Figure 5.28 - Comparison of Temperature Change and Strain Variation for Instruments Located Near the Top of the Capital

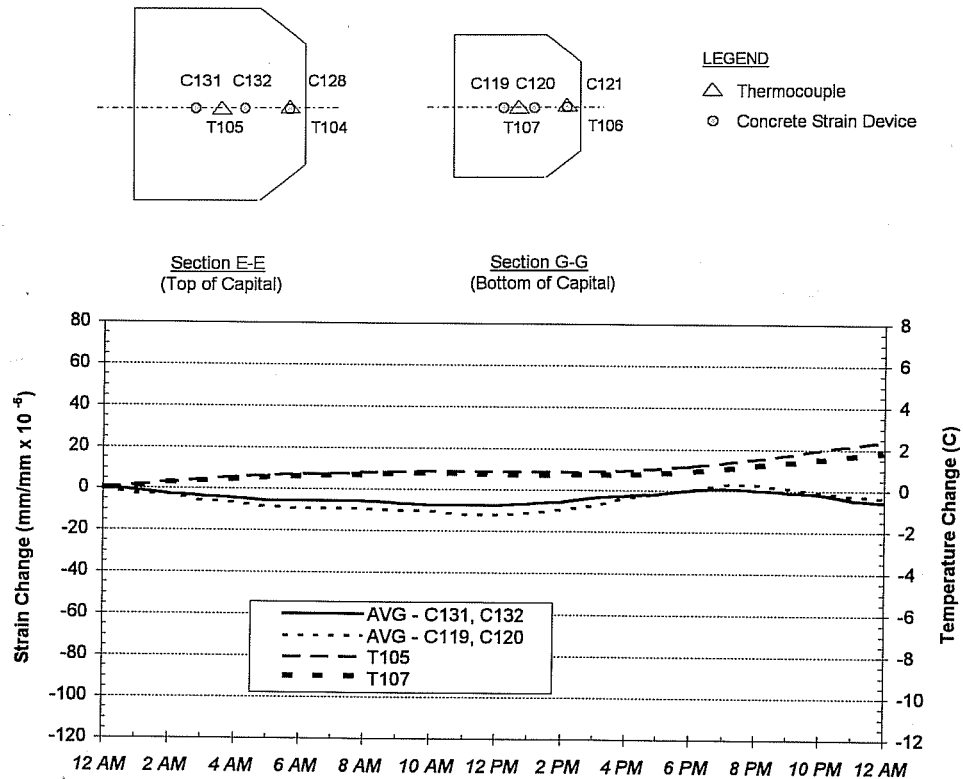
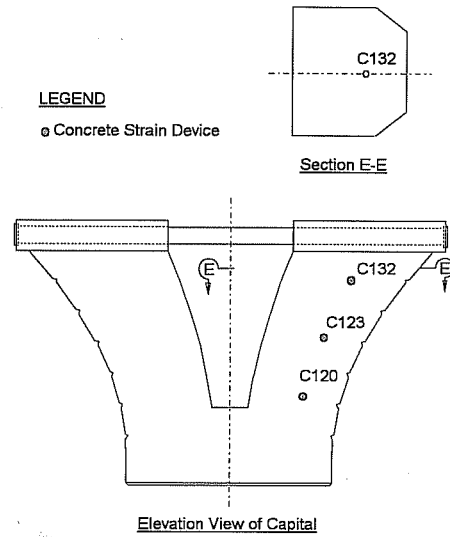
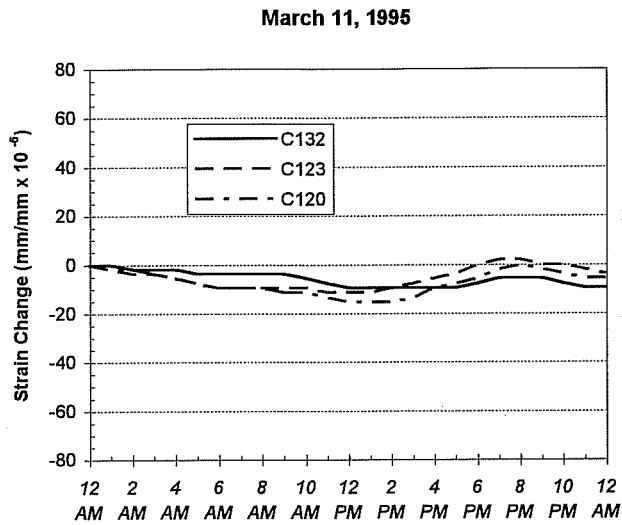
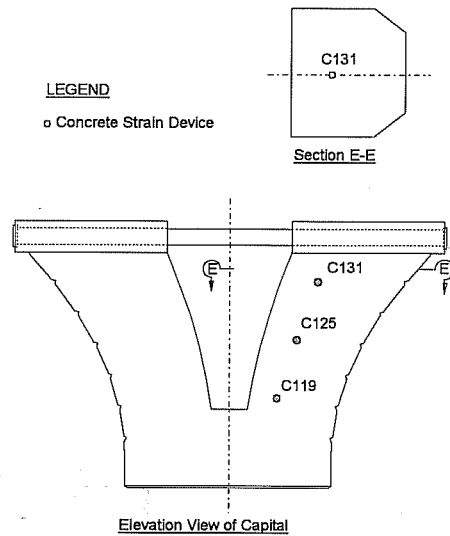
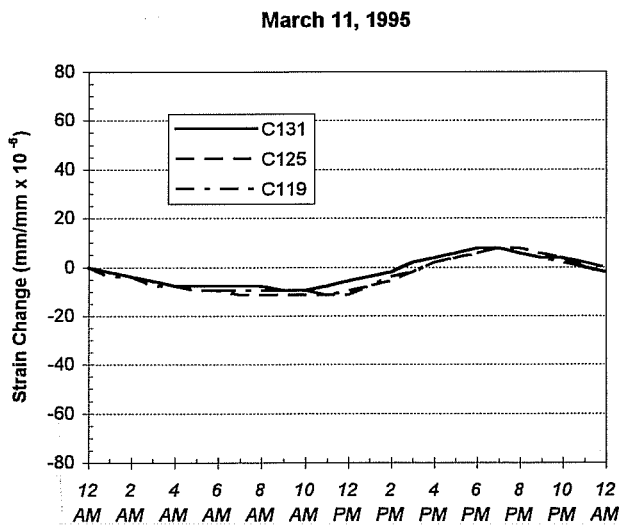


Figure 5.29 - Comparison of Temperature Change and Strain Variation for Instruments Located Near the Bottom of the Capital



**Figure 5.30 - Variation of Strain Vertically Along the "Y": Concrete Core**



**Figure 5.31 - Variation of Strain Vertically Along the "Y": Concrete Core**

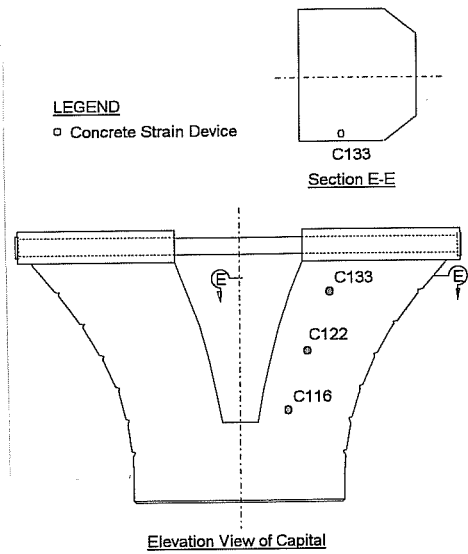
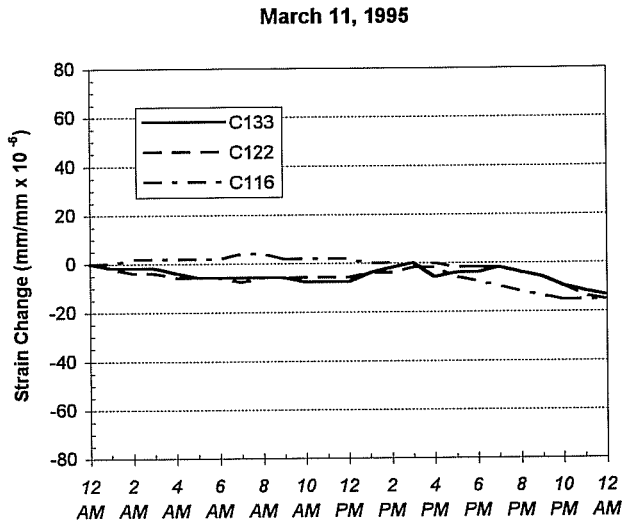


**Figure 5.32 - Variation of Strain Vertically Along the "Y": Concrete Shell**

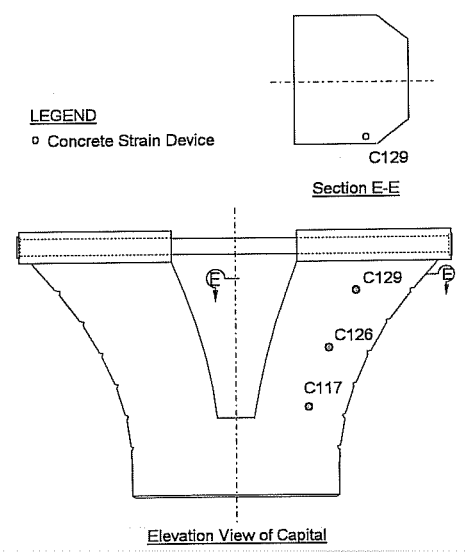
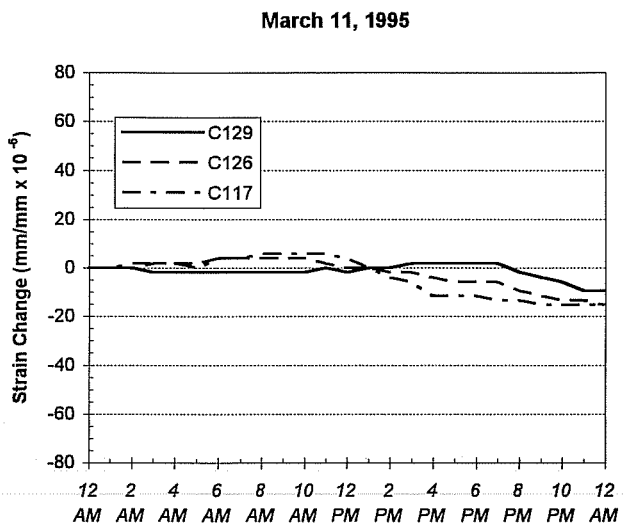
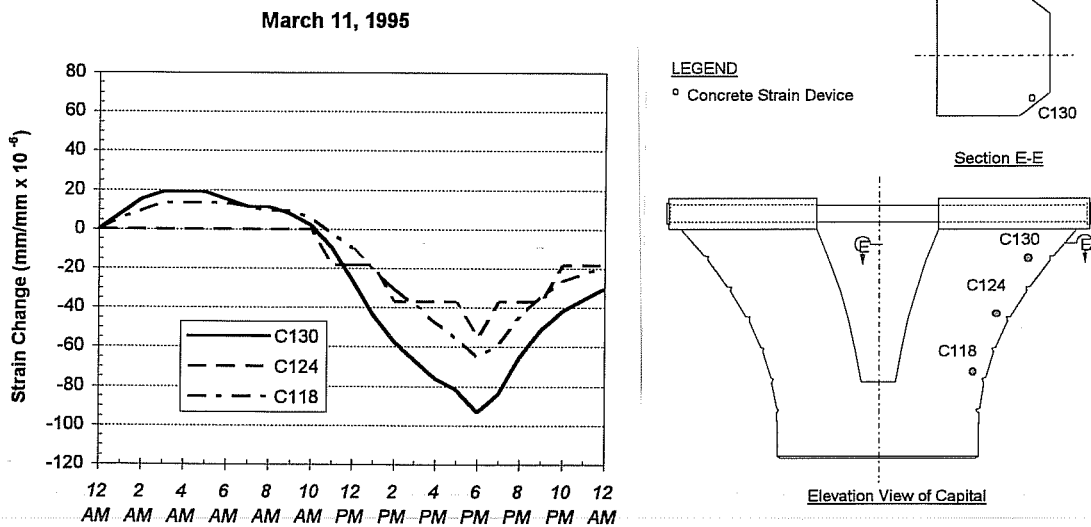
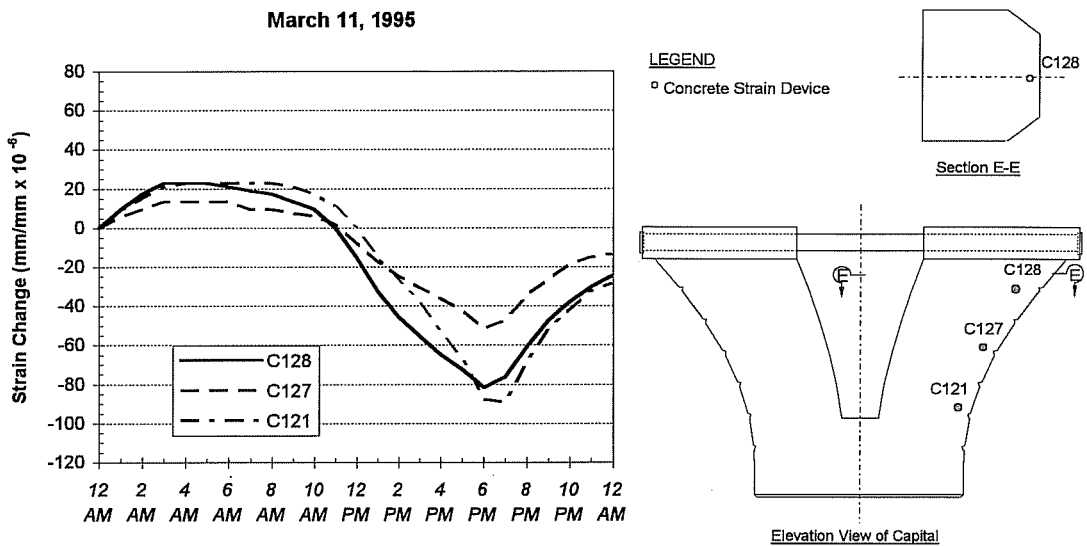


**Figure 5.33 - Variation of Strain Vertically Along the "Y": Concrete Shell**



#### *5.3.4 Shaft Strains - Typical Sunny Day*

The locations of concrete strain devices in the column portion of pier D6 are shown in Figure 5.36. Strain changes for these devices for March 11, 1995, are shown in Figure 5.37 through Figure 5.39. Negative strain variations indicate compressive strains.

Figure 5.37 shows strain changes over the course of a typical day for concrete strain devices located near the top of the column or "shaft" portion of the pier. The devices located in the shell of the pier exhibit tensile strain changes during temperature increases and compressive strain changes during temperature decreases. Compressive strain changes occur in the core during temperature increases. As temperatures decrease, core devices indicate tensile strain changes.

Interesting to note is the fact that the concrete strain device located on the corner of the shell, C112, undergoes a much larger strain change in the afternoon than do any of the other strain devices in this section. This may be due to the orientation of the pier with respect to the sun. Strain device C112 is approximately perpendicular to the afternoon sun.

Figure 5.38 shows strain changes for devices located near the middle of the column. Behavior similar to that seen in the top of the column can be observed here. As in the section located near the top of the column, the strain device C106 indicates much higher strain changes in the afternoon than do other gages in the shell of the column.

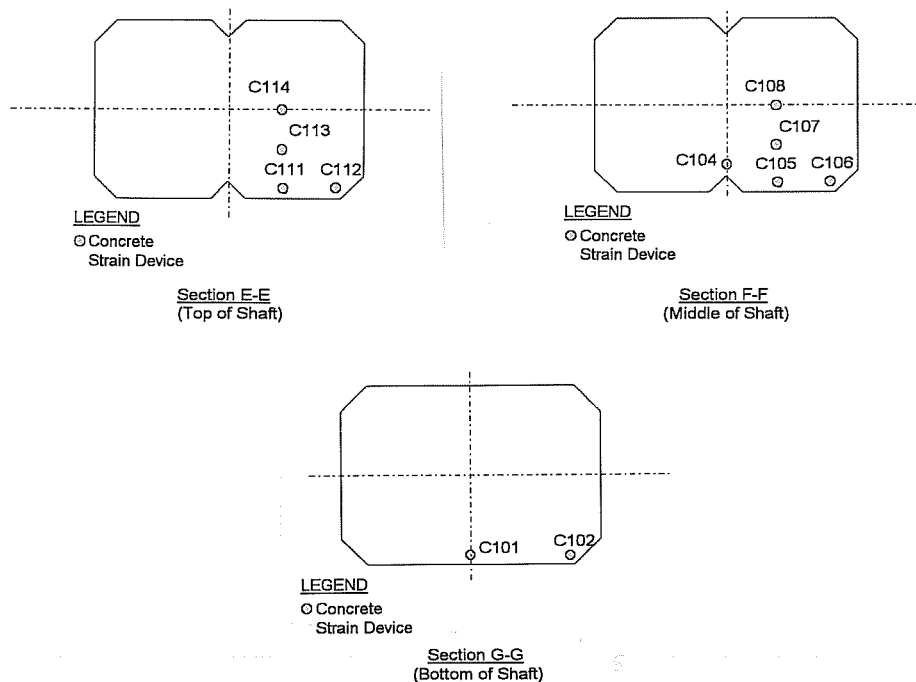
Figure 5.39 shows strain changes for concrete strain devices located at the bottom of the column. These devices exhibit similar behavior to the top and middle sections of the column. These devices are below grade, and as a result are less affected by the sun's radiation than devices at other levels. Device C102, located on the corner of the pier, exhibits larger strain changes than C101.

Thermocouples were not installed in the shaft of pier D6. If the assumption is made that the surface temperature of the column is approximately the same as the surface temperature of the capital, a comparison of temperature change and strain variation of instruments located near the surface of the concrete can be made. Figure 5.40 shows a comparison of instruments C112 and T104 during March 11. As the surface of the concrete heats up in the afternoon, a compressive strain change takes place. As mentioned in Section 5.3, this is due to the uneven heating and cooling trends across the section of the concrete.

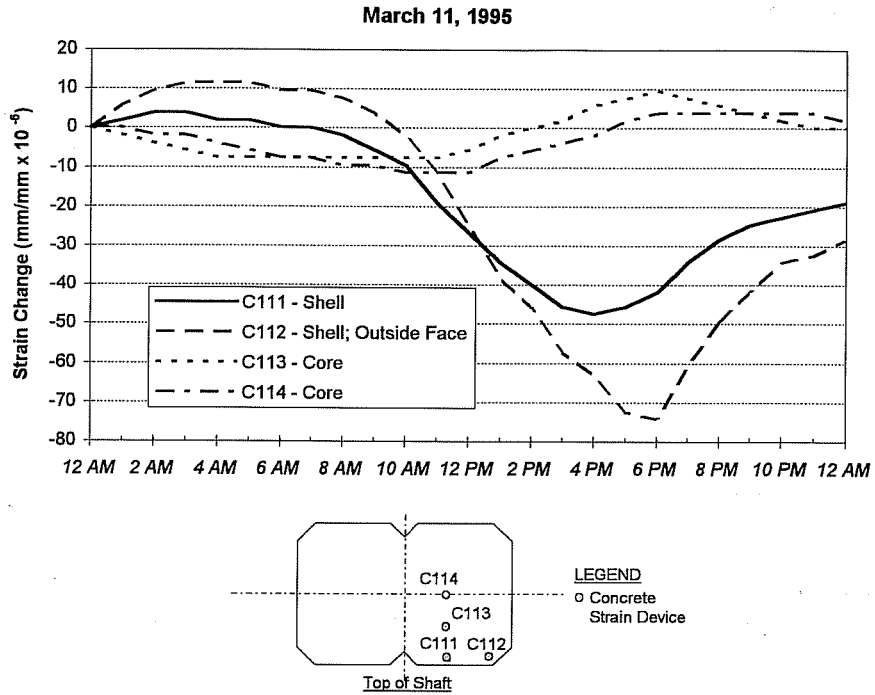
Figure 5.41 shows a comparison of instruments C113, T105, and T104. Instruments C113 and T105 are located in the core concrete. Instrument T104 is located near the surface. The assumption is made that the behavior of the column core and capital core is similar.

Figure 5.42 and Figure 5.43 show strains tracked vertically through the column. Instruments C102, C106, and C112 are shown in Figure 5.42. These instruments undergo fairly large strain changes throughout the day. Instrument C102 is less affected by temperature since it is located below grade and is therefore insulated from the sun.

Instruments C107 and C113 are shown in Figure 5.43. These core instruments do not exhibit strain changes as large as the instruments located near the concrete surface.



**Figure 5.36 - Locations of Instruments in Column**



**Figure 5.37 - Strain Variation: Top of Column**

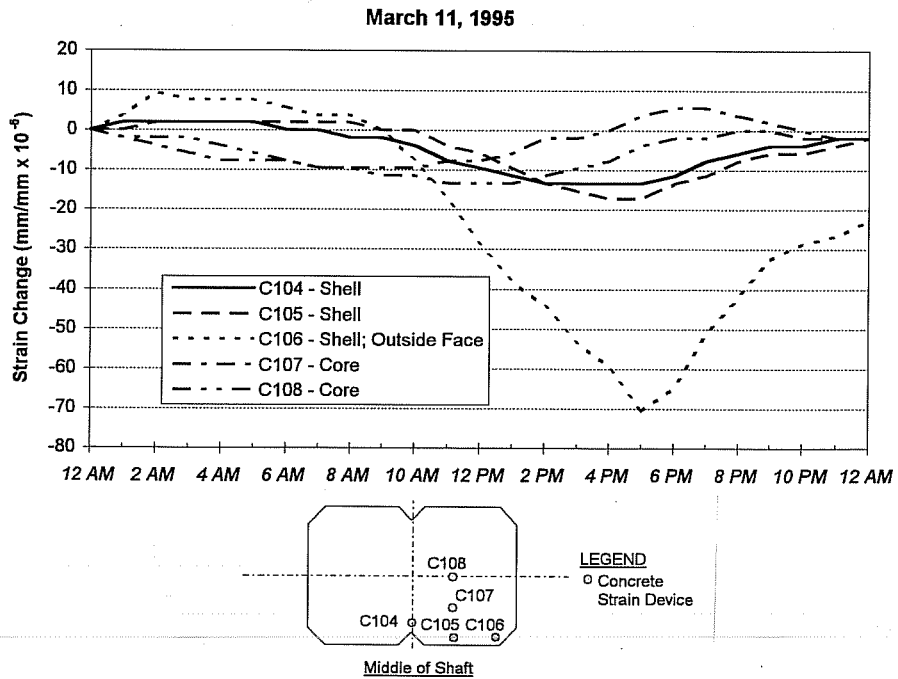


**Figure 5.38 - Strain Variation: Middle of Column**



March 11, 1995

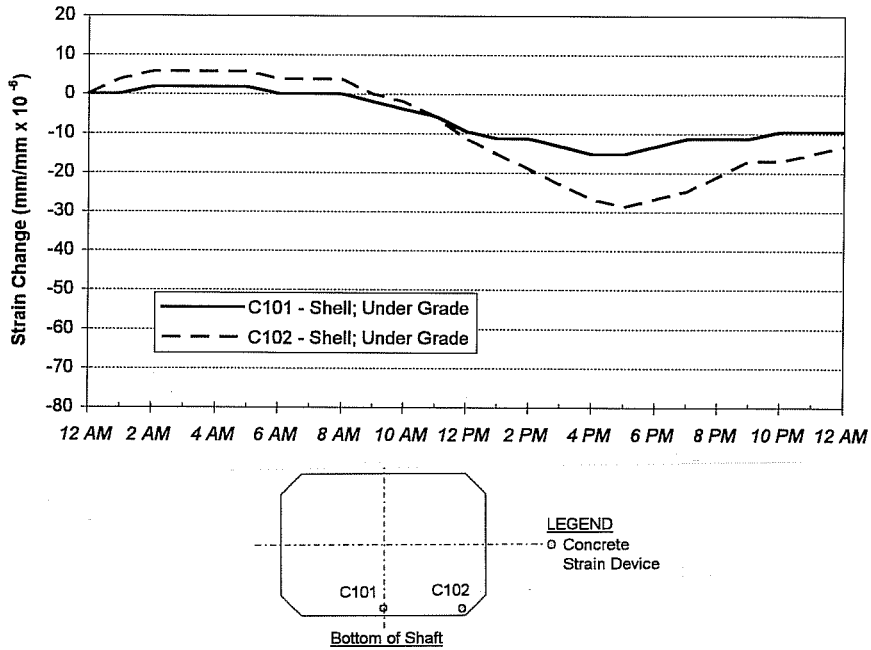


Figure 5.39 - Strain Variation: Bottom of Column

March 11, 1995

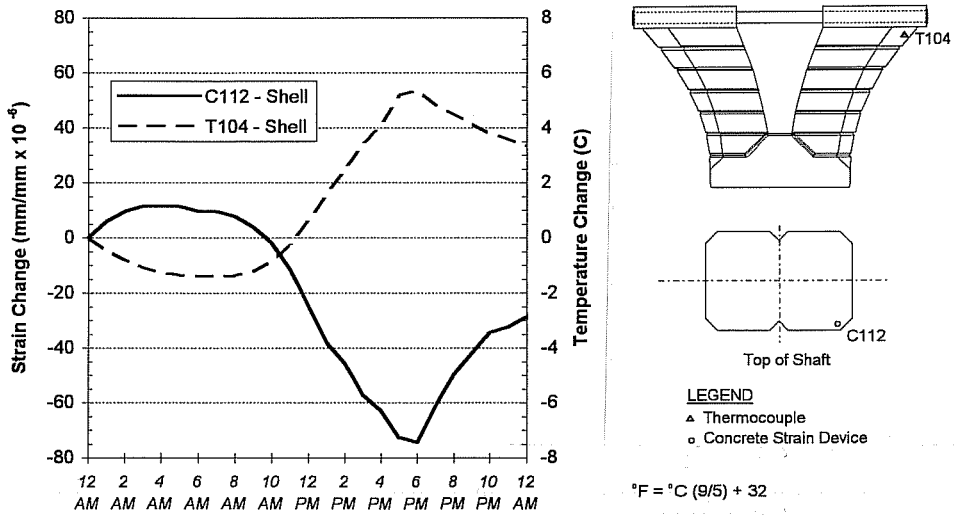


Figure 5.40 - Comparison of Column Strain Variation and Surface Temperature Change: Concrete "Shell"

March 11, 1995

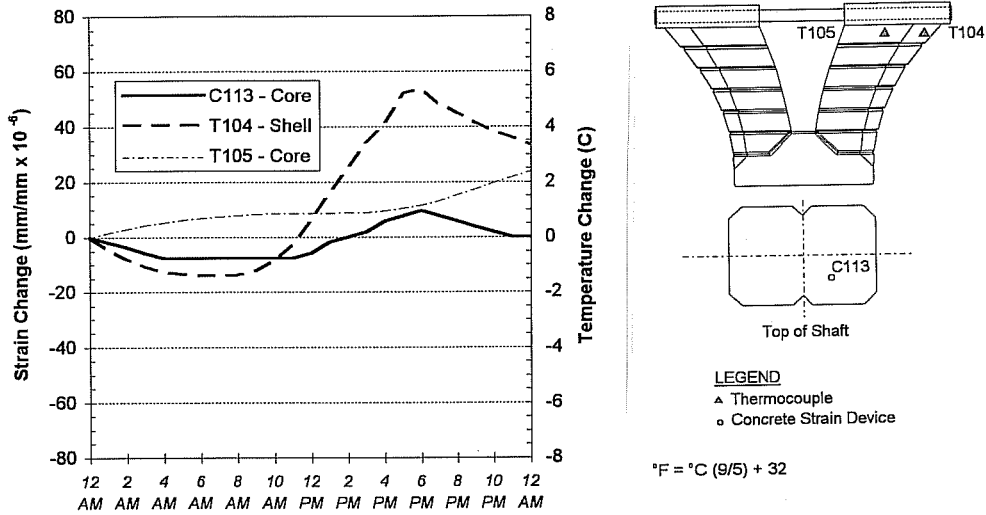


Figure 5.41 - Comparison of Column Strain Variation and Surface Temperature Change: Core Concrete

March 11, 1995

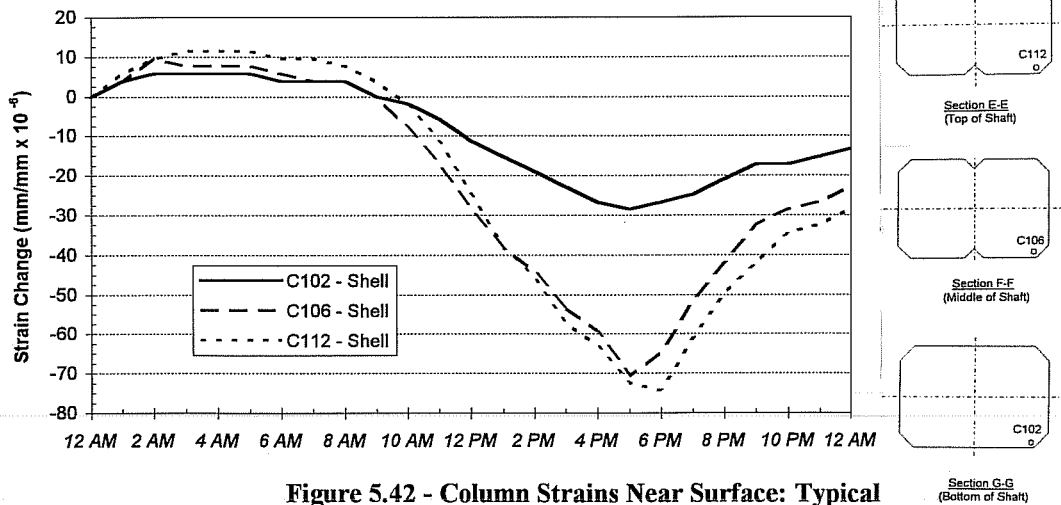


Figure 5.42 - Column Strains Near Surface: Typical

March 11, 1995

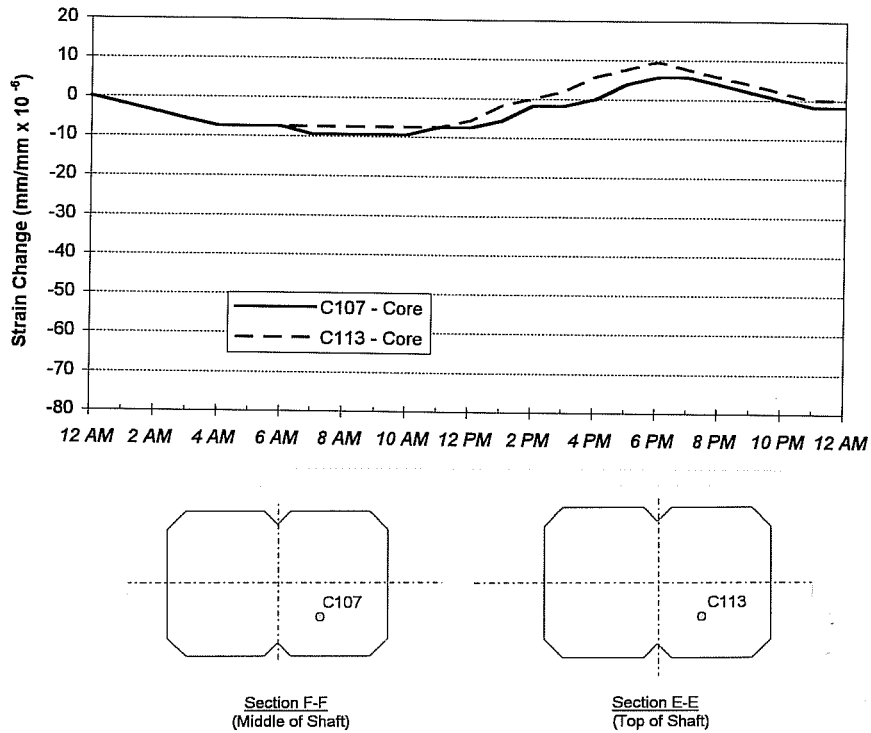


Figure 5.43 - Column Strains in Core: Typical

#### 5.4 Measurements - During Superstructure Erection

This section presents field measurements made during the erection of Spans 5 and 6 of US 183, both of which are supported by Pier D6. The purpose of this section is to present the total strains on Pier D6 due to combined thermal and gravity loads during erection of the superstructure over the instrumented pier. These spans were erected over a period of eleven days, from March 16 - 26, 1995. Because of this, the total measured strain changes due to total load include thermal as well as gravity strains. Separation of thermal strains from total measured strains in order to compare measured forces with those predicted by a strut-and-tie model is discussed in Chapter 6.

Span 5 was the first span erected and placed on the bearings of the instrumented pier. The erection process for this span was monitored closely during stressing until the

span was placed on the bearings. Continuous hourly readings were taken after Span 5 erection through the erection of Span 6. The construction process is discussed in Chapter 4.

The erection schedule for Spans 5 and 6 is shown in Table 5.1. The initial load on the shaft occurred on March 17 with the placement of the truss for erection of Span 5. The initial load on the capital and on the structural steel pipes occurred on March 22 with the stressing of the post-tensioning tendons in Span 5 when the spans begin to be supported on the bearings.

#### *5.4.1 Temperature Measurements*

Ambient temperatures measured during the erection of the superstructure are shown in Figure 5.44a. A slight warming trend occurred during the time period from March 16 - 26. Temperatures measured during this time from thermocouples located in the capital and on the structural steel pipes of the pier are shown in Figure 5.45 - Figure 5.48. The general warming trend exhibited for the ambient temperature is reflected in each of the thermocouples.

Temperatures measured from thermocouples located on the structural steel pipe are shown in Figure 5.45. Thermocouple T103, located in the center of the structural steel pipe, was most directly affected by ambient temperature change. Thermocouple T102, located at the concrete/steel interface experienced less temperature change than T103. Thermocouple T101 is embedded in the concrete and exhibits the least temperature change of the thermocouples located on the pipe. This temperature trend is consistent with thermal trends discussed in Section 5.3. The concrete surrounding the pipe insulates the pipe from the sun's radiation and absorbs heat from the exposed portion of the pipe.

Temperatures from thermocouples T104 and T105, located near the top of the capital, are shown in Figure 5.46. Daily temperature fluctuations for thermocouple T104 are greater than those for T105. This is due to the fact that thermocouple T104 is located in the shell of the concrete and T105 is located in the core.

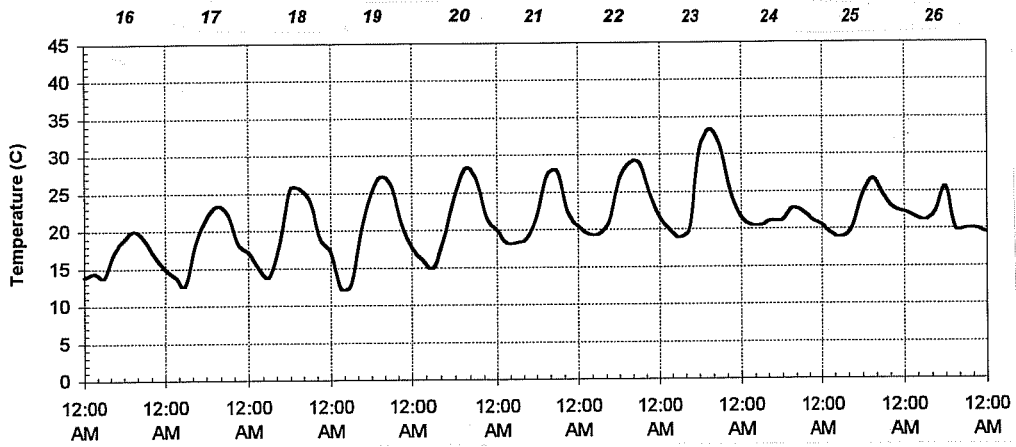
Figure 5.47 shows temperatures measured from thermocouples T106 and T107. These thermocouples are located near the bottom of the capital with the same relative position as T104 and T105, respectively. Thermocouples T106 and T107 exhibit trends and temperatures very similar to T104 and T105.

Temperature measurements across the concrete capital section as measured for the 5 days of erection operations indicate that the daily maximum temperature gradient as shown in Figure 5.44b across the concrete capital section varied from +5 °C (9 °F) to -3 °C (5.4 °F). A positive gradient indicates that the shell is warmer than the core.

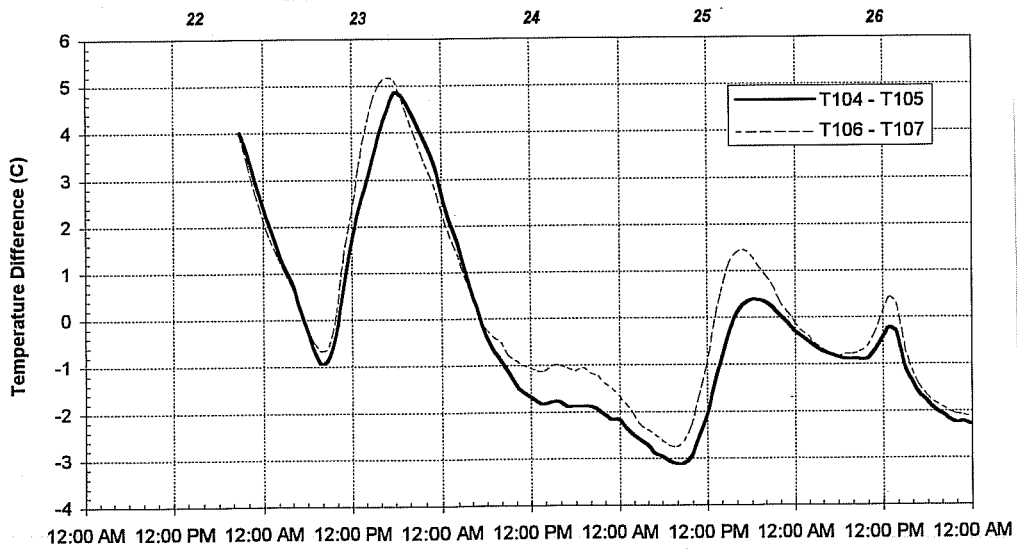
Temperatures measured from T108 and T109 are shown in Figure 5.48. Neither of these thermocouples show large temperature fluctuations. Although T108 is located near the surface of the concrete, the shade provided by the capital during the latter part of the day protects it from the temperature fluctuations experienced by other thermocouples located near the surface of the concrete.

**Table 5.1 - Superstructure Erection Sequence Over Pier D6**

EVENT	DATE
Truss advanced to Pier D6 for Span 5 Erection	March 17, 1995
Span 5 segments placed on truss	March 17 - 19, 1995
Instrumentation of Span 5 (Data acquisition system disconnected)	March 19 - 22, 1995
(Data acquisition system re-connected) Span 5 segments post-tensioned	March 22, 1995
Hydraulic jacks released - Span 5 placed on Pier D6 bearings	March 22, 1995 (Approximately 8:00 P.M.)
Truss advanced for Span 6 erection; segments placed on truss and post-tensioned	March 23 - 26, 1995
Hydraulic jacks released - Span 6 placed on Pier D6 bearings	March 26, 1995 (Approximately 8:00 P.M.)

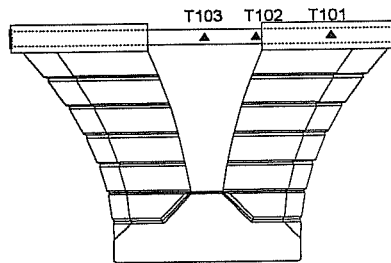
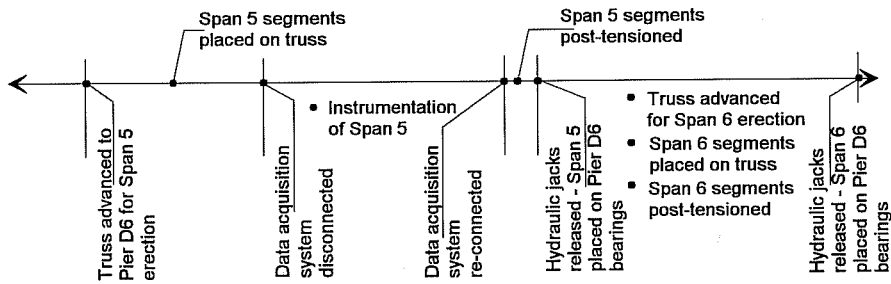
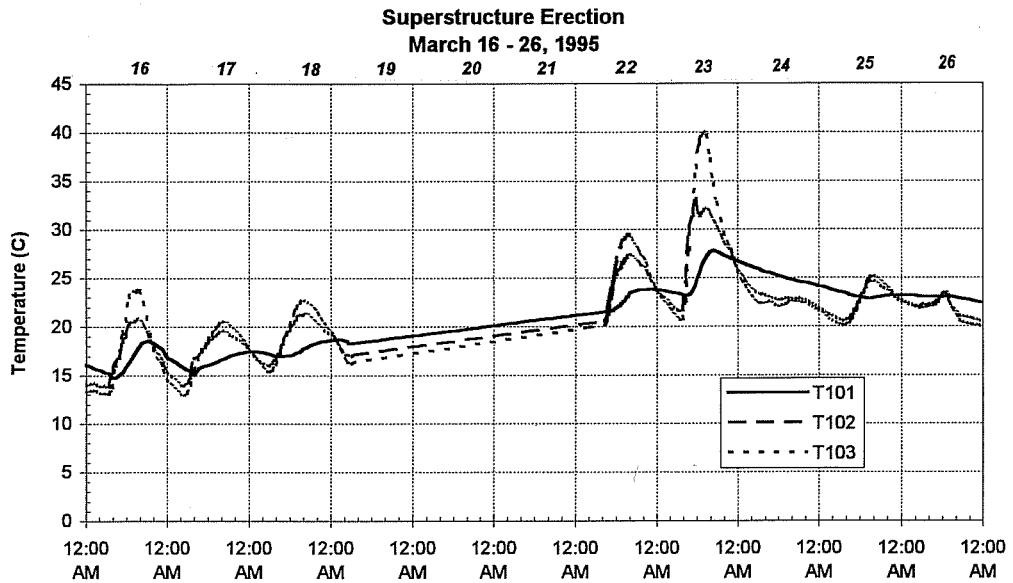


a) Ambient Temperatures - Superstructure Erection, March 16-26, 1995



b) Temperature Gradient Across Concrete, March 22-26, 1995

Figure 5.44 Temperature Readings During Superstructure Erection



**LEGEND**  
▲ Thermocouple

$$^{\circ}\text{F} = ^{\circ}\text{C} (9/5) + 32$$

**Figure 5.45 - Temperatures Measured on the Structural Steel Pipe During Construction**



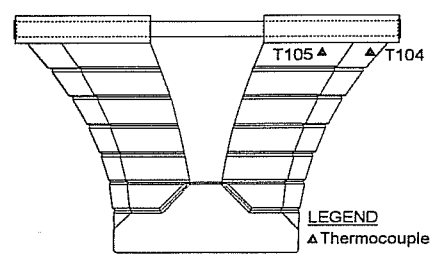
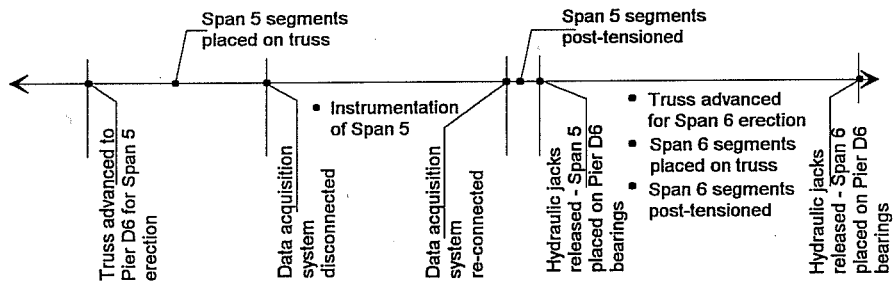
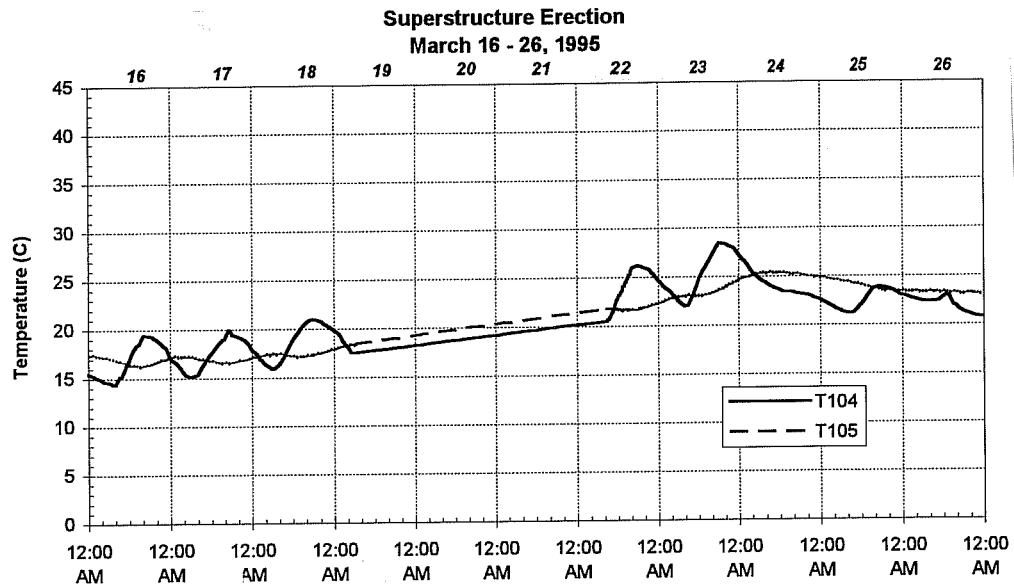


**Figure 5.46 - Concrete Temperatures Measured Near the Top of the Capital During Construction**

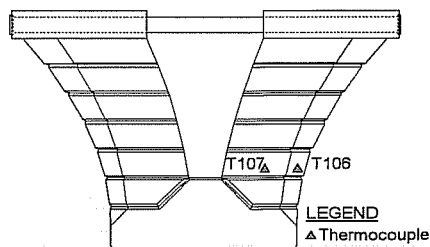
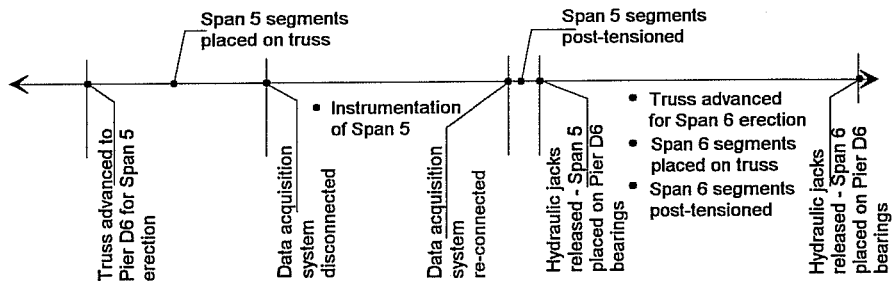
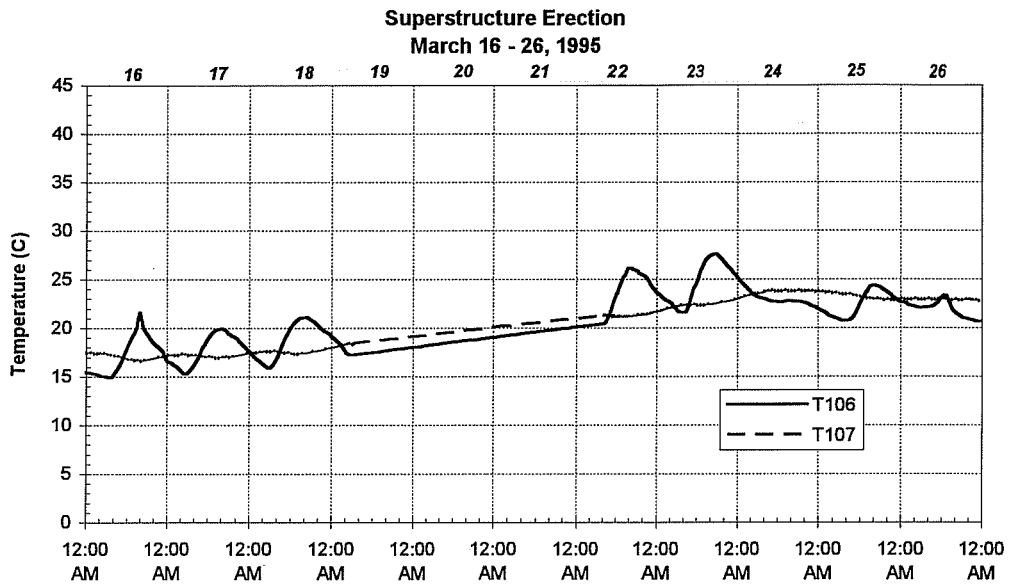


**Figure 5.47 - Concrete Temperatures Measured Near the Bottom of the Capital During Construction**

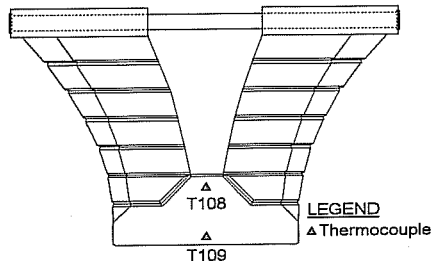
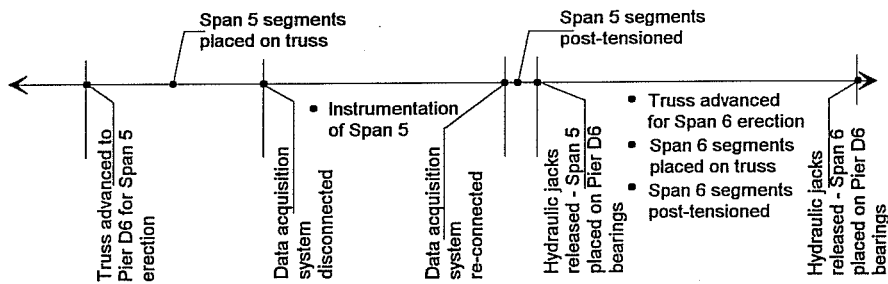
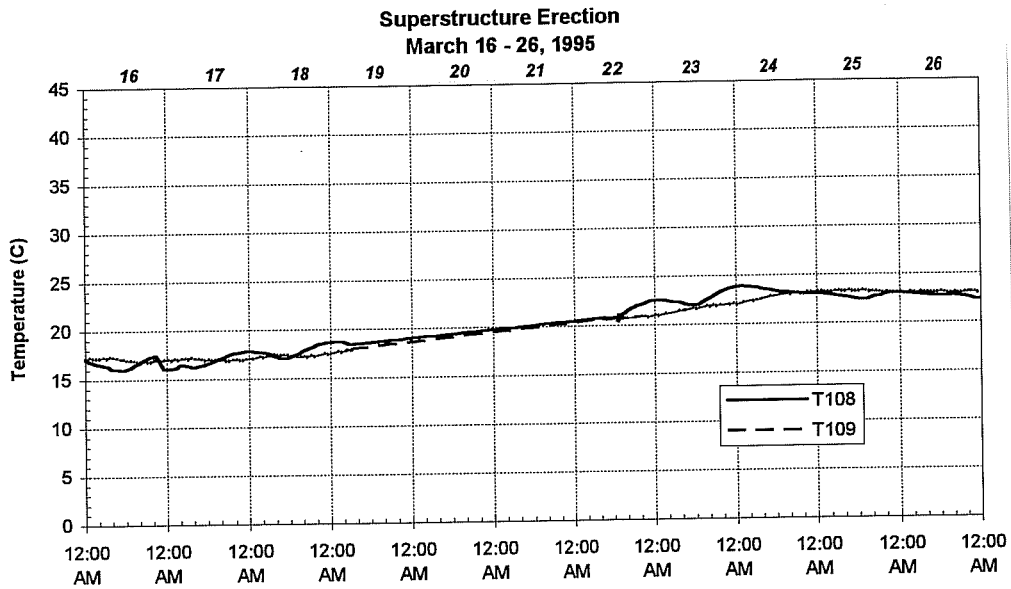


**Figure 5.48 - Concrete Temperatures Measured at the Base of the Capital During Construction**

#### **5.4.2 Structural Steel Pipe Strains**

The strain change measured on the structural steel pipes during the superstructure erection is shown in Figure 5.49 and Figure 5.50. The initial point of these plots was taken immediately prior to stressing, before any load had been transferred to the bearings of the pier.

During stressing of the tendons in Span 5, some load is transferred to the pipes. A small tensile strain change is exhibited during this time period in all locations except at the ends of the pipes.

As Span 5 is placed on the bearings of the pier, a tensile strain change occurs along the pipes. Strain gages located in the center of the pipes (S129, S130 and S117, S118) exhibit the largest strain change. Strain gages located at the concrete/steel interface (S125-S128 and S113-S116) also exhibit a significant tensile strain change due to Span 5 placement on the bearings. The strain change is, however, smaller than that exhibited at the center of the pipes.

The force due to loading is dissipated along the entire pipe length. Along the length of the pipe, the strain change due to loading approaches zero as the gage distance from the centerline of the pier increases. The strain change is dissipating along the length of the pipe because the load is being transferred to the concrete along the length of the pipe. A large portion of the force is dissipated between the concrete/steel interface and the next set of gages along the pipe (S123, S124 and S111, S112). Beyond this point, the strain change due to loading is very close to zero.

As Span 6 was placed on the bearings, the strain gages at the center (S129, S130 and S117, S118) and at the concrete/steel interface (S125-S128 and S113-S116) exhibited approximately the same tensile strain change. The strain change due to Span 5 loading was larger than that due to Span 6 since the instrumented pipes are located on the Span 5 side of the pier. A small tensile strain change in strain devices S123, S124 and S111, S112 was exhibited. The strain gages located at the ends of the pipes exhibited virtually no strain change due to Span 6 loading.

Both pipes exhibit similar total strain changes along their lengths. Trends in strain change during construction are also similar. Total strain change measured due to thermal

and gravity loading is less for the interior pipe. This could be due to the fact that the interior pipe is more insulated by the concrete.

#### **5.4.3 Capital Strains**

Strain measurements made in the capital are shown in Figure 5.51 - Figure 5.53. Strain change during the superstructure erection was made by assuming an initial point directly prior to stressing of Span 5 tendons. Figure 5.51 shows strain change at a section near the top of the capital. Figure 5.52 shows strain change at a section near mid-height of the capital. Strain change near the bottom of the capital is shown in Figure 5.53.

Prior to stressing, the erection truss and the segments are supported at the bottom of the “Y”. Strain change in the compressive direction occurred for most strain devices as the tendons of Span 5 were stressed. This indicates that the span is being partially supported by the capital during stressing.

When the hydraulic jacks are released and Span 6 is placed on Pier D6 bearings, a significant compressive strain change is seen in strain devices along the centerline of the pier. Strain devices located on the Span 5 side of the pier show small tensile strain changes due to placement of Span 6 on the pier bearings.

Consistently, strain devices located closer to the transverse centerline of the pier (C119, C125, C131) show a lower compressive strain change than those devices located toward the outside face of the capital (C121, C127, C128). This is likely due to the expansion and contraction of the pipe caused by temperature changes.

Also, strain devices located in the concrete core (C131, C132; C119, C120; C125, C123) show small fluctuation in daily strain change due to what appears to be thermal strains. On March 23, the load on the capital is approximately constant. During the second half of the day, as ambient temperature is increasing, devices C119 and C120 show small tensile strain change. Device C121, which is located in the shell of the concrete, shows a large compressive strain change during the same period.

These trends in strain change follow thermal effects discussed in Section 5.2. Across a section of the concrete, as ambient temperature increases the shell is put into compression and the core into tension. This is due to the temperature lag across the section caused by the fact that the concrete is so massive. The expansion of the pipe during this

time period causes large compressive strains in devices located on the outside face of the “Y”.

Figure 5.54 - Figure 5.56 show a comparison of strain devices located on the transverse centerline of the capital in the same relative position in each respective section of the capital. Each “vertical line” of strain devices shows very similar behavior, indicating that the devices are positioned along the load path. Again, devices located on the outside face of the “Y” (C121, C127, C128) exhibit larger strains than devices located in the core (C119, C125, C131).

**Superstructure Erection**  
**March 22 - 26, 1995**

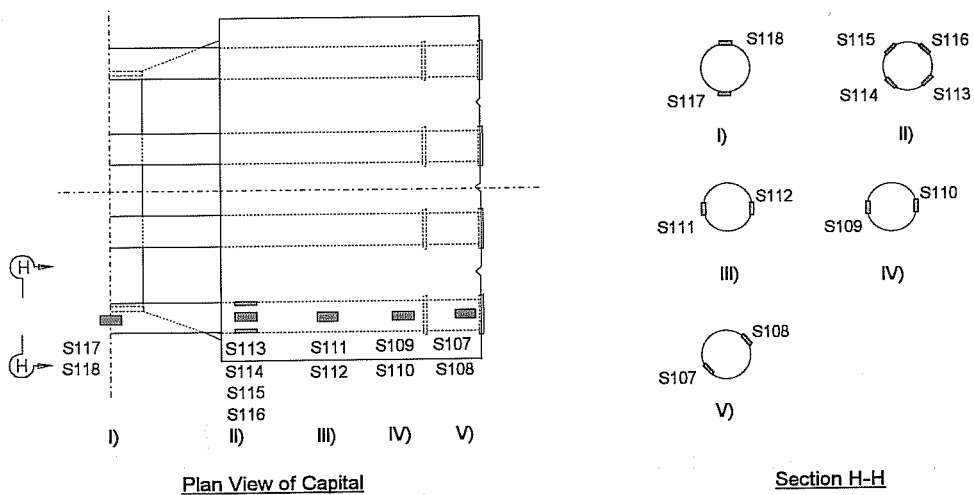
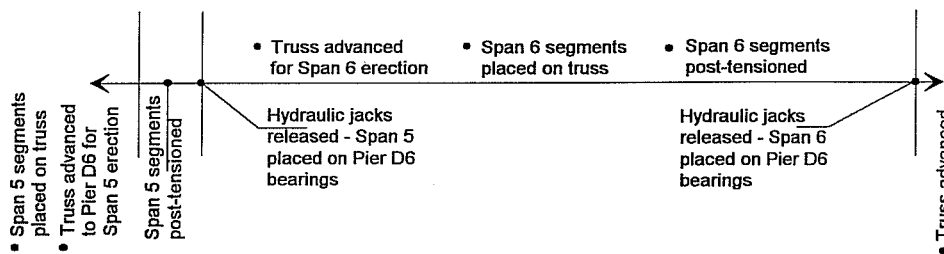
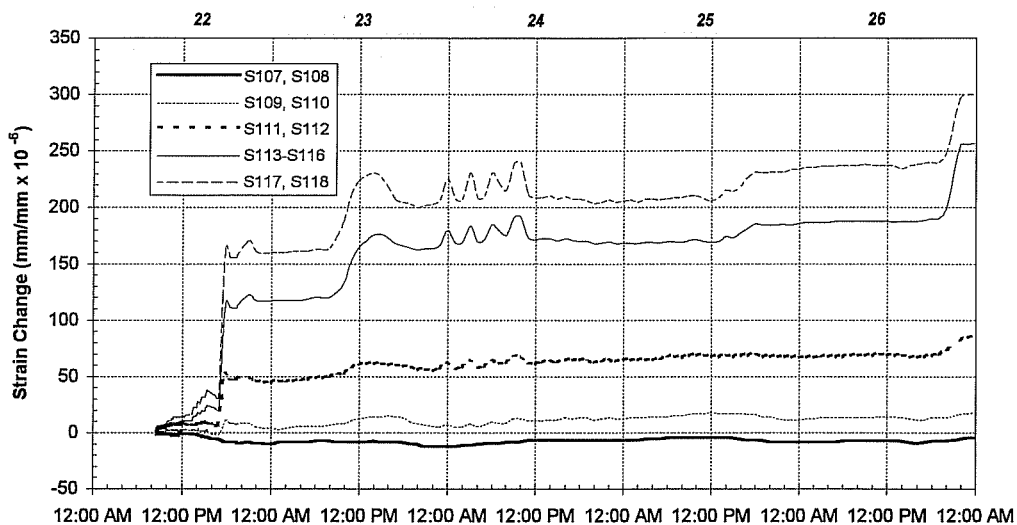
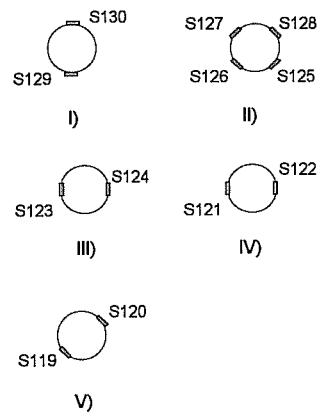
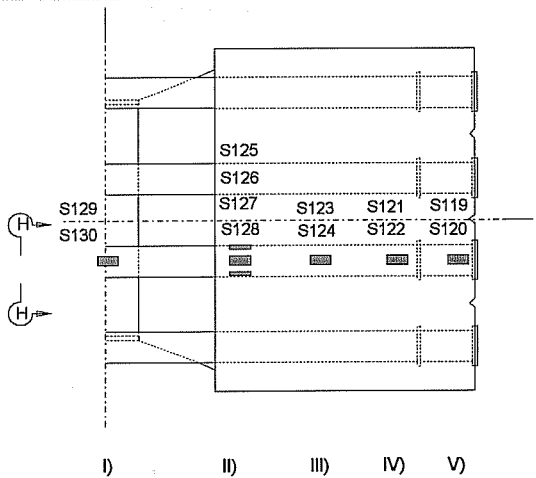
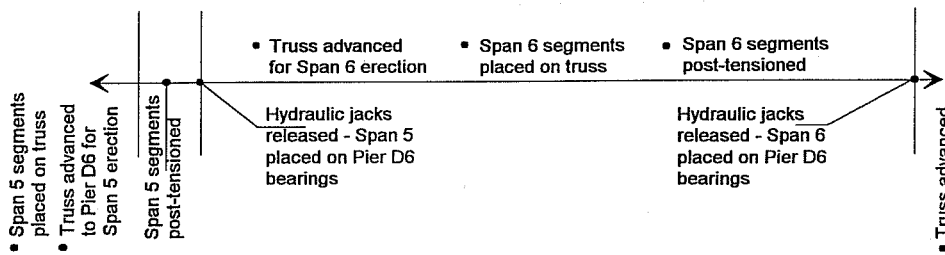
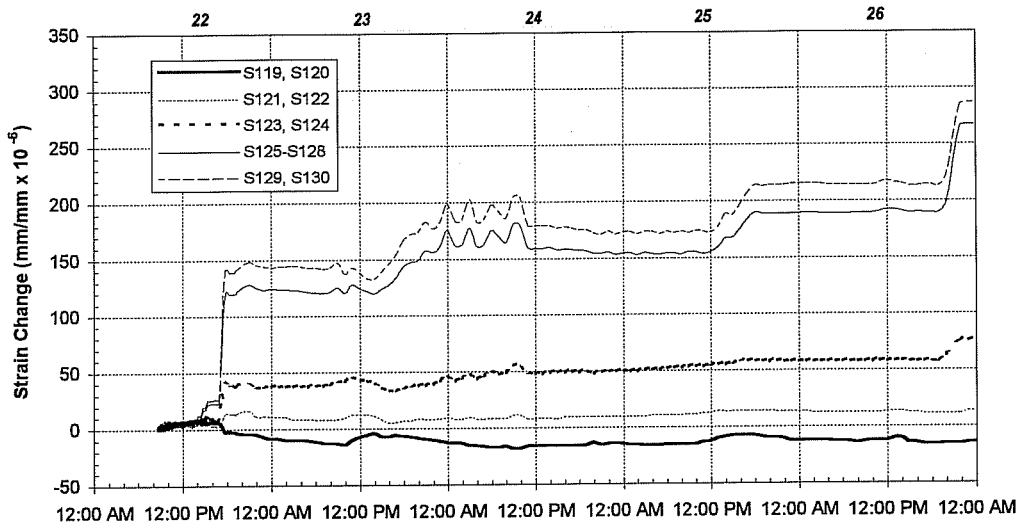


**Figure 5.49 - Strain Change Measured in the Interior Structural Steel Pipe During Construction**

**Superstructure Erection  
March 22 - 26, 1995**



Plan View of Capital

Section H-H

**Figure 5.50 - Strain Change Measured in the Exterior Structural Steel Pipe During Construction**



**Superstructure Erection**  
**March 22 - 26, 1995**

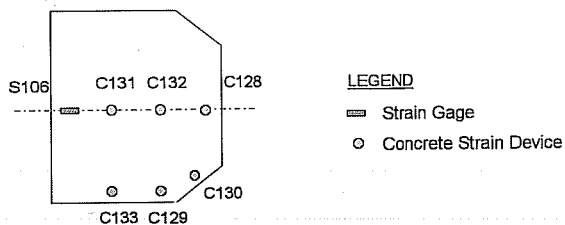
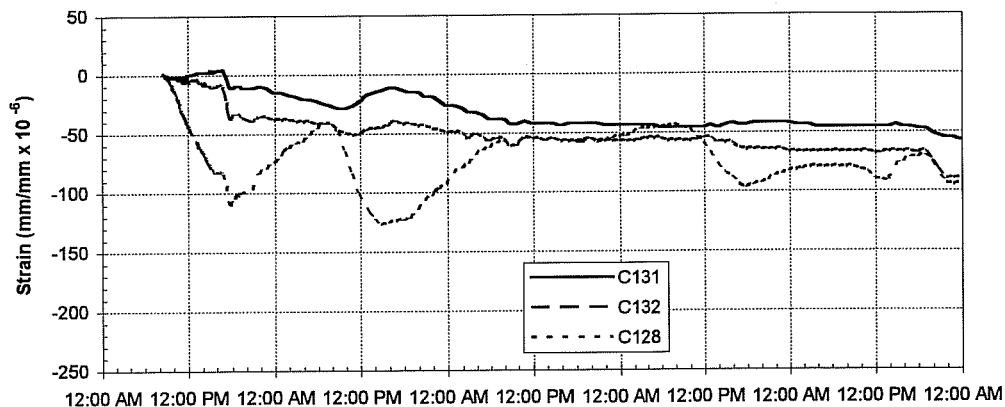
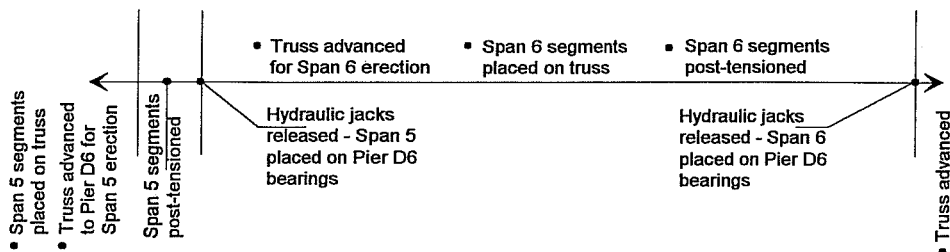
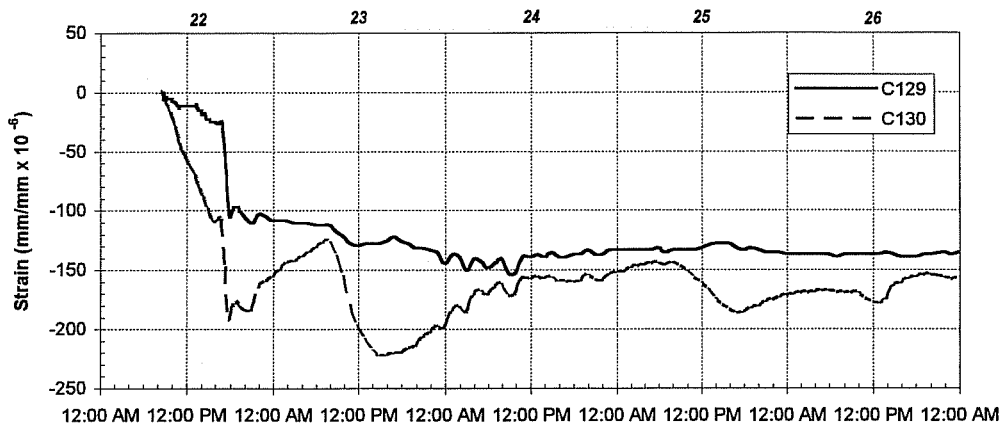


**Figure 5.51 - Strain Change Measured Near Top of Capital During Superstructure Erection**

**Superstructure Erection**  
**March 22 - 26, 1995**

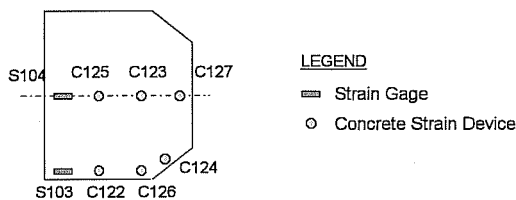
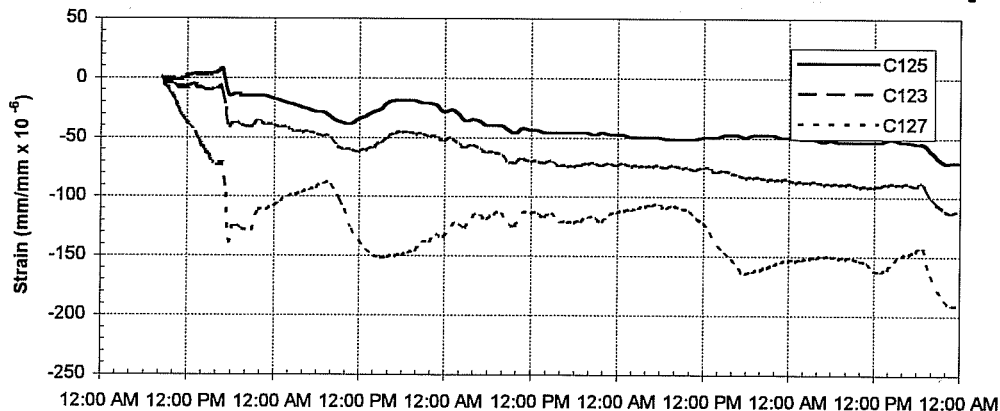
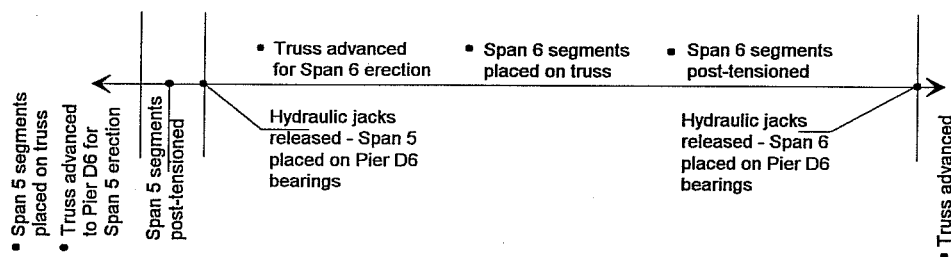
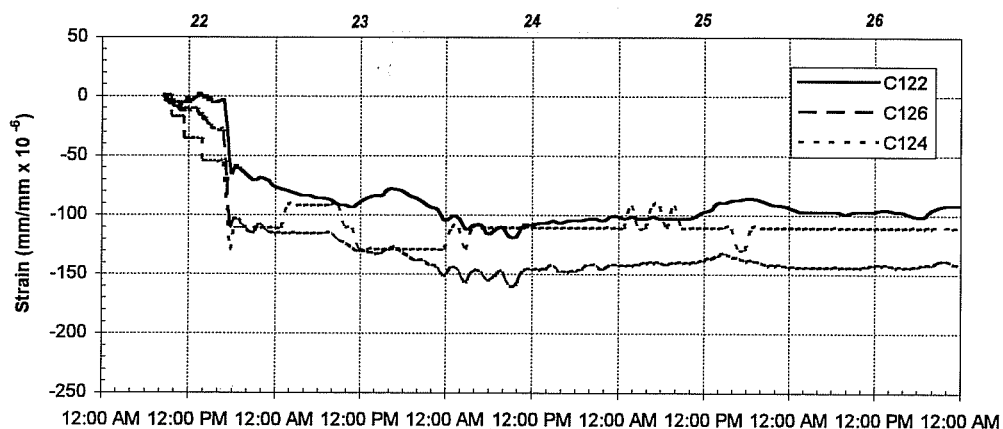


**Figure 5.52 - Strain Change Measured Near Mid-Height of Capital During Superstructure Erection**

**Superstructure Erection  
March 22 - 26, 1995**

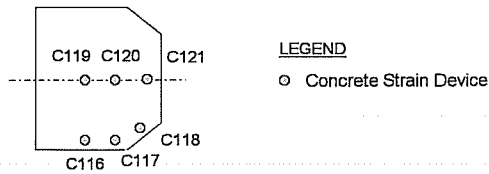
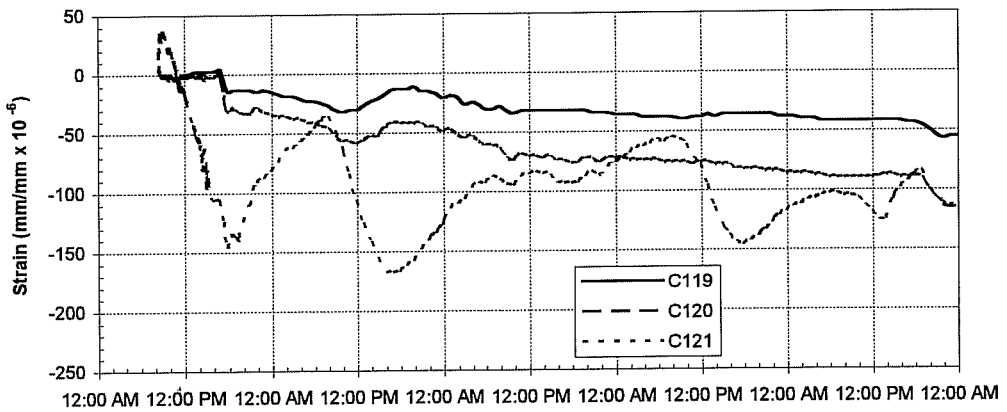
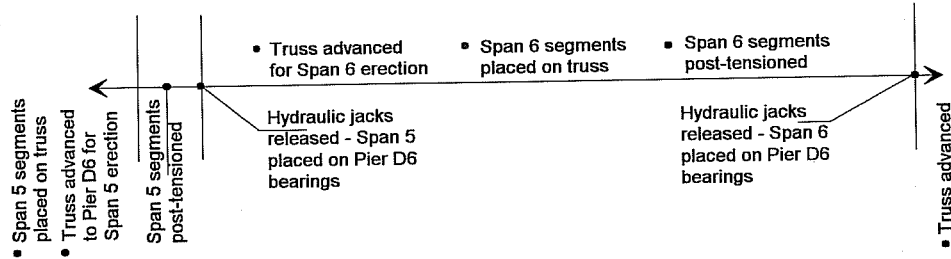
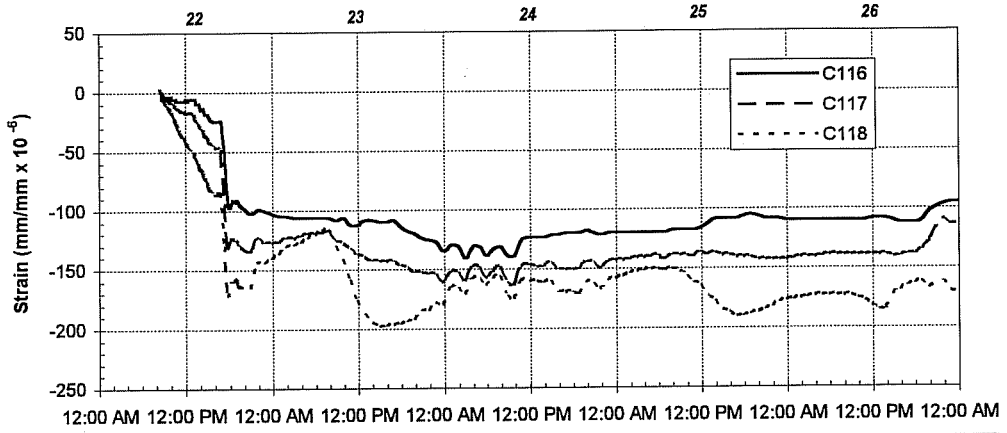


**Figure 5.53 - Strain Change Measured Near Bottom of Capital During Superstructure Erection**

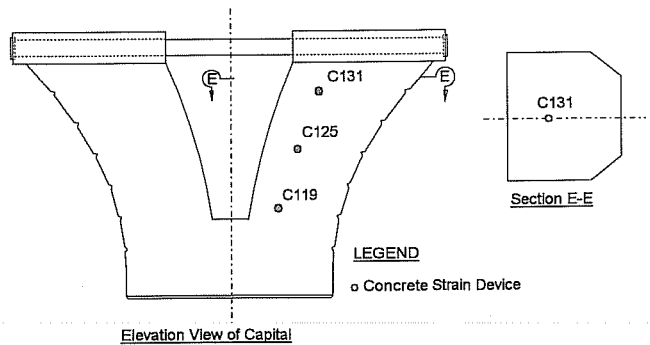
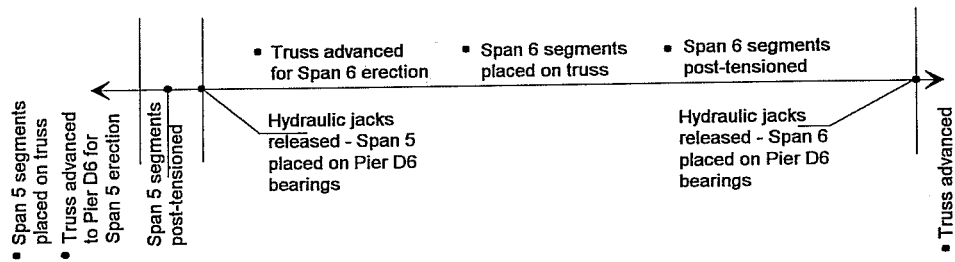
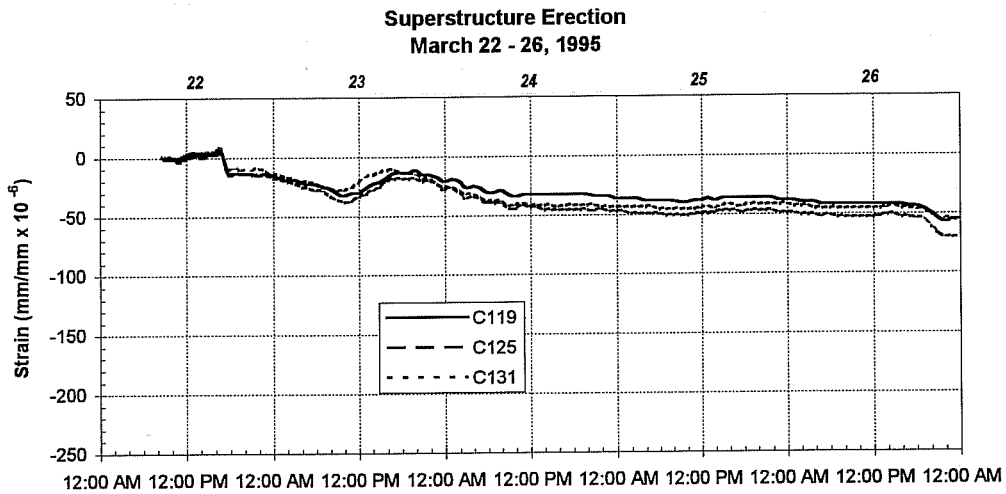


**Figure 5.54 - Comparison of Strain Change "Vertically" on Capital During Superstructure Erection: Core Near Inside Face of "Y"**

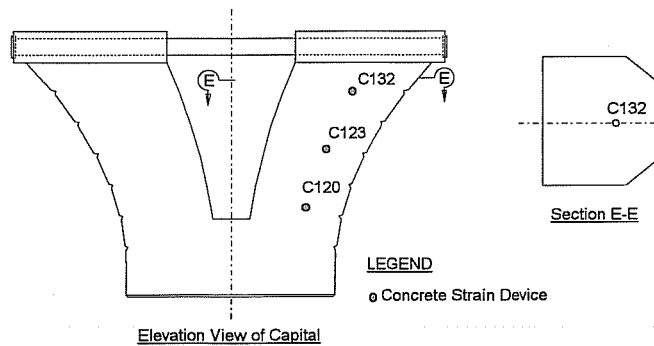
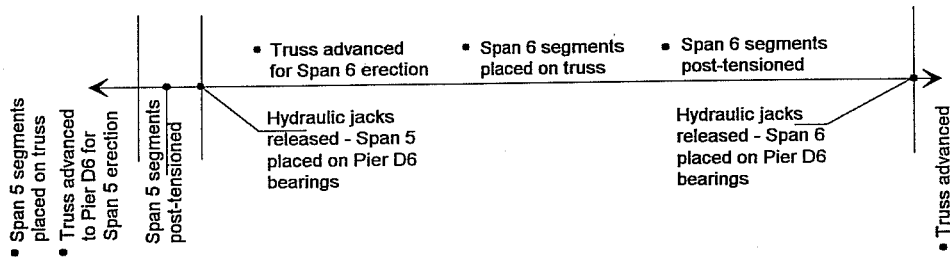
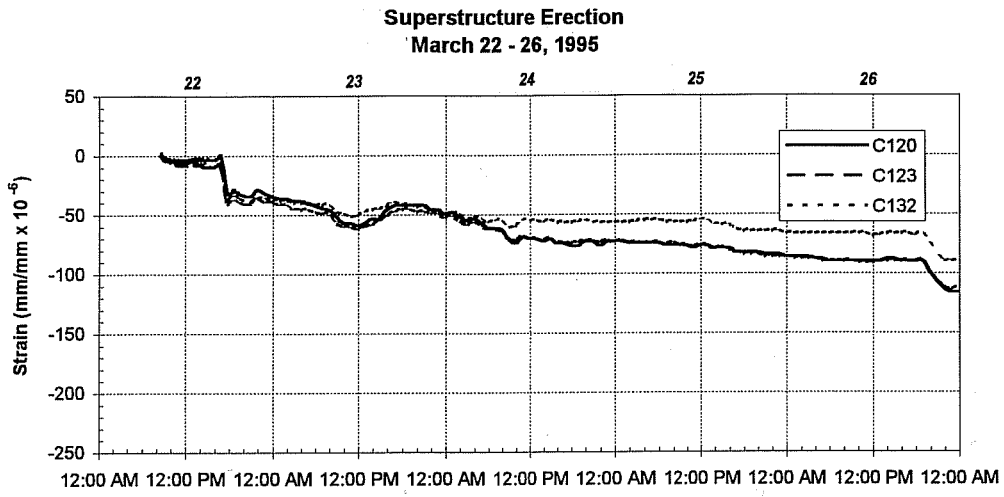


**Figure 5.55 - Comparison of Strain Change "Vertically" on Capital During Superstructure Erection: Core Near Outside Face of "Y"**

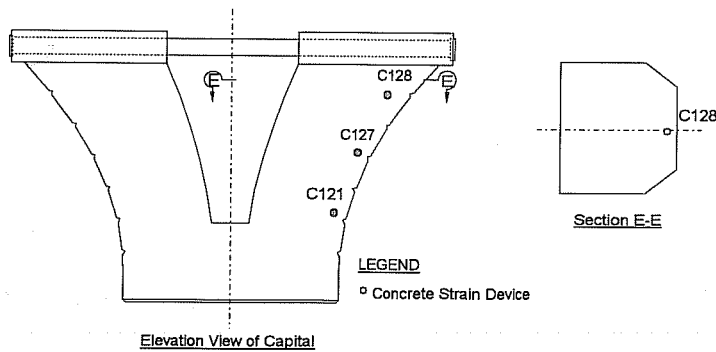
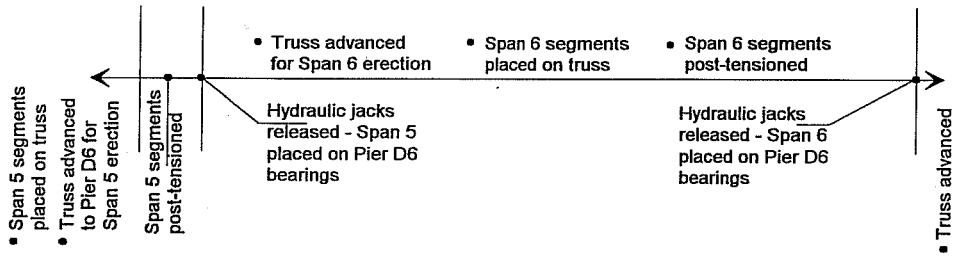
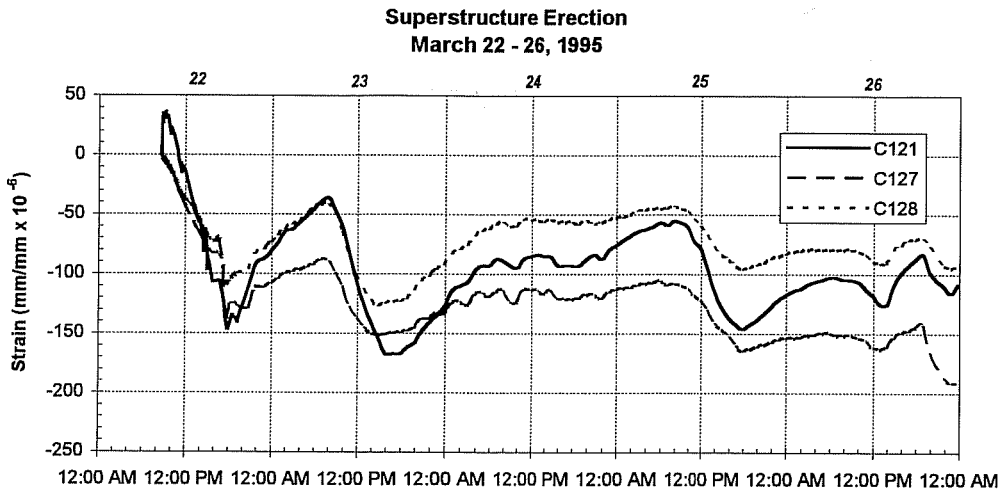


**Figure 5.56 - Comparison of Strain Change "Vertically" on Capital During Superstructure Erection: Shell Near Outside Face of "Y"**

#### **5.4.4 Shaft Strains**

Strains measured in the shaft of the pier are shown in Figure 5.57 and Figure 5.58. Strain change was calculated using a point in time prior to any load placement on the shaft. March 16 preceded advancement of the erection truss to Pier D6 and was chosen for use as an initial point.

As the tendons of Span 5 were stressed, strain devices in the shaft exhibited strain change, indicating that the load was partially transferred from the bottom of the “Y” to the capital during the stressing operation. Strain devices located on the Span 5 side of the centerline of the pier (C111, C112, C113; C104, C105, C106, C107) experienced compressive strain changes. Strain devices located on the transverse centerline of the pier experienced tensile strain changes. This intuitively makes sense due to the fact that Span 5 is not centered on the bearing, but is placed on the Span 5 side of the pier. Bending is induced in the pier, causing tensile strain changes along the transverse centerline of the pier.

When the hydraulic jacks are released and Span 5 is placed on the bearing, a noticeable compressive strain change occurs in devices located on the Span 5 side of the pier. Devices located along the transverse centerline of the pier (C114, C108) do not exhibit a distinct strain change.

The placement of Span 6 on the bearings has an effect which is the reverse of that caused by placement of Span 5 on the bearings. When Span 6 is placed on the bearings of the pier, devices C113 and C107 exhibit a distinct tensile strain change. Devices C114 and C108 experience a compressive strain change.

Devices located in the shell of the shaft (C112; C104, C105, C106) exhibit a tensile strain change when Span 6 is placed on the bearings. This tensile strain change is approximately equal to the compressive strain change caused by placement of Span 5 on the bearings.

Figure 5.59 shows a comparison of devices located in the same relative position in the cross section of the shaft. Devices C104 and C101 experience less strain change due to the superstructure load than do devices C112 and C106. All of these devices located in the shaft of the concrete exhibit a distinct compressive strain change when Span 6 is placed on the bearings. Strain devices C114 and C108 are located in the core of the concrete. They do

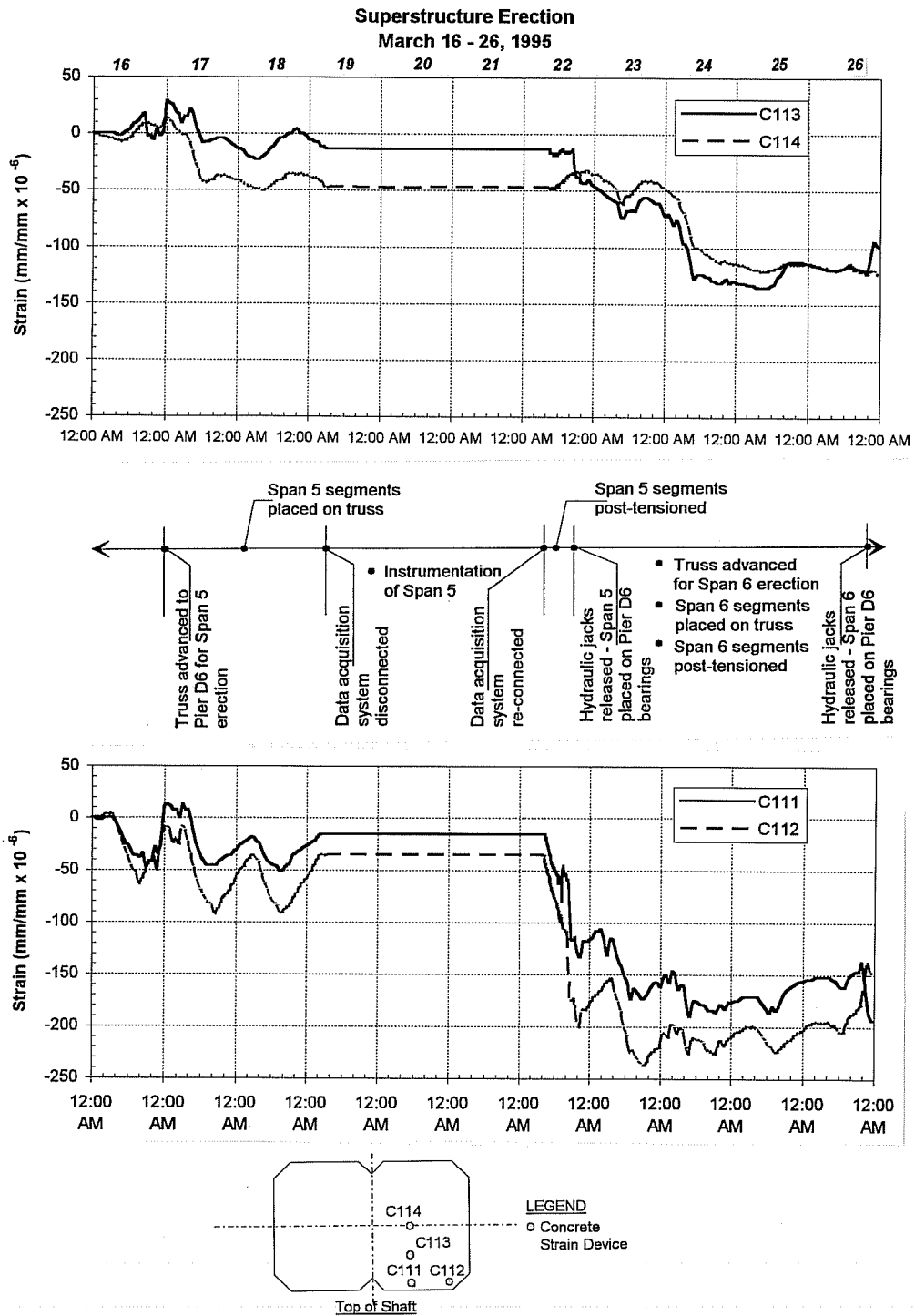
not exhibit a distinct strain change when Span 5 is transferred from the bottom of the “Y” to the bearings.

Figure 5.60 and Figure 5.61 show a comparison of strain changes in devices located at mid-height of the shaft. When Span 5 is placed on the bearings, C108 experiences no distinct strain change. Strain device C107, which is located just off the transverse centerline, experiences a small compressive strain change during the release of Span 5 onto the bearings. Strain device C105, which is located near the surface of the concrete, exhibits a compressive strain change significantly larger than C107.

When Span 6 is placed on the bearings, C108 experiences no distinct strain change. Strain device C107, which is located just off the transverse centerline, experiences a small tensile strain change approximately equal to the compressive strain change caused by the placement of Span 5 on the bearings. Strain device C105, which is located near the surface of the concrete, exhibits a tensile strain change significantly larger than C107 and approximately equal to the compressive strain change caused by placement of Span 5 on the bearings. These trends are reasonable since the load is merely transferred from a centered position on the shaft to a position which produces unbalanced load on the shaft.

As mentioned previously, the strain changes presented in this section contain thermal as well as gravity load effects. In order to compare the measured loads due to gravity to the loads predicted by a strut-and-tie model, thermal strains must be separated from the total measured strains presented in this chapter. A procedure for separating thermal strains from total strains is discussed in Chapter 6.





**Figure 5.57 - Strain Change Near Top of Shaft Measured During Superstructure Erection**

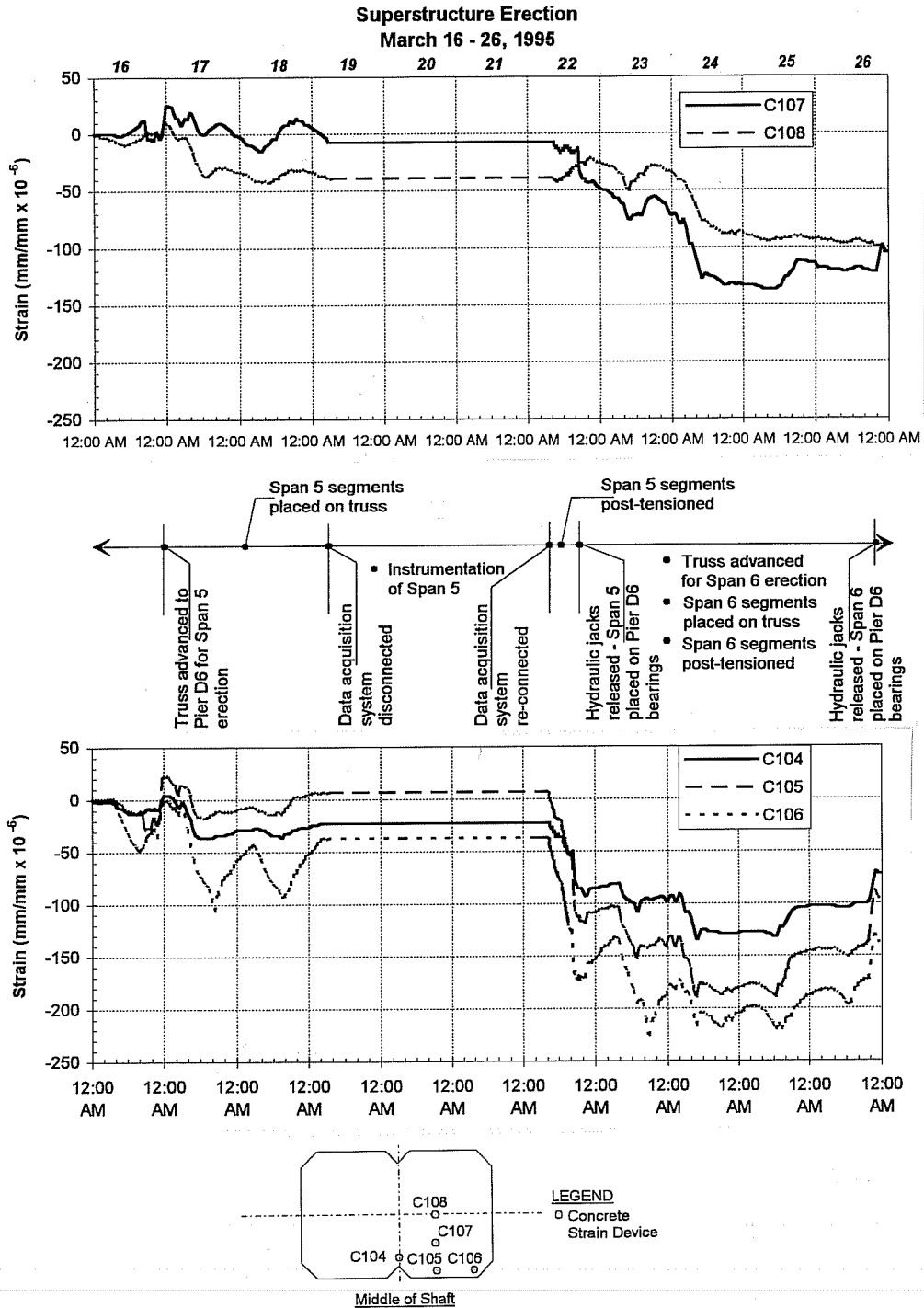


**Figure 5.58 - Strain Change Near Mid-Height of Shaft Measured During Superstructure Erection**

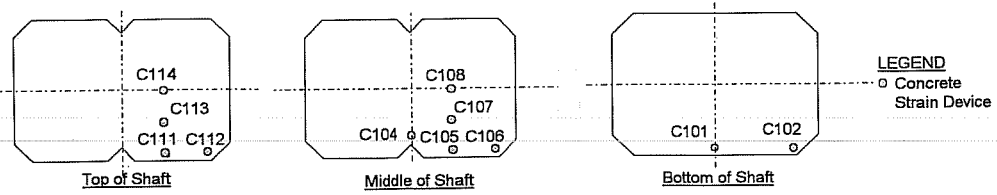
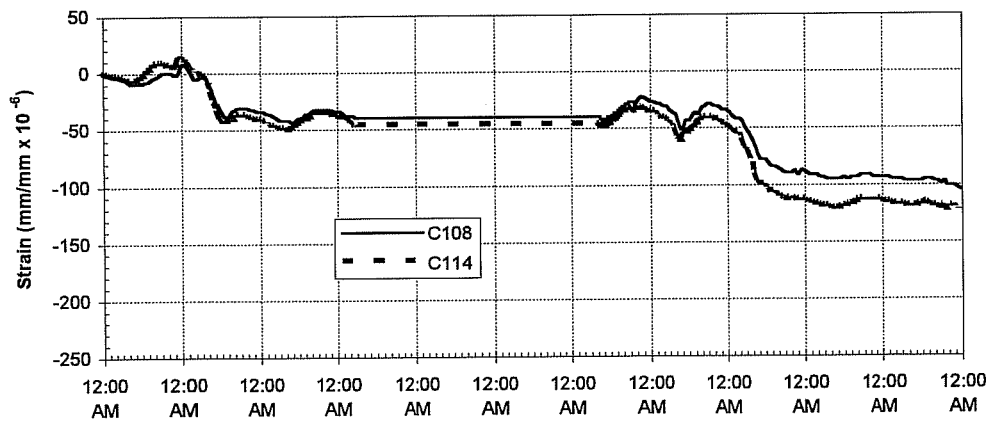
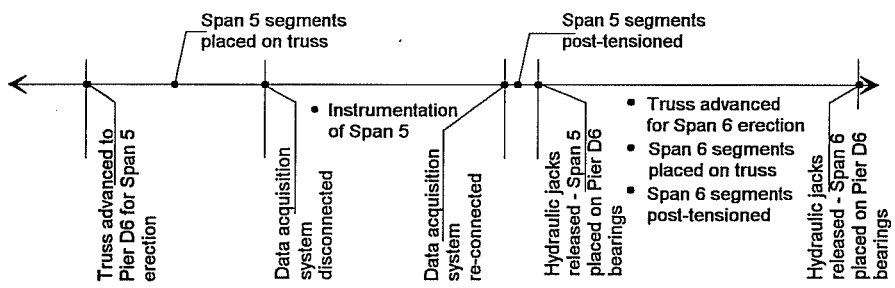
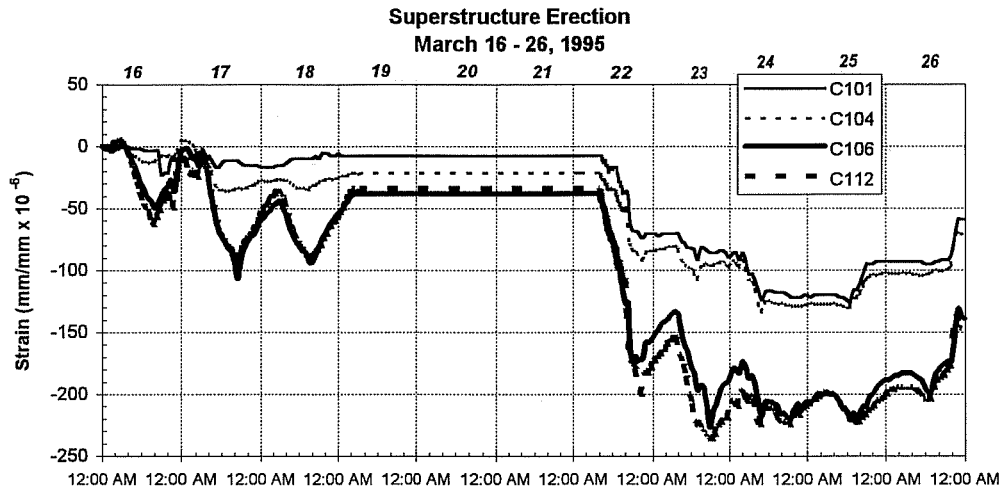


**Figure 5.59 - Comparison of Strain Changes "Vertically" in Shaft During Construction of Superstructure**

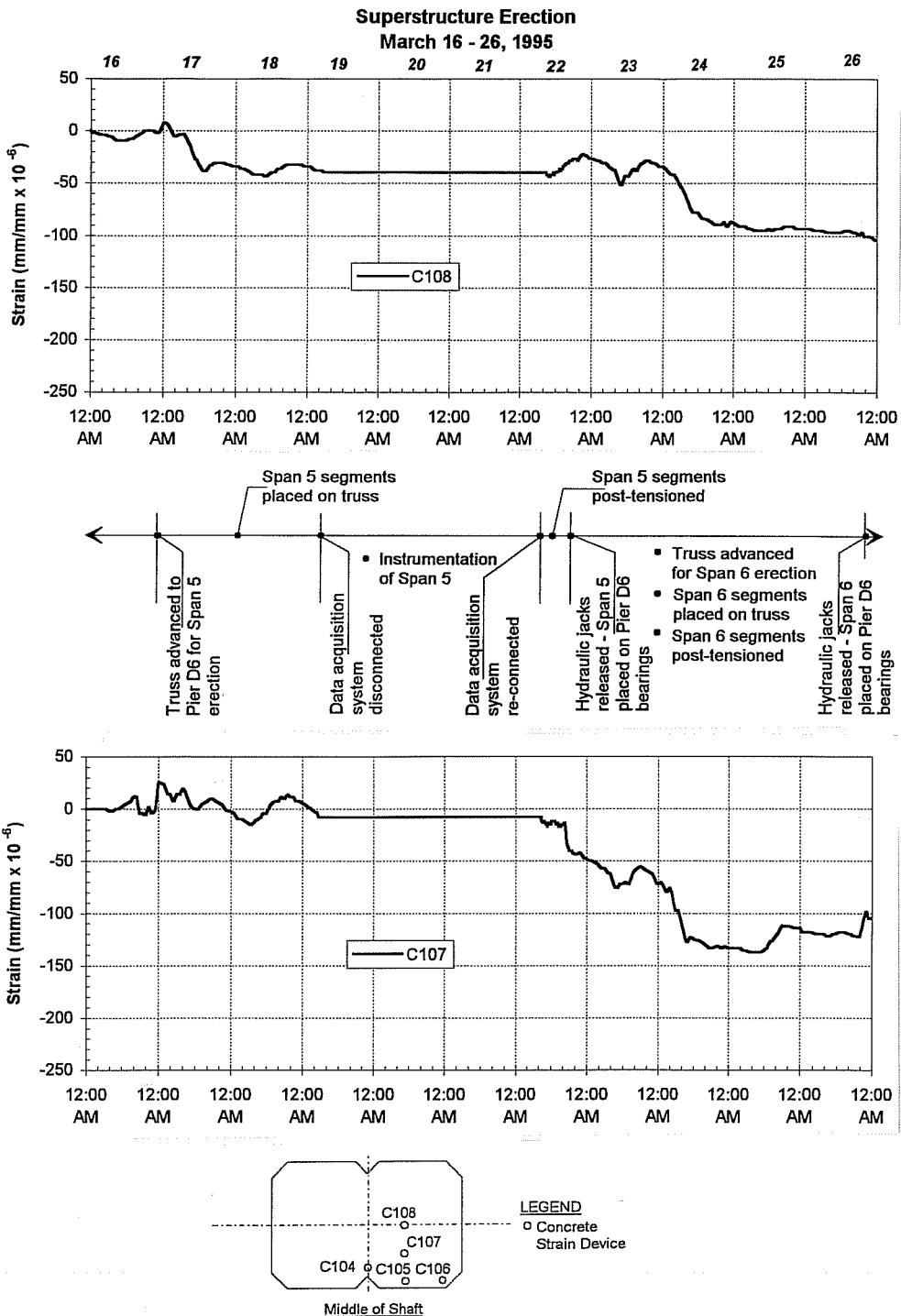


**Figure 5.60 - Comparison of Strain Changes at Varying Distances from the Transverse Centerline of the Pier During Superstructure Construction (C107, C108)**

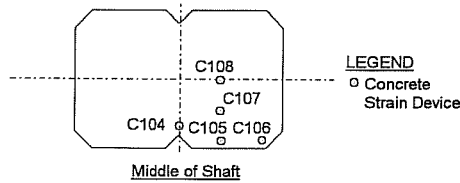
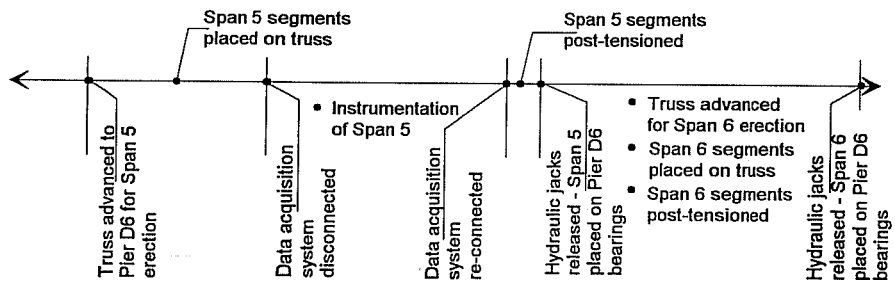
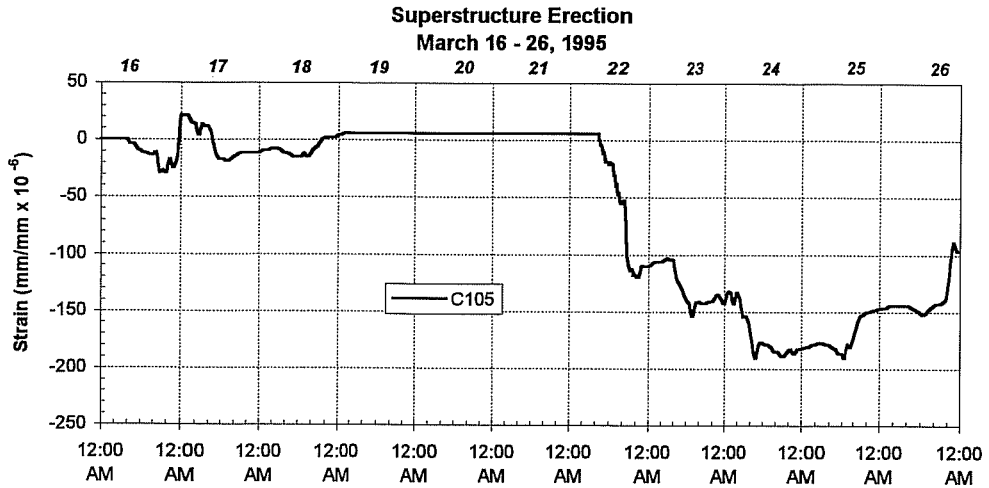


**Figure 5.61 - Comparison of Strain Changes at Varying Distances from the Transverse Centerline of the Pier During Superstructure Construction (C105)**

## CHAPTER 6

### SUPERSTRUCTURE DEAD LOAD DATA ANALYSIS

#### 6.1 Introduction

The purpose of this chapter is to compare measured forces due to superstructure dead load with those predicted by a strut-and-tie model for the instrumented US 183 mainlane pier. In order to use measured dead load induced strains for comparison purposes, thermal strains must be separated from total strains measured during application of the dead load since the superstructure construction extended over several days. A procedure for extracting thermal strains from total measured strains is discussed in this chapter. A strut-and-tie model for the US 183 mainlane pier is also presented and used to compare predicted and measured forces.

#### 6.2 Thermal Strains

As indicated in Chapter 5, temperature changes induce thermal strains in the mainlane piers of US 183. The following sections describe the significance of thermal strains as related to the total measured strains due to the superstructure dead load and suggest a procedure for separating these thermal strains from the total measured strains.

##### 6.2.1 Significance of Thermal Strains

A comparison of expected gravity strains due to placement of the superstructure dead load,  $\epsilon_{gravity}$ , and measured thermal strains during these construction operations,  $\epsilon_{thermal}$ , is shown in Table 6.1. Expected gravity strains were calculated based on the gross cross-sectional area of the concrete and a simplified load distribution of P/A (gravity load/cross-sectional area). Calculations can be found in the Appendix. Measured thermal strains were taken from data presented in Chapter 5 for March 11, 1995.

**Table 6.1 - Comparison of Expected Gravity Strains and Measured Thermal Strains**

	<i>Pipe</i>	<i>Capital</i>		<i>Shaft</i>	
		<i>Shell</i>	<i>Core</i>	<i>Shell</i>	<i>Core</i>
$\epsilon_{\text{gravity}} (\mu\epsilon)$	210	40-80	40-80	70	70
$\epsilon_{\text{thermal}} (\mu\epsilon)$	10	80-95	20	70	10-50
$(\epsilon_{\text{thermal}} / \epsilon_{\text{gravity}}) \times 100$	5	40-200	25-50	100	15-70

Although  $\epsilon_{\text{thermal}}$  is only approximately 5% of  $\epsilon_{\text{gravity}}$  for the structural steel pipe, it ranges from 15 to 200% of  $\epsilon_{\text{gravity}}$  for the capital and the shaft. Thermal strains can be expected to be the same order of magnitude as gravity strains in certain cases. For this reason, the extraction of thermal strains from the total strains which were presented in Chapter 5 as measured during superstructure erection must be addressed.

### **6.2.2 Procedure for Extraction of Thermal Strains from Measured Strains**

As indicated in Chapter 5, temperature differentials across the concrete section and between the concrete and the structural steel pipes induce thermal strains in the pier. If temperature differentials on the pier are the same for two separate times, the induced thermal strains should be the same for the two times regardless of the individual temperatures at each thermocouple location.

Data collected immediately prior to and subsequent to Span 5 and Span 6 erection over Pier D6 was investigated to determine if temperature differentials on the pier were the same for any two times. Several relative locations for temperature comparisons were considered to be of importance and are listed in Table 6.2.

Stable temperature trends were observed on March 15-16, prior to superstructure erection, and March 30-31, subsequent to superstructure erection. During these times, no significant heating or cooling trends occurred, and the gravity load was constant. Relative temperatures were calculated for thermocouples located as indicated in Table 6.2 for these days. Temperature differentials prior to and subsequent to superstructure erection were compared. Close inspection of the differentials indicated that at 4:00 A.M. on March 16 and

4:00 A.M. on March 30, the variance in the differentials was less than 1 °C (1.8 °F) for each location comparison. These relative temperatures are shown in Table 6.3.

**Table 6.2 - Temperature Differential Locations Compared for Thermal Strain Extraction**

<i>Thermocouple Designation</i>	<i>Location in Pier</i>
T103 - T101	Exposed Pipe - Embedded Pipe
T103 - T105	Exposed Pipe - Concrete Core
T103 - T104	Exposed Pipe - Concrete Shell
T104 - T105	Concrete Shell - Concrete Core
T106 - T107	Concrete Shell - Concrete Core

**Table 6.3 - Relative Temperatures for March 16 and March 30, 1995**

<i>Date</i>	<i>Time</i>	<i>Differential (°C)</i>				
		T103-T101	T103-T105	T103-T104	T104-T105	T106-T107
March 30	4:00 A.M.	-1.83	-3.28	-0.98	-2.30	-2.22
March 16	4:00 A.M.	-2.33	-3.92	-1.59	-2.33	-2.22
Variance	4:00 A.M.	0.50	0.64	0.61	0.03	0

Since the temperature differentials for these times are very close, the assumption was made that the strains measured at 4:00 A.M. on March 16 prior to the superstructure erection could be directly subtracted from the strains measured at 4:00 A.M. on March 30 subsequent to the placement of Spans 5 and 6 on Pier D6, and thermal strains would in effect be negated.

### **6.3 Superstructure Dead Load Strains in Pier**

As mentioned previously, strut-and-tie modeling has a limited capability to detect compatibility and constraint induced stresses. For this reason, the procedure discussed in



Section 6.2.2 was used to correct the total measured strains induced in the pier due to the total superstructure load in order to eliminate any thermal effects. The known weight of the superstructure produced a load on each branch of the pier capital of 4430 kN (996 kips). The following sections present these strains after they were adjusted for temperature effects.

### 6.3.1 Pipe Strains

The superstructure dead load induced strains measured on the structural steel pipes are shown in Table 6.4. Thermal strains have been extracted from these strains. Both pipes show very similar trends along their lengths. Strain gage locations are shown in Figure 6.1. The force is greatest in the exposed portion of the pipe. Once the pipe enters the concrete, force begins to rapidly transfer to the concrete through the steel/concrete bond. At the ends of the pipe, negligible strains exist.

**Table 6.4 - Superstructure Dead Load Strains Measured in Structural Steel Pipes:  
Thermal Strains Extracted**

<i>Single Exterior Pipe</i>		<i>Single Interior Pipe</i>	
<i>Strain Gage</i>	<i>Strain</i> ( $\mu\epsilon$ )	<i>Strain Gage</i>	<i>Strain</i> ( $\mu\epsilon$ )
S107, S108	-12	S119, S120	3
S109, S110	12	S121, S122	22
S111, S112	58	S123, S124	85
S113 - S116	230	S125 - S128	266
S117, S118	251	S129, S130	258

### 6.3.2 Capital Strains

Concrete strain devices were used in the capital to measure strains. Strains due to total superstructure dead load after extraction of thermal strains are shown in Figure 6.2. For evaluation purposes, strains were averaged as shown in Table 6.5. As the distance from the inside face of the "Y" increases, the strains are increasingly compressive.

The strain distribution across each section is shown in Figure 6.3. The outside face at each section is in compression. Strain distribution is approximately linear for both the mid-height and bottom sections. Although the strain gages located on the inside face of the “Y” were damaged during construction, extrapolation of the measurements indicates that the inside face of the “Y” at both of these latter sections would also be in tension.

Measurements along the top section of the pier indicate a more non-linear strain distribution than those at the mid-height and bottom sections. This may be due to the fact that the strain gages at this level are located closer to the points of load application. The load may not have fully dissipated across the section at this location.

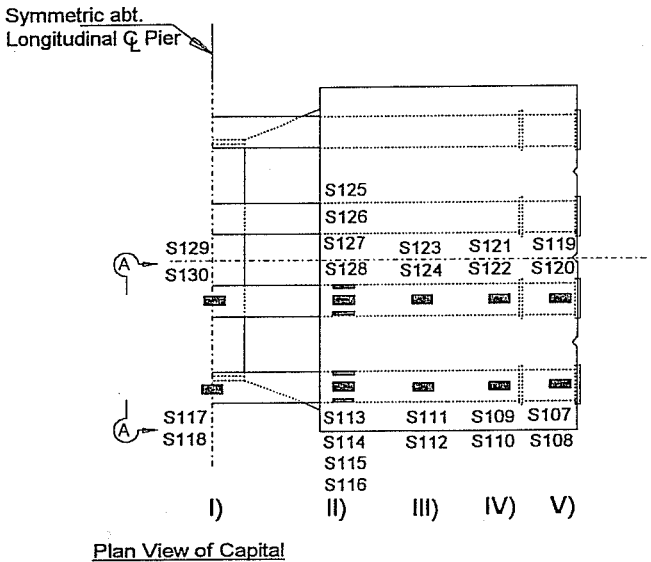
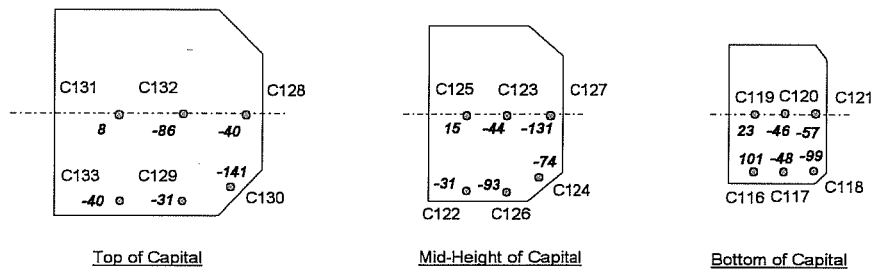


**Figure 6.1 - Strain Gage Locations on Structural Steel Pipes**



NOTE: Measured strains are indicated in italics in  $\mu\epsilon$ .

**Figure 6.2 - Strains Measured in Capital due to Superstructure Dead Load: Thermal Strains Extracted**

**Table 6.5 - Average Superstructure Dead Load Strains Measured in the Capital: Thermal Strains Extracted**

<i>Bottom of Capital</i>		<i>Mid-Height of Capital</i>		<i>Top of Capital</i>	
<i>Concrete Strain Device</i>	<i>Strain (<math>\mu\epsilon</math>)</i>	<i>Concrete Strain Device</i>	<i>Strain (<math>\mu\epsilon</math>)</i>	<i>Concrete Strain Device</i>	<i>Strain (<math>\mu\epsilon</math>)</i>
C119, C116	-17	C125, C122	-8	C131, C133	62
C120, C117	-58	C123, C126	-69	C132, C129	-47
C121, C118	-90	C127, C124	-102	C128, C130	-78

**Average Strains Across Capital Sections**

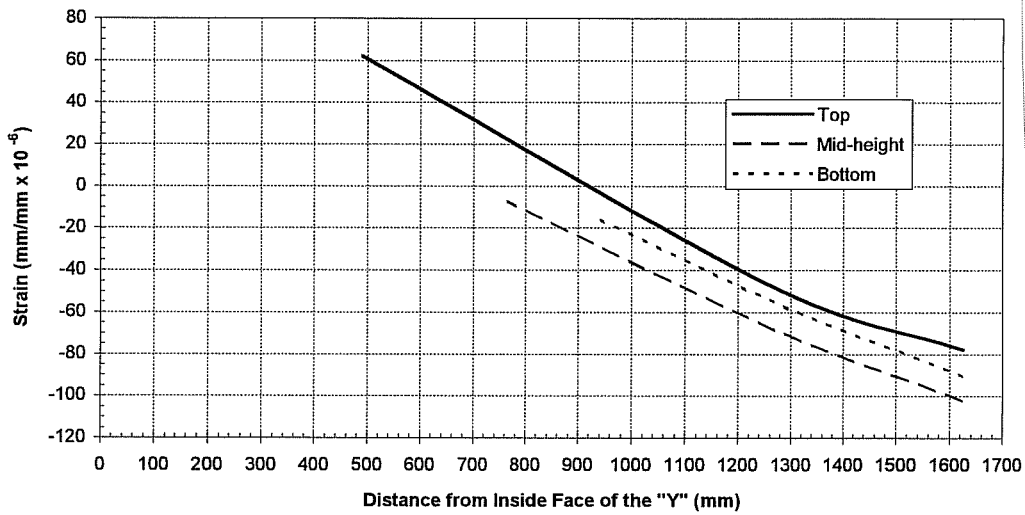
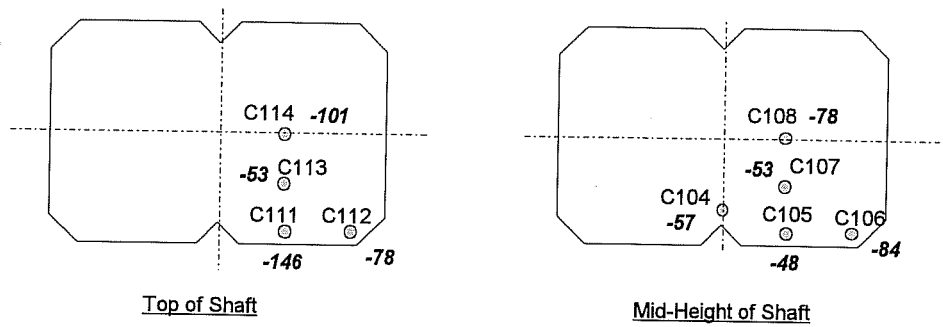


**Figure 6.3 - Strain Distribution Across Each Section of the Capital: Thermal Strains Extracted**

### 6.3.3 Shaft Strains

Strains measured in the shaft of the pier due to the superstructure dead load are shown in Figure 6.4. All strains are compressive. Average strains are shown in Table 6.6. Average strains at the top of the shaft are substantially larger than at mid-height. After the correction for thermal strains was made, calculated strains at the bottom of the shaft were highly erratic and unexplainable. Therefore, they were neglected.



**NOTE:** Measured strains are indicated in italics in  $\mu\epsilon$

**Figure 6.4 - Strains Measured in the Shaft due to Superstructure Dead Load: Thermal Strains Extracted**

**Table 6.6 - Average Measured Strains in Shaft due to Superstructure Dead Load: Thermal Strains Extracted**

<i>Top of Shaft</i>		<i>Mid-Height of Shaft</i>	
<i>Average Strain Across Section (<math>\mu\epsilon</math>)</i>	-95	<i>Average Strain Across Section (<math>\mu\epsilon</math>)</i>	-64
<i>Average Strain in "Core" (<math>\mu\epsilon</math>) (C113, C114)</i>	-77	<i>Average Strain in "Core" (<math>\mu\epsilon</math>) (C107, C108)</i>	-66
<i>Average Strain in "Shell" (<math>\mu\epsilon</math>) (C111, C112)</i>	-112	<i>Average Strain in "Shell" (<math>\mu\epsilon</math>) (C104, C105, C106)</i>	-63

#### 6.4 Superstructure Dead Load Forces in Pier

Strains measured in the pier were converted to forces and are shown in this section. Calculations are presented in the Appendix.

##### 6.4.1 Pipe Forces

Pipe forces were calculated from the strains presented in Table 6.4 using a Young's modulus of 199,955 MPa (29,000 ksi) and a cross sectional area of 8258 mm<sup>2</sup> (12.8 in<sup>2</sup>). The forces are shown in Table 6.7 for the single pipes instrumented. The effective pipe force of the tension tie would be the sum of the forces in the four pipes.

**Table 6.7 - Forces Measured in Pipes due to Gravity Load**

<i>Single Exterior Pipe</i>		<i>Single Interior Pipe</i>	
<i>Strain Gage</i>	<i>Force</i> kN (kips)	<i>Strain Gage</i>	<i>Force</i> kN (kips)
S107, S108	-19.8 (-4.5)	S119, S120	4.89 (1.1)
S109, S110	19.8 (4.5)	S121, S122	36.3 (8.2)
S111, S112	95.6 (21.5)	S123, S124	140 (31.6)
S113 - S116	380 (85.4)	S125 - S128	399 (98.7)
S117, S118	415 (93.2)	S129, S130	426 (95.8)

##### 6.4.2 Capital Forces

Compressive forces measured in the capital due to gravity load were calculated from the averaged concrete strains presented in Table 6.5 and are shown in Table 6.8. Only compressive stress areas were used in calculations since the tensile capacity of concrete is neglected in strut-and-tie modeling. These forces were calculated based on a Young's modulus of 28,270 MPa (4100 ksi). This modulus was measured in the laboratory using concrete specimens taken from the casting of the capital for Pier D6.

### 6.4.3 Shaft Forces

Shaft forces were calculated from the averaged measured strains presented in Table 6.6 using a Young's modulus of 24,130 MPa (3500 ksi). This modulus was measured in the laboratory using test specimens taken from the concrete during casting of the shaft for Pier D6. Forces were calculated based on the average core strains and one half the cross sectional area of the shaft at the location of the instrumented section. Forces are presented in Table 6.9.

**Table 6.8 - Compressive Forces Measured on One Branch of the Capital due to Superstructure Dead Load**

<i>Compressive Force</i>	
kN (kips)	
<i>Mid-Height of Capital</i>	2215 (498)
<i>Bottom of Capital</i>	1637 (368)
<i>Average</i>	1926 (433)

**Table 6.9 - Forces Measured in One Half of Shaft due to Superstructure Dead Load**

<i>Force</i>	
kN (kips)	
<i>Top of Shaft</i>	3683 (828)
<i>Mid-Height of Shaft</i>	3157 (710)
<i>Average</i>	3420 (769)

### 6.5 Strut-and-Tie Model for US 183 Mainlane Pier

A strut-and-tie model (STM) was developed for the US 183 mainlane pier to compare predicted forces with measured service load forces. Strut-and-tie modeling is an *ultimate load model* developed for reinforced concrete design. Strut-and-tie modeling serves

the designer by allowing efficient proportioning of reinforcement in patterns and quantities that satisfy equilibrium assuming that predicted force paths are followed by the applied load. Since STM is strictly speaking only applicable to ultimate load conditions, the only purpose of comparing the strut-and-tie model with *measured service load* forces is to investigate the general agreement of strut-and-tie modeling in predicting the basic flow of forces in a structure. A detailed discussion of strut-and-tie modeling can be found in Chapter 2.

The US 183 mainlane piers provide an excellent opportunity for the use of strut-and-tie models. A STM typical for a reinforced concrete wall is shown in Figure 6.5a. Dashed lines represent compression struts, and solid lines represent tensile ties. The US 183 pier is shown in Figure 6.5b with the same general force path illustrated as for the wall. In areas of the reinforced concrete wall where the concrete is not necessary for the flow of forces, the concrete has been removed to form the US 183 pier. The flow of forces is easily visualized due to the shape of the structure. Figure 6.5 shows the efficiency of the basic shape chosen for the US 183 mainlane piers. The basic force path of Figure 6.5b was used to develop a strut-and-tie model for the instrumented pier.

The following paragraph refers to Figure 6.5b. The superstructure dead load is assumed to be evenly distributed across the bearing pads. For this reason, the assumption is made that the compressive struts transferring the force through the capital must pass through the centroid of the applied load at the center of the bearing pad, or at node (A). The load is assumed to be evenly distributed at the bottom of the shaft. Therefore, the compressive struts in the shaft must pass through the location of the half-pier force resultants of the distributed load at the bottom of the pier, or node (B). The location of the intermediate node (C) is somewhat arbitrary and will vary according to the particular model assumed. Thus, the angle  $\theta$  is a variable assumed by the designer in choosing a STM. Node (C) should be chosen so that the force centroid on the path between nodes (A) and (C) lies well within the concrete capital cross section.



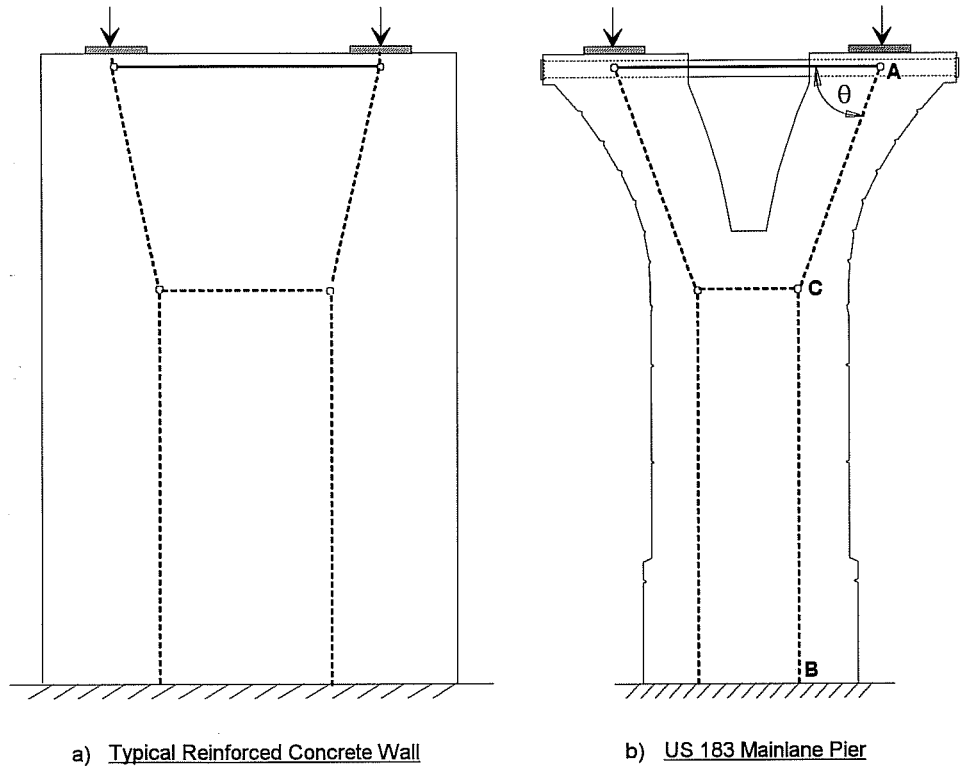


**Figure 6.5 - Basic Force Path in the US 183 Mainlane Piers**

### **6.5.1 *Strut-and-Tie Model Based on Measured Forces***

Two approaches were investigated for selection of a strut-and-tie model of the pier based on measured forces. These approaches are discussed in the following sections.

#### **6.5.1.1 *Strut-and-Tie Model Based on Compressive Force Resultants in the Capital***

In order to investigate the actual force path as indicated by measured compression strains, the force path in the pier was determined by assuming that the compression strut of

the capital follows the location of the compressive force resultant at each instrumented level. The compression strut of the capital is also assumed to meet the tension tie of the pipe directly below the center of the bearing.

A graphical representation of this procedure is shown in Figure 6.6. In Figure 6.6a, a strain diagram for each instrumented section is shown. These strain diagrams were obtained by using the average measured strains across each section as shown in Figure 6.3. The average strain at the outside face of the “Y” was assumed to be valid. An approximate linear fit was made through the measured data, and the linear fit was extrapolated to the inside face of the “Y”.

The neutral axis was then graphically measured, and the location of the compressive force resultants were calculated for each section assuming that the resultant force acts at a centroid located at the “1/3 points” of the compressive portion of the stress diagram. This assumption assumes the section is rectangular in shape, which is a reasonable approximation for the capital section. This measured “1/3 point” at the mid-height of the capital was calculated to be approximately 330 mm (13 in) from the outside face of the “Y”. The “1/3 point” at the bottom of the capital was similarly calculated to be about 356 mm (14”) from the outside face of the “Y”. These calculations can be seen in the Appendix.

In order to calculate the angle  $\theta$ , through which the compressive strut of the capital acts, a line was drawn through these points as shown in Figure 6.6a. The angle was measured to be approximately  $70^\circ$ . As shown in Figure 6.6b, if the angle  $\theta$  is  $70^\circ$  for an applied superstructure dead load of 4430 kN (996 kips), from geometry the pipe force is 1612 kN (363 kips) and the compressive strut force is 4715 kN (1060 kips). These forces are also shown in Figure 6.7a.

#### 6.5.1.2 Measured Force Distribution

The previous section indicated that from measured superstructure dead load compressive force paths, the angle  $\theta$  is  $70^\circ$ . Individual measured pipe forces were presented in Table 6.7. The total pipe force across the tension tie was calculated to be 1681 kN (378 kips) by adding these measured forces and multiplying them by two. The compressive force in the compression strut of the capital as measured by the embedded strain devices, as shown in Table 6.8, was 1926 kN (433 kips), the average of the compressive forces at the mid-

height and bottom of the capital. Table 6.9 shows the compressive force in each compressive strut in the shaft as measured by the embedded strain devices to be 3420 kN (769 kips). These forces do not satisfy equilibrium at any node and thus the basic accuracy of the measurements is questionable. These forces are also shown in Figure 6.7b.

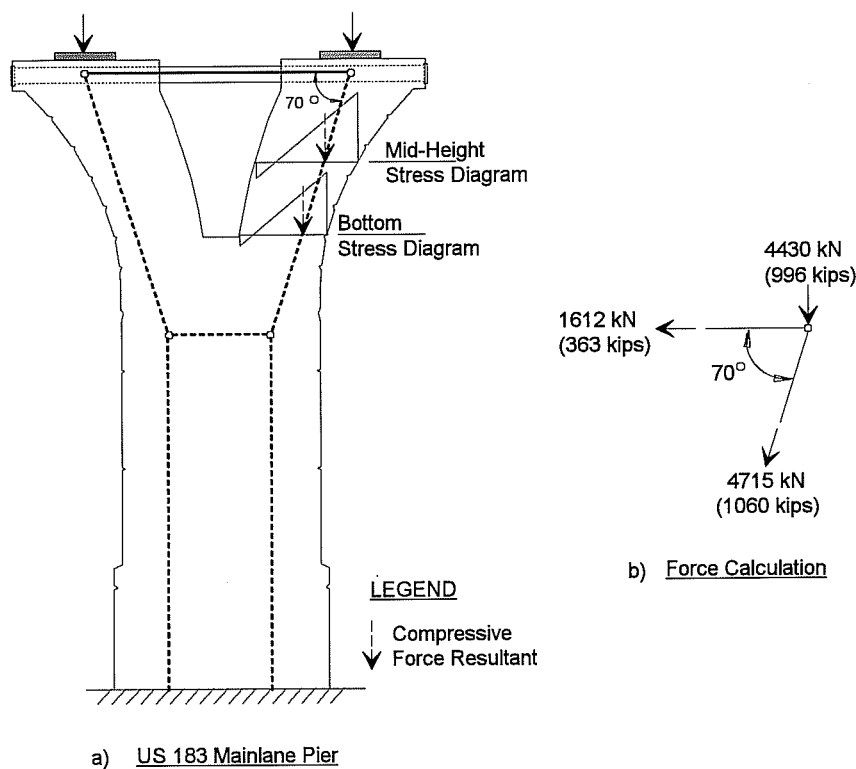


**Figure 6.6 - Calculation of the Orientation of the Compression Strut in the Capital Based on Measured Compressive Centroids**

### 6.5.2 *Strut-and-Tie Model Based on an Elastic Frame Analysis*

An elastic frame analysis was performed for the capital of the pier to estimate the force in the structural steel pipes. Varying stiffnesses were used for the “Y” branch of the capital. The base of the “Y” was assumed to be fixed. The superstructure dead load of 4430

kN (996 kips) was applied on each branch of the “Y”. Calculations for section properties and dimensions for the model are shown in the Appendix. The total force across the tension tie was determined by the elastic frame analysis of the capital as 1368 kN (308 kips). Based on this force and the known superstructure dead load, the angle  $\theta$  was determined from equilibrium to be  $73^\circ$ . This would be possible since the compression strut path would still fall within the capital branch concrete section. The corresponding compression force in the compression strut along the capital was calculated from equilibrium to be 4635 kN (1042 kips). These forces are also shown in Figure 6.7c.

## 6.6 Comparison of Forces and Force Paths

Figure 6.7 shows a comparison of the measured forces with the forces determined from the various strut-and-tie analyses. Figure 6.7a shows the STM with forces in equilibrium based on an angle  $\theta$  of  $70^\circ$  as indicated from the centroids of the measured compressive force path. Figure 6.7b shows the measured forces. These measured forces do not satisfy equilibrium, and are thus questionable. Figure 6.7c also shows a STM with the forces in equilibrium. This STM is based on an assumed angle  $\theta$  of  $73^\circ$  as indicated from the elastic frame analysis results.

The measured pipe forces, shown in Table 6.7, show very similar trends across the pipe lengths. Also, similar forces were measured in both pipes. For these reasons, the measured pipe forces are thought to be very reliable. The very close agreement (within approximately 4%) of the measured pipe force shown in Figure 6.7b with that predicted by the strut-and-tie model in Figure 6.7a appears to confirm the validity of the  $70^\circ$  STM.

Assuming the measured pipe force due to superstructure dead load is known with reasonable certainty, the pipe force predicted by the strut-and-tie model of Figure 6.7a is much closer to the actual force in the pipe than the pipe force predicted by the elastic frame analysis shown in Figure 6.7c. Interesting to note is the fact that while both strut-and-tie models provide estimates of the pipe force that are unconservative, the STM based on the frame analysis is more unconservative, agreeing within approximately 22%.

The point should be made that the strut-and-tie model presented in Figure 6.7a was developed by basing the design variable,  $\theta$ , on measured forces. A designer would obviously

not have these measured forces on which to base a selection of  $\theta$ . However, the selection of the location of the compressive strut in the branch of the capital by an experienced designer would likely be fairly close to  $70^\circ$  based on the geometry of the pier. A smaller  $\theta$  would require the compressive strut to approach an area of the capital branch where, intuitively, tensile forces are quite possible. A larger  $\theta$  would allow the compressive strut to approach the exterior face of the “Y” and eventually exit the concrete capital cross section, which is inadmissible.

The STM strut forces in Figure 6.7a, calculated based on the compressive strut orientation indicated by the location of the measured compressive force resultants, do not agree with the measured strut forces shown in Figure 6.7b. The measured concrete strains are substantially lower than those calculated based on an angle  $\theta$  of  $70^\circ$ . The calculated pipe force of 1612 kN (363 kips) agrees very well with the measured pipe force of 1681 kN (378 kips).

Several observations may explain the fact that the measured concrete forces do not agree with those predicted by the strut-and-tie model shown in Figure 6.7a. Figure 6.2 shows the strains measured in the capital. These individual strain measurements are somewhat erratic and do not present any general trends across the sections. Figure 6.4 shows that the strains measured in the shaft also exhibit unexplainable erratic behavior. Strain devices located directly above one another do not agree at most locations. These behaviors may be due to lack of instrument sensitivity in reading the low strains produced in the concrete due to the superstructure dead load. Such low strain readings are difficult to measure electronically and can be affected by slight resistance changes.

The difference in the forces measured in the capital and those predicted by the strut-and-tie model may also be explained by assumptions inherent to strut-and-tie modeling. Strut-and-tie modeling is an ultimate load model. The strut-and-tie model presented in this chapter for the US 183 pier was based on service loads. As indicated by the strains measured at each section of the capital, tensile strains are present at levels below those needed to crack the concrete. The tensile capacity of the concrete is neglected for most practical cases with the use of strut-and-tie modeling. The concrete can be assumed to be

carrying tensile loads in those areas where tensile strains were measured. The strut-and-tie model does not account for this concrete tensile capacity.

Strut-and-tie modeling is a design tool and is not intended for use in analysis. As such, exact agreement between measured forces and strut-and-tie model forces is not expected. The force path used for the strut-and-tie model of Figure 6.7a was very close to the measured force path. Thus the angle  $\theta$  used in the STM agrees very well with reality. The calculated tie force is in close agreement with the measured tie force when this angle is used, indicating the ability of a strut-and-tie model to accurately determine the reinforcement (the structural steel pipes in this case) needed in a structure.

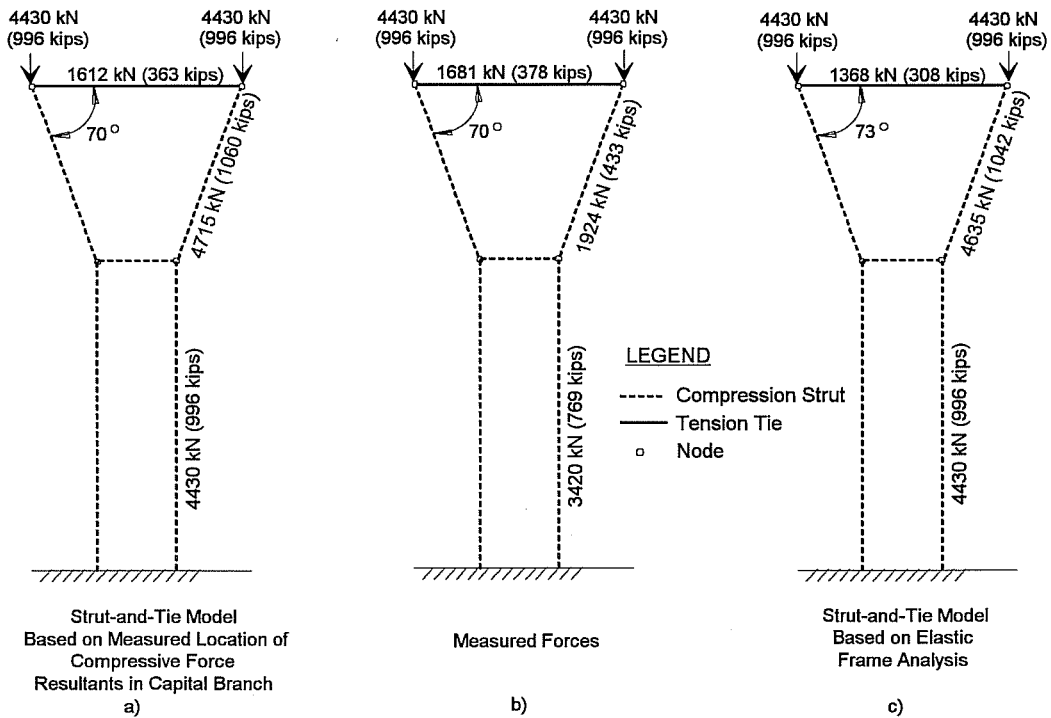


**Figure 6.7 - Comparison of Measured Forces and Strut-and-Tie Model Forces**

## **CHAPTER 7**

### **CONCLUSIONS, RECOMMENDATIONS, & SUMMARY**

#### **7.1 Introduction**

This chapter presents an overview of the instrumentation, data collection, data analysis, and results for the field instrumentation of a mainlane bridge pier of the US 183 Elevated highway located in Austin, Texas.

#### **7.2 Project Overview**

The study of the force distribution through the innovative US 183 Elevated mainlane bridge piers was performed in order to further evaluate the use of strut-and-tie modeling (STM) for reinforced concrete design and to familiarize designers with the concept of STM and its possible uses. Chapter 2 provides detailed background information on the development and use of strut-and-tie modeling.

In order to investigate the behavior of a US 183 mainlane pier, one of these piers was instrumented during construction. The purpose of the instrumentation was to measure the flow of forces through the pier due to the superstructure dead load so that these forces could be compared to the forces predicted by a strut-and-tie model of the pier. Concrete strain devices and strain gages were used to measure strains in the concrete and on the structural steel pipes. Due to the limitations of STM in detecting compatibility and constraint induced stresses, temperature measurements were made using thermocouples to determine the effects of thermal gradients on the pier. Chapter 3 describes the instrumentation procedures and instrument locations.

The instrumented US 183 mainlane pier was constructed several months prior to the erection of the superstructure supported by the pier. Data was therefore collected prior to, during, and subsequent to the placement of dead load on the pier. Chapter 4 presents the construction and data collection procedures.

Data collection prior to the construction of the superstructure allowed researchers to investigate the thermal strains induced in the pier. The thermal gradient across the structural steel pipes as well as the thermal gradients across the concrete sections were found to produce strains in some areas on the same order of magnitude as the strains expected from

the dead load. Thermal effects were therefore considered to be of significance regarding the comparison of measured forces to a strut-and-tie model of the pier. Chapter 5 presents background information on thermal induced strains and stresses and investigates the thermal strains in the pier on both a typical sunny and a typical cloudy day prior to superstructure erection. Data was collected during and after the erection of the superstructure and is also presented in Chapter 5.

The construction of the superstructure extended over several days. As such, thermal induced strains had to be separated from the total strains measured during this time since the measured forces due to superstructure dead load were to be compared to strut-and-tie models. A procedure for separating thermal strains from total measured strains is discussed in Chapter 6. The resulting strains were due only to superstructure dead load. These strains were converted to forces and compared to two strut-and-tie models. One of the strut-and-tie models was based on measured forces, and one was based on forces predicted by an elastic frame analysis. The measured forces, the strut-and-tie models, and a comparison of the two is presented in Chapter 6.

### **7.3 Conclusions and Recommendations**

Several conclusions and recommendations can be made regarding the instrumentation of the US 183 Elevated mainlane pier and the subsequent analysis of measurements made during the erection of the superstructure over the pier. The comparison of measured forces with those predicted by strut-and-tie models provided information regarding evaluation of strut-and-tie modeling for use with reinforced concrete design.

#### **7.3.1 Temperature Measurements**

Observation of measurements made prior to superstructure erection provided much insight concerning the extent of and the effects of temperature change on the pier. Thermal strains induced in the pier were found to be on the same order of magnitude, in some locations, as the expected strains due to the superstructure dead load.

Trends in temperature measurements and in thermal strains across sections of the concrete portion of the pier followed basic thermal principles regarding thermal stresses due to a temperature gradient across the concrete section. Due to the massive proportions of the



concrete, a temperature lag was found to exist across the concrete section. As ambient temperatures increased, the outer “shell” of the concrete was immediately affected. The inner “core” of the concrete was not affected by ambient temperature changes until a later time. This temperature lag across the section induced thermal stresses in the pier.

Since the superstructure erection on the instrumented pier extended over several days, these thermal strains were included in the strain measurements made during the superstructure erection. The comparison of the force distribution in the pier due to superstructure dead load with strut-and-tie models of the pier necessitated the separation of thermal strains from total measured strains due to the previously mentioned limitations of strut-and-tie modeling.

A simplified procedure was used in an attempt to separate the thermal strains from total measured strains. The extent of the effect of thermal strains on the behavior of the pier was not anticipated. Due to this fact, the number of thermocouples placed in the pier to record temperatures was insufficient to perform a detailed study of the thermal effects. Placement of more thermocouples across each cross section instrumented would have facilitated the analysis of the thermal effects in the pier. Placement of thermocouples in the shaft of the pier would have provided very clear information concerning the thermal effects, since the shape of the pier is symmetric in the shaft.

### ***7.3.2 Superstructure Dead Load Measurements***

The separation of thermal strains from total measured strains determined the strains due to the superstructure dead load. These strains due to dead load provided insight concerning the force distribution in the pier. They also provided insight concerning the field instrumentation of concrete structures subjected to low strains.

The strains measured in the structural steel pipes of the pier provided forces which were similar to those predicted by a STM of the pier. The strains measured in the concrete portion of the pier indicated forces which were not consistent in the capital and shaft. These forces were also not similar to those expected from simple analysis of the pier. The measured compression forces were on the order of half of what was expected and required due to the superstructure dead load. The expected strains in the concrete due to service loads are very small. The possibility exists that these strains were so small that the measurements

were affected by small fluctuations in the resistance of the data acquisition system. Further investigation of this possibility is recommended.

### *7.3.3 Comparison of Measured Forces with Strut-and-Tie Models*

Comparison of measured forces with strut-and-tie models of the pier provided insight concerning the use of strut-and-tie modeling with reinforced concrete design. The forces measured in the pier were compared with two strut-and-tie models. One of the strut-and-tie models was based on an angle  $\theta$  determined by the measured location of the neutral axis and hence centroid of compressive forces, while the other was based on forces predicted by an elastic frame analysis.

The strut-and-tie model based on the angle  $\theta$  determined by the measured compressive path was developed based on the known superstructure dead load and assuming uniform force distribution at the base of the pier. Although the measured forces in the concrete struts did not agree with those predicted, the force path from the point of superstructure dead load through the capital to the shaft of the pier indicated by the measured strains in the capital provided a reasonable force path. This force path was used to determine the orientation of the compressive strut in the capital of the pier. The full strut-and-tie model for the pier was then developed. The resulting tie force was in very good agreement (within 4%) with the measured tie force.

The strut-and-tie model based on forces predicted by an elastic frame analysis of the pier was developed based on the known superstructure dead load and the structural steel pipe force predicted by the frame analysis. The pipe force predicted by the frame analysis was 22% less than the measured value. The two strut-and-tie models developed provided generally similar compression force paths, indicating the ability of strut-and-tie modeling to reasonably trace the flow of forces through a structure.

Strut-and-tie modeling is a design tool and is not intended for use in analysis. The point should be made that one of the strut-and-tie models used for comparison was developed with information that a designer would not have: measured forces and force paths. Although this information would not be known by a designer, the orientation of the compressive strut in the capital selected by an experienced designer would likely be close to the strut based on measured forces.

#### **7.4 Summary**

In summary, the field instrumentation of a US 183 Elevated mainlane bridge pier successfully provided researchers with valuable information regarding the distribution of forces in the pier. Information regarding temperature effects in the pier can be used to further study the behavior of similar structures. The measurements made prior to and during construction of the superstructure furnished researchers with the information needed to evaluate the use of strut-and-tie modeling for reinforced concrete design. The comparison of strut-and-tie models based on measured and predicted forces indicated the ability of strut-and-tie modeling to allow a designer to trace the flow of forces through a structure. Strut-and-tie models redirect the designer's focus to the overall flow of forces in a structure and provide a rational framework to aid in the visualization of structural behavior.

## APPENDIX - CALCULATIONS

### Estimation of Expected Strains

US 183

V. ANDRES  
7-OCT-95

#### CONVERSION OF MEASURED STRAINS TO FORCES:

PIPE:  
AVG. OF 2 PIPES:

$$\text{CENTER: } 254 \times 10^{-6} \text{ in/in}$$

$$\begin{aligned} \sigma_{\text{pipe}} &= E_{\text{pipe}} \cdot \epsilon_{\text{pipe}} \\ &= 29,000 \text{ ksi} (254 \times 10^{-6} \text{ in/in}) = 7.37 \text{ ksi} \end{aligned}$$

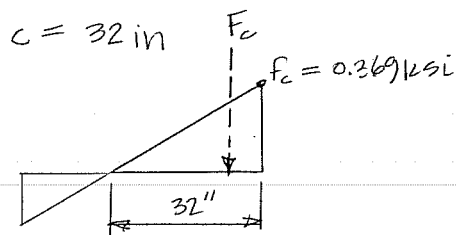
$$\begin{aligned} F_{\text{pipe}} &= \sigma_{\text{pipe}} \cdot A_{\text{pipe}} \\ &= 7.37 \text{ ksi} (12.8 \text{ in}^2) = 94.3 \text{ k} \end{aligned}$$

CAPITAL:

BOTTOM:

$$\text{AT OUTSIDE FACE OF "Y": } \epsilon_c = -90 \mu\epsilon$$

$$\begin{aligned} f_c &= E_c \epsilon_c \\ &= 4100 \text{ ksi} (-90 \mu\epsilon) = 0.369 \text{ ksi} \end{aligned}$$

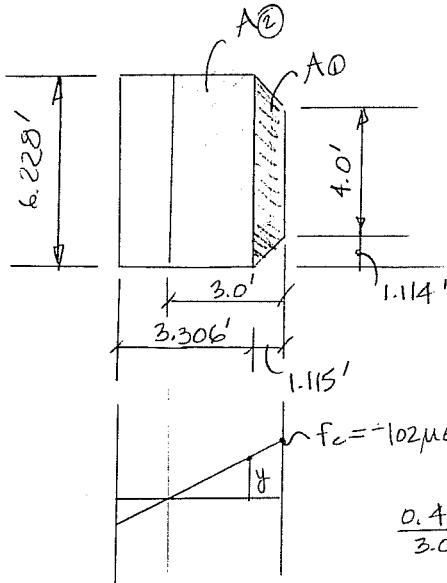


Estimation of Expected Strains

V. ANDRES  
7 OCT - 95

CAPITAL:

MID-HEIGHT:



$$f_c = -102 \mu \epsilon (4100 \text{ ksi}) = 0.418 \text{ ksi}$$

$$\frac{0.418}{3.0} = \frac{y}{(3 \downarrow 1.115)}$$

$$y = 0.26 \text{ ksi}$$

COMPRESSIVE FORCE:

$$F_c = (1.115) \left( \frac{1}{2} (4 + 6.228) \right) \left( \frac{0.418 + 0.26}{2} \right) \left( \frac{144 \text{ in}^2}{\text{ft}^2} \right)$$

$$+ (3 - 1.115) (6.228) \left( \frac{1}{2} (0.26) \right) \left( \frac{144 \text{ in}^2}{\text{ft}^2} \right)$$

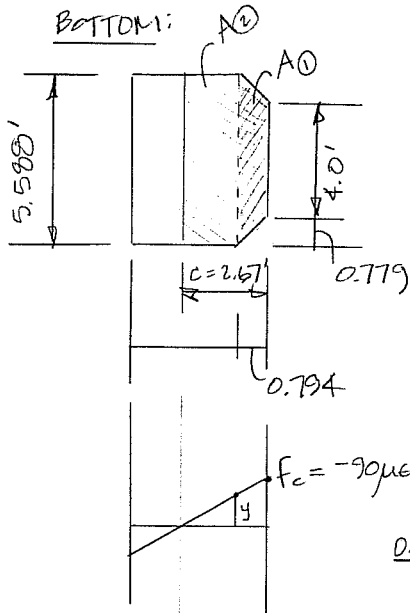
$$= 278 \text{ k} + 220 \text{ k} = 498.1 \text{ k}$$

Estimation of Expected Strains

V. ANDRES  
7-OCT-95

CAPITAL:

BOTTOM:



$$f_c = -90\mu\epsilon(4100 \text{ ksi}) = 0.369 \text{ ksi}$$

$$\frac{0.369 \text{ ksi}}{2.67'} = \frac{y}{(2.67' - 0.794')}$$

$$y = 0.259 \text{ ksi}$$

COMPRESSIVE FORCE:

$$F_c = A_0 \text{ avg}_0 + A_2 \text{ avg}_2$$

$$= (0.794') \left( \frac{1}{2} (4' + 5.588') \right) \left( \frac{0.369 + 0.259}{2} \right) \left( \frac{144 \text{ in}^2}{\text{ft}^2} \right) \\ + (2.67' - 0.794') (5.588') \left( \frac{1}{2} (0.259) \right) \left( \frac{144 \text{ in}^2}{\text{ft}^2} \right)$$

$$F_c = 172.11 \text{ k} + 195 \text{ k} = 367.6 \text{ k}$$

### Estimation of Expected Strains

US 103

V. ANDRES

#### CONVERSION OF MEASURED STRAINS TO FORCES:

##### SHAFT:

##### MID-HEIGHT:

$$\text{AVG STRAIN} = 66 \mu\epsilon \quad (\text{CORE})$$

$$\text{AREA SHAFT} = 42.67 \text{ ft}^2$$

$$E = \frac{\sigma}{\epsilon} \quad ; \quad \sigma = \epsilon \cdot E$$

$$\begin{aligned} \sigma &= 66 \times 10^{-6} \text{ in/in} (3500 \text{ ksi}) \\ &= 0.231 \text{ ksi} \end{aligned}$$

$$\begin{aligned} F &= \sigma \cdot A = 0.231 \text{ ksi} \left( 42.67 \text{ ft}^2 \right) \left( \frac{144 \text{ in}^2}{\text{ft}^2} \right) \\ F &= 1419 \text{ kips} \end{aligned}$$

### Conversion of Measured Strains to Forces

PIPE:

FROM FRAME ANALYSIS:

$$F_{\text{PIPE}} = 77 \text{ KIPS (TENSION)}^*$$

$$A_{\text{PIPE}} = 12.8 \text{ in}^2$$

$$b = \frac{F}{A} = \frac{77 \text{ K}}{12.8 \text{ in}^2} = 6.015 \text{ ksi}$$

$$e_{\text{PIPE}} = \frac{b}{E} = \frac{6.015 \text{ ksi}}{29,000 \text{ ksi}} = 2.07 \times 10^{-4} \text{ in/in}$$



### Conversion of Measured Strains to Forces

#### CAPITAL:

##### TOP OF CAPITAL

$$A = 5.50 \text{ ft} (7.0 \text{ ft}) = 38.5 \text{ ft}^2$$

$$F = 995.78 \text{ k}$$

$$b = \frac{995.78 \text{ k}}{38.5 \text{ ft}^2} \left( \frac{1 \text{ ft}^2}{144 \text{ in}^2} \right) = 0.1796 \text{ ksi}$$

$$\begin{aligned} \epsilon &= \frac{0.1796 \text{ ksi}}{4500 \text{ ksi}} = 3.99 \times 10^{-5} \text{ in/in} \\ &= 39.9 \times 10^{-6} \text{ in/in} \end{aligned}$$

##### BOTTOM OF CAPITAL

$$A = (5.588 \text{ ft})(3.500 \text{ ft}) = 20.05 \text{ ft}^2$$

$$b = \frac{995.78 \text{ k}}{20.05 \text{ ft}^2} \left( \frac{1 \text{ ft}^2}{144 \text{ in}^2} \right) = 0.345 \text{ ksi}$$

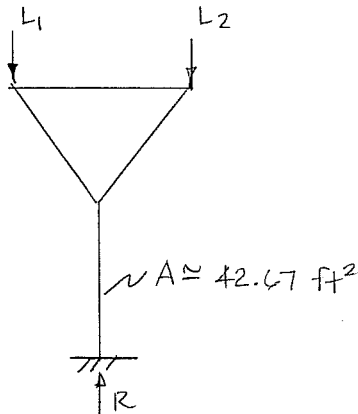
$$\begin{aligned} \epsilon &= \frac{0.345 \text{ ksi}}{4500 \text{ ksi}} = 7.67 \times 10^{-5} \text{ in/in} \\ &= 76.7 \times 10^{-6} \text{ in/in} \end{aligned}$$

Note: THESE STRAINS ARE DUE TO AXIAL LOAD ONLY. BENDING MAY CAUSE EVEN GREATER STRAINS, ESPECIALLY ON THE OUTSIDE FACE OF THE "Y".

Conversion of Measured Strains to Forces

SHAFT:

BASED ON AXIAL LOAD ONLY



NOTE:  $L_1 = L_2$  FOR ALL LOAD CASES

STATICS:

OVERALL EQUILIBRIUM:  $L_1 + L_2 = R$

LET  $L_1 + L_2 = L$

LOAD CASES:

SPAN 5  $L_1 = L_2 \cong 497.89 \text{ K}$

SPAN 6  $L_1 = L_2 \cong 497.89 \text{ K}$

$\therefore L_1 + L_2 = R \rightarrow R = 995.78 \text{ (ONE SPAN)}$

BOTH SPANS:  $R = 1991.56 \text{ K}$

STRESS:

$$\delta = \frac{P}{A} = \frac{1991.56}{42.67 \text{ ft}^2} = 46.674 \text{ K/ft}^2 \left( \frac{1 \text{ ft}^2}{144 \text{ in}^2} \right)$$

$$\delta = 0.324 \text{ K/in}^2$$

### Conversion of Measured Strains to Forces

SHAFT:

STRAIN:

$$E = \frac{\sigma}{\epsilon} \quad ; \quad \epsilon = \frac{\sigma}{E}$$

$$= \frac{0.324 \text{ ksi}}{4500 \text{ ksi}} = 7.2 \times 10^{-5} \text{ in/in}$$

$$\epsilon_{\text{SHAFT}} = 7.2 \times 10^{-5} \text{ in/in}$$

## Calculation of Measured Compressive Force Resultant Location

### MEASURED STRAINS IN "Y":

FOR BOT. & MID-HEIGHT SECTIONS OF THE CAPITAL, MEASURED STRAINS WERE LINEAR ACROSS THE SECTION.

SINCE SID3 & SID4 WERE LOST, THE LINEAR STRAINS WERE EXTRAPOLATED TO THE INSIDE FACE OF THE "Y". FROM THIS, THE COMPRESSIVE RESULTANT FORCE FOUND (AT THE 1/3 PT. OF THE TRIANGULAR STRESS PATTERN).

AT THE BOTTOM OF THE CAPITAL:

COMPRESSIVE FORCE ACTS  $\cong$  14" FROM THE OUTSIDE FACE OF THE "Y"

AT MID-HEIGHT:

COMPRESSIVE FORCE ACTS  $\cong$  12.7" FROM THE OUTSIDE FACE OF THE Y.

AT TOP OF CAPITAL, MEAS. STRAIN DIST IS NOT LINEAR. AT THE LOCATION OF THESE GAGES, THE FORCE HAS NOT HAD A CHANCE TO DISTRIBUTE ACROSS THE SECTION.

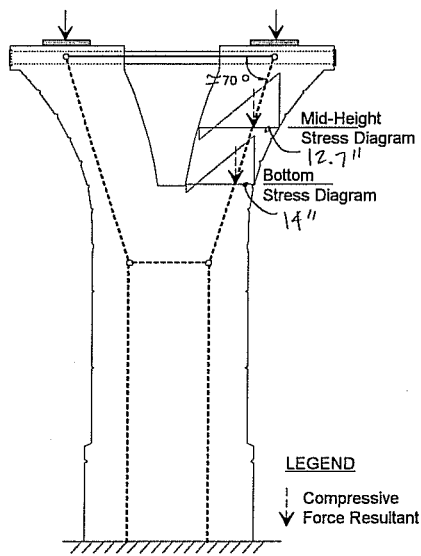
IF THE BOT. & MID. FORCE RESULTANTS ARE LOCATED ON A SCALE DRAWING OF THE PIER, ASSUMING THE COMPRESSIVE STRUT STARTS AT THE CENTER OF THE BEARING PAD AND PROCEEDS THROUGH THE RESULTANT COMP. FORCES,  $\theta$  CAN BE MEASURED. THIS ANGLE WAS DETERMINED AS:

$$\theta = 70.5^\circ$$

Calculation of Measured Compressive Force Resultant Location

MEASURED STRAINS IN "Y":

LOCATION OF COMPRESSIVE FORCE RESULTANTS ON SCALE DRAWING;  
DETERMINATION OF  $\theta$ .

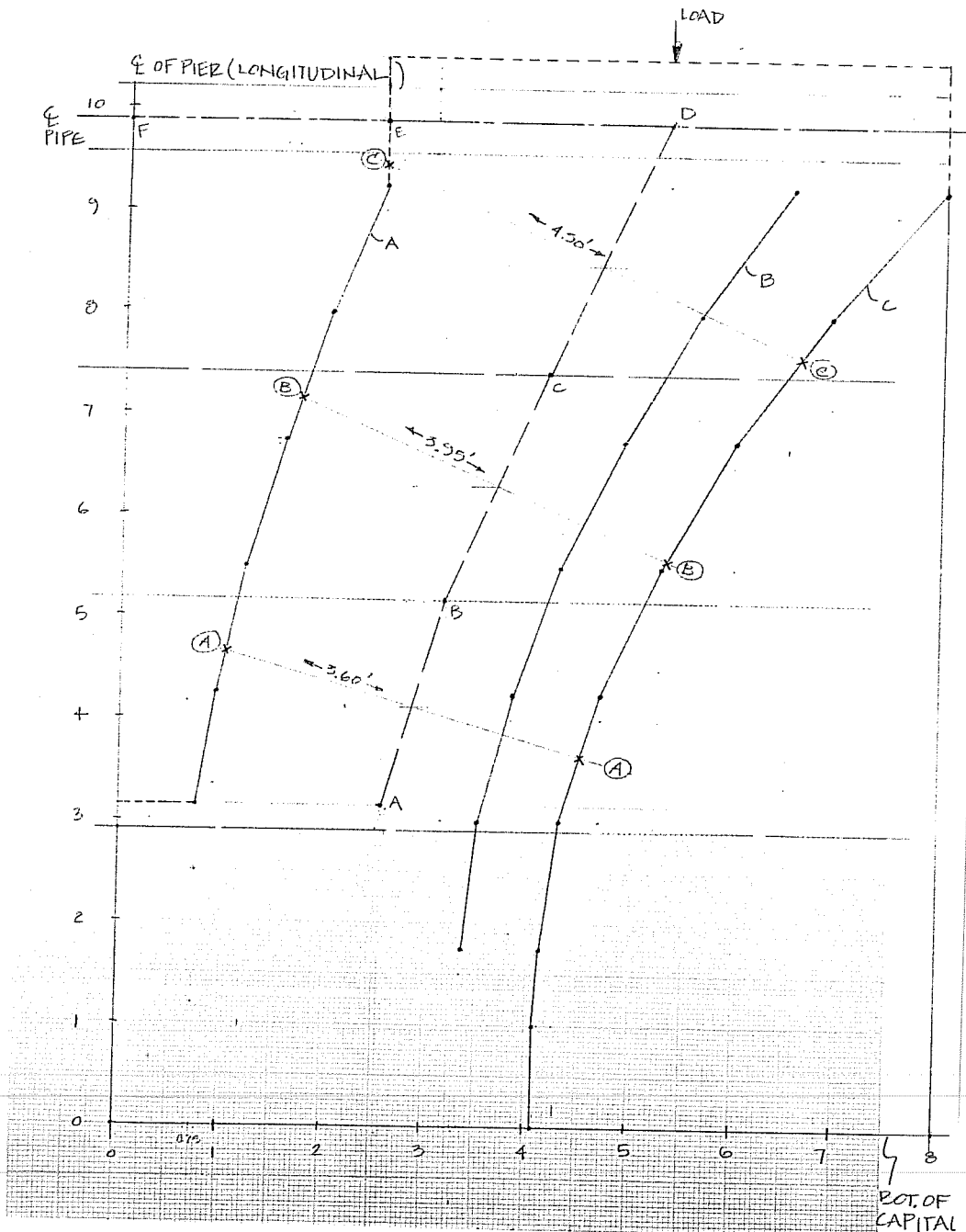


Frame Analysis for Capital

FRAME ANALYSIS  
FOR CAPITAL

PIER D6

V. ANDRES  
22-APR-95

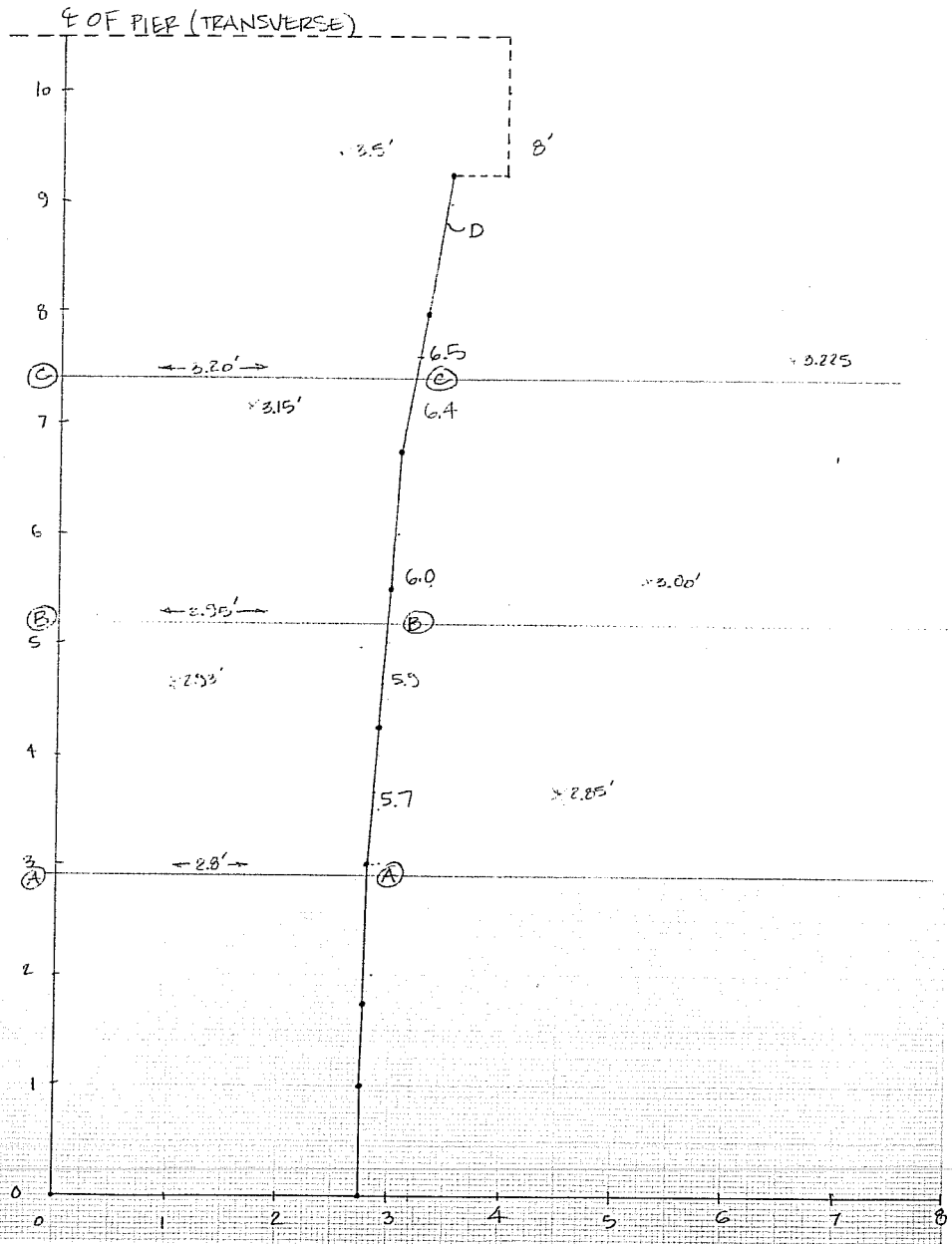


### Frame Analysis for Capital

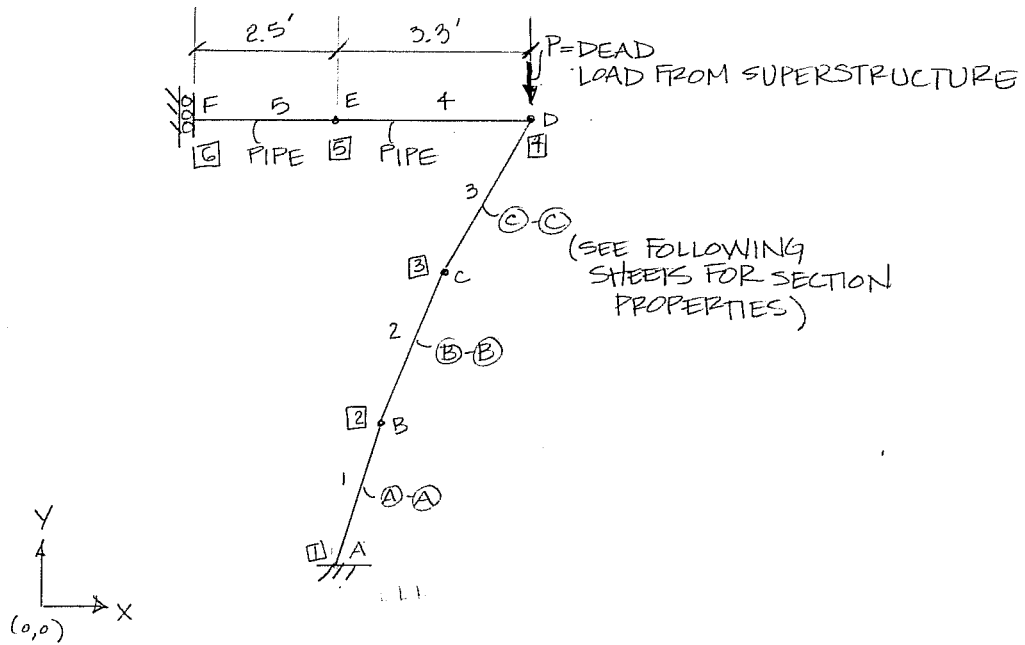
FRAME ANALYSIS  
FOR CAPITAL

PIER DL

V. ANDRES  
22-APR-95



### Frame Analysis for Capital



COORDINATES:

<u>POINT</u>	<u>"X"</u> (FT)	<u>"Y"</u> (FT)
A	2.55	3.25
B	3.25	5.17
C	4.25	7.40
D	5.275	9.875
E	2.56	9.875
F	0.00	9.875

LOAD: (SEE LOAD CALCULATIONS SHEETS)

$$P = \text{LOAD ON BEARING} \cdot 2 = (497.89)(2) = 995.78 \text{ K}$$



## Frame Analysis for Capital

### CALCULATION OF AREA FOR SECTIONS:

AREA (A-A):

$$(3.60')(\frac{1}{2}(5.9+5.7)) = 20.88 \text{ FT}^2$$

AREA (B-B):

$$(3.95')(\frac{1}{2}(6.4+6.0)) = 24.49 \text{ FT}^2$$

AREA (C-C):

$$(4.50')(\frac{1}{2}(8+6.5)) = 32.63 \text{ FT}^2$$

$$\begin{aligned} \underline{\underline{\text{AREA OF STEEL PIPE}}} &= 12.8 \text{ IN}^2 && (8" \phi \text{ EXTRA STRONG}) \\ &= 0.0888 \text{ FT}^2 \end{aligned}$$

### MOMENTS OF INERTIA:

$$I_{\text{PIPE}} = 106 \text{ in}^4 = 5.11 \times 10^{-3} \text{ FT}^4$$

(A-A):

$$\begin{aligned} I &= \frac{1}{12} b h^3 \\ &= \frac{1}{12} (3.60') (\frac{1}{2}(5.9+5.7))^3 \\ &= 22.55 \text{ FT}^4 \end{aligned}$$

(B-B):

$$\begin{aligned} I &= \frac{1}{12} (\frac{1}{2}(6.4+6.0)) (3.95)^3 \\ &= 31.84 \text{ FT}^4 \end{aligned}$$

(C-C):

$$\begin{aligned} I &= \frac{1}{12} (\frac{1}{2}(8+6.5)) (4.50)^3 \\ &= 55.05 \text{ FT}^4 \end{aligned}$$

## Frame Analysis for Capital

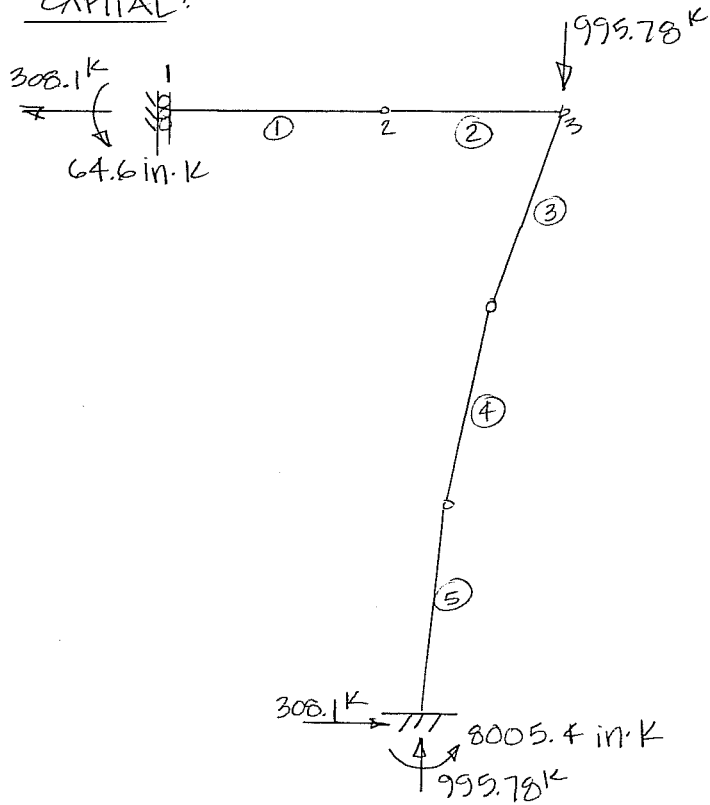
### SUMMARY:

<u>SEGMENT</u>	<u>AREA</u>	<u>I</u>
4 PIPES	51.2 in <sup>2</sup>	424 in <sup>4</sup>
(A-A)	20.88 ft <sup>2</sup>	22.55 ft <sup>4</sup>
(B-B)	24.49 ft <sup>2</sup>	31.84 ft <sup>4</sup>
(C-C)	32.63 ft <sup>2</sup>	55.05 ft <sup>4</sup>

### Frame Analysis for Capital

#### FRAME ANALYSIS RESULTS:

CAPITAL:



	<u>E (ksi)</u>	<u>A (in<sup>2</sup>)</u>
①	29,000	51.2
②	4,000	432 (AREA OF CAP. TOP)
③	4,000	3,007
④	4,000	3,530
⑤	4,000	4,699

## REFERENCES

1. Breen, J.E. "Why Structural Concrete?". IABSE Colloquium: Structural Concrete. Stuttgart, Germany, 1991.
2. Bergmeister, K. et al.. "Detailing for Structural Concrete". Center for Transportation Research Report 1127-3F. Austin, TX. May 1993.
3. Breen, J.E. et al. "Anchorage Zone Reinforcement for Post-Tensioned Concrete Girders". NCHRP Report 356. National Academy Press. Washington, D.C. 1994.
4. Schlaich, J. et al. "Toward a Consistent Design of Structural Concrete". PCI Journal. Vol. 32, No.3. Prestressed Concrete Institute. May/June 1987.
5. Leonhardt, F., E. Monnig. "Lectures on Reinforced Concrete Structures. Part 2: Special Cases of Calculations for Reinforced Concrete Construction." 3rd ed. Springer Verlag Publishers. Berlin. 1986.
6. AASHTO Standard Specifications for Highway Bridges. 15th ed. American Association of State Highway and Transportation Officials. 1992.
7. AASHTO LRFD Bridge Design Specifications. 1st ed. American Association of State Highway and Transportation Officials. 1994.
8. ACI 318-89 Building Code Requirements for Reinforced Concrete. American Concrete Institute. Detroit, MI. 1989.
9. Higdon, A. et al.. *Mechanics of Materials*. 4th ed. John Wiley & Sons, Inc. New York, NY. 1985.
10. Arréllaga, J.A. "Instrumentation Systems for Post-Tensioned Segmental Box Girder Bridges". Master's Thesis. The University of Texas at Austin. Austin, TX. December, 1991.
11. Roberts, C. "Measurement Based Revisions for Segmental Bridge Design and Construction Criteria". PhD Dissertation. The University of Texas at Austin. Austin, TX. December, 1993.
12. Stone, William C. "Design Criteria for Post-Tensioned Anchorage Zone Tensile Stresses". PhD Dissertation. The University of Texas at Austin. Austin, TX. 1980.
13. *Campbell Scientific 21X Micrologger Operator's Manual*. Campbell Scientific. Logan, Utah. 1992.

14. Den Hartog, J.P. *Strength of Materials*. 1st ed. McGraw-Hill Book Company, Inc. New York, NY. 1949.
15. National Oceanic and Atmospheric Administration. "Local Climatological Data: Monthly Summary - Austin, TX." National Climactic Data Center. Asheville, NC. 1994-95.

## VITA

Valerie Ann Andres was born at Scott Air Force Base in Belleville, Illinois, on February 10, 1970. She grew up in the southern part of Indiana in Jeffersonville and New Albany. She completed her work at Our Lady of Providence High School in Clarksville, Indiana, in May of 1988. She entered Purdue University in August of 1988. She completed the Cooperative Education Program while at Purdue and graduated in May of 1993 with highest distinction. She entered The University of Texas at Austin in August of 1993. While at The University of Texas, she was the 1994-1995 American Concrete Institute Katharine and Bryant Mather Fellow.